Computational Optimization of the Thermal Performance of Internally Finned Ducts

by

Eric Duplain

Department of Mechanical Engineering

McGill University
Montréal, Québec, Canada

August, 2006

A thesis submitted to McGill University
in partial fulfillment of the requirements for the degree of
Master of Engineering

Library and
Archives Canada

Bibliothèque et
Archives Canada

Published Heritage
Branch

Direction du
Patrimoine de l'édition

395 Wellington Street
Ottawa ON K1A 0N4
Canada

395, rue Wellington
Ottawa ON K1A 0N4
Canada

Canada

Abstract

A computational methodology for the optimization of the thermal performance of straight ducts with non-twisted, uninterrupted, longitudinal internal fins is formulated and demonstrated in the context of steady, laminar, fully-developed forced convection, accounting for conjugate heat conduction in the fins. The fluid flow and heat transfer problems are solved using control-volume-based finite difference and finite element methods. The optimization is done using a gradient method. The fins shapes are approximated using non-uniform rational B-splines (NURBS). The control points of the NURBS curves are among the design variables. In the demonstration problems, the objective was to maximize the total rate of heat transfer to the fluid per unit length of the duct, subject to the constraint of keeping the corresponding pumping power constant. Results pertaining to four sample ducts with fins made of stainless steel, aluminum, and copper, and air as the working fluid, are presented and discussed.

Résumé

Une méthodologie utilisant des outils numériques est formulée et démontrée pour l'optimisation des performances thermiques de tuyaux rectilignes à ailettes internes non-rotationnelles et non-interrompues pour un écoulement développé, laminaire et constant, considérant la conduction de chaleur à l'intérieur des ailettes. La solution aux problèmes fluidique et thermique est obtenue à l'aide des méthodes d'éléments finis et de différences finies. L'optimisation est performée avec la méthode du gradient. La forme des ailettes est approximée à l'aide d'une courbe B-spline non-uniforme et rationnelle (NURBS), où les points de contrôle font partie des variables de design. Pour les problèmes démonstratifs, l'objectif est de maximiser le taux total de transfert de chaleur au fluide par unité de longueur de tuyau, assujetti à la contrainte de garder la puissance de pompage correspondante fixe. Les résultats obtenus pour quatre tuyaux dont les ailettes sont faites d'acier inoxydable, d'aluminium et de cuivre, sont ensuite présentés et discutés.

Acknowledgements

I would like first to express my gratitude to my mentor and supervisor, Professor B. Rabi Baliga, whose teachings, guidance, support and sense of humour have made my experience at McGill an enjoyable and rewarding journey. I also thank him for giving me the opportunity to work on this very exciting and challenging project.

Thanks to my colleagues and friends from the Heat Transfer Laboratory, Nima Atabaki, David Scott, Nirmalakanth Jesusathan, Alexandre Lamoureux, and Lorena Camargo, whose camaraderie and support I have deeply appreciated.

I would like to thank the Mechanical Engineering Administrative Staff, and especially Joyce Nault, Barbara Lapointe, and Jean Milliken for their help with all the paperwork and administrative details.

I would like to thank my dear parents, Denis and Louise, for their continuous love, support and wisdom.

Finally, I would like to thank my beloved Stephanie for her love, patience, understanding and invaluable support during those last two years.

Eric

Table of Contents

List of Figures

List of Tables

Nomenclature

a	coefficients of the discretization equation
A	Basis matrix that defines a constraint hyper-plane
$A_{c\text{-}s}$	Cross sectional area of the ducts
b	Absolute source term
C	NURBS curve vector
c_p	Specific heat capacity
D_h	Hydraulic diameter
f	Objective function
f_D	Darcy friction factor
g	Constraint function
$\tilde{g}$	Component of the gravitational acceleration in the z direction
h	Control point height above the fin central axis for the circular duct
H	Height of the rectangular and triangular ducts
h_{av}	Average heat transfer coefficient
J	Diffusion flux
k	Thermal conductivity
l^*	Normalized fin length
l_f	Fin length for the circular duct
$\dot{m}$	Mass flow rate
$\mathbf{n}$	Unit outward vector normal to differential area element ds
N	NURBS basis function
n_{fin}	Number of fins for the circular duct
Nu	Nusselt number
p	Static pressure
P	Reduced pressure
$\mathbf{P}$	NURBS control point (with subscript)
$\mathbf{P}$	Projection matrix (without subscript)
$Peri_{wetted}$	Wetted perimeter of the duct
pp	Pumping power
pp_{target}	Desired pumping power
Pr	Prandtl number
q	Heat input
r	Radius of the circular duct
Re	Reynold number
S	Volumetric source term
$\mathbf{S}$	Gradient-based search direction

t	Fin thickness
T	Temperature
$\mathbf{U}$	NURBS knot vector
$\mathbf{V}$	Constraint hyper-plane basis vector
x	Cartesian coordinate component
X	Dimensionless cartesian coordinate component
$\mathbf{X}$	Design vector
y	Cartesian coordinate component
Y	Dimensionless cartesian coordinate component
w	Axial velocity
W	Non dimensional axial velocity
W	Width of the rectangular and triangular ducts
z^*	Dimensionless length of the ducts

Greek letters

ε	Convergence criterion
ϕ	General scalar dependent variable
η	Thermal effectiveness
η	Dimensionless thickness of the duct
φ	Non dimensional temperature for the thermal boundary condition T
λ	Step size
μ	Viscosity
θ	Non dimensional temperature for the thermal boundary condition H
ρ	Density
σ	Half base angle of the fin for the circular duct
τ	Half aperture angle of the triangular duct
ξ	Dimensionless width of the duct
Γ	Diffusion coefficient
Ω	Fin conductance

Subscripts

av	Average value
b	Bulk value
circ	Relative to the circular duct
const	Relative to the Constraint function

e, E   East

  f   Fluid

  l   Lower fin surface

n, N   North

 obj   Relative to the objective function

 rect   Relative to the rectangular duct

s, S   South

  tri   Relative to the triangular duct

tri_y   Component of the half-fin thickness *t* in the *y* direction

  u   Upper fin surface

w, wall   Wall

w, W   West

  ϕ Relative to the general scalar dependent variable

  $\perp$ perpendicular component

Superscripts

  H   Pertaining to the thermal boundary condition involving uniform heat input per unit axial length and uniform cross-sectional temperature

  T   Pertaining to the thermal boundary condition involving constant wall temperature

Chapter 1. Introduction

1.1 OVERALL GOAL, MOTIVATION, AND BACKGROUND

The overall goal of this research is to propose, implement, and demonstrate a computational methodology for the optimization of the convective heat transfer in internally finned ducts. The particular optimization criterion adopted in this work is to maximize the rate of heat transfer for a fixed value of pumping power, and also other constraints, as required. In internally finned ducts, the number of fins, the base thickness of the fins, the height (length) of the fins, the shape of the fins and the flow passage, and the thermofluid properties of the fluid influence the pumping power needed to force the fluid through it at the desired rate. These parameters, as well as the thermal conductivity of the fin material, influence the rate of heat transfer from the internally finned duct to the fluid, or vice versa. Hence, all combinations of these parameters must be explored to find one that meets the thermal optimization criteria. The computational methodology put forward in this thesis is formulated to achieve such thermally optimal designs of internally finned ducts.

The proposed optimization methodology does not depend on the specific application. In this work, it is demonstrated in the context of steady, fully-developed, laminar forced convection in straight internally finned ducts; the fins considered are straight, continuous, and longitudinal; the fluid considered is air; and in the range of operation considered, the average thermofluid properties of the fluid and the fin material are assumed to remain essentially constant. The reasons for the choice of this particular demonstration problem are the following: it is conceptually simple, yet practical; and the mathematical models for the associated fluid flow and heat transfer are well established.

The motivation for this thesis is derived from a desire, on the part of both the author and his supervisor, to contribute to ongoing global efforts of heat transfer engineers to improve and optimize the thermal performance of energy exchange and conversion devices. Such efforts translate directly into improved energy utilization and reduced energy wastage, and thus have significant economic, social, and health-related benefits.

Figure 1.1 presents some typical tube heat exchangers and cooling blocks with internal flow passages. In this figure, the parts number 2, 5, 6, 8, and 12 have embedded ducts with smooth (finless) circular and oval internal cross-sections. Part number 1 is an example of an arrangement with internally finned annuli. Parts number 9 and 10 have internally finned ducts with longitudinal rectangular fins; and parts number 3, 4, 7, and 11 have externally finned ducts. Additional examples of internally finned ducts and annuli are given in Figure 1.2.
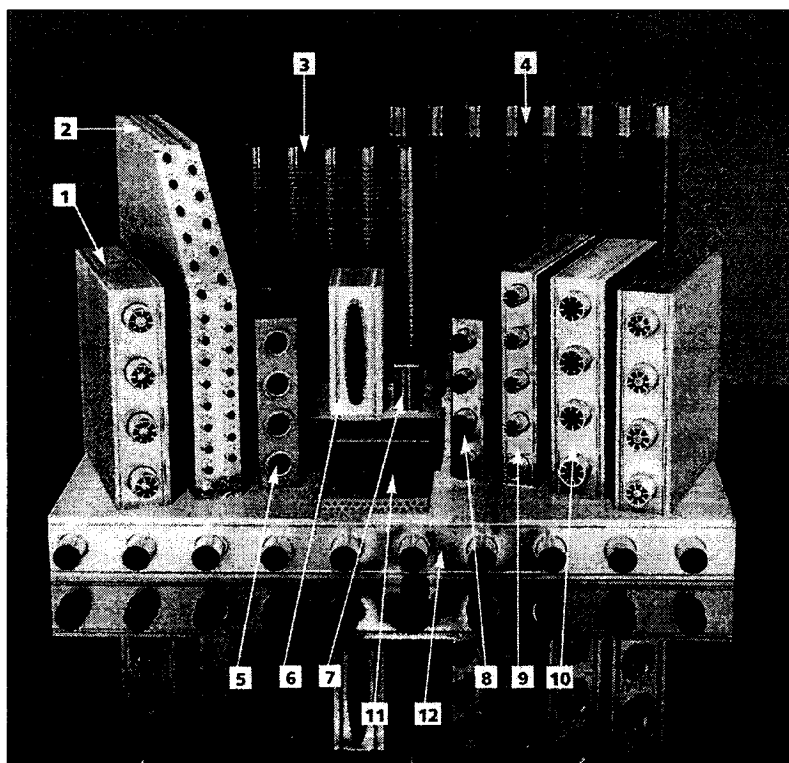
Figure 1.1 Tubular and finned heat exchange surfaces (courtesy Britannia Heat Transfer)

Internally finned ducts are routinely encountered in the cores of compact heat exchangers. These heat exchangers are characterized by cores in which the heat-transfer-area-to-volume ratio (or area density) exceeds 700 m^2/m^3. They are commonly used in the chemical, aeronautical, automotive, and heating, ventilating and air-conditioning (HVAC) industries, and also in industrial gas turbine engines and cooling systems for electronics. They are also extensively used for heat recovery and steam generation applications in thermal and nuclear power plants. The cores of compact heat exchangers

are often constructed out of plates and fins that together create so-called plate-fin ducts or flow passages. The fins, which are placed in between the plates, enhance the rate of heat transfer, and often play a secondary role as structural spacers and supports. A wide variety of fins, such as continuous, rectangular offset, zigzag, chevron, perforated, and louvered fins, are used in the cores of compact heat exchangers [Kays (1972); Kays and London (1964, 1984); Shah et al. (2001); Kakaç and Liu (2002)].
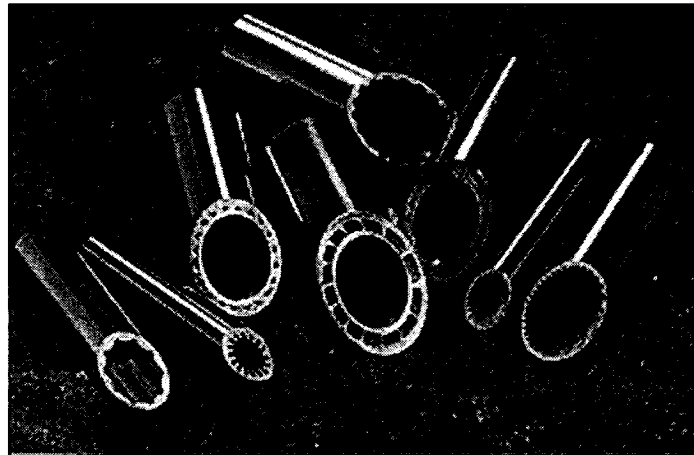
Figure 1.2 Photograph of some commonly used internally finned tubes (courtesy Wolverine Tube)

Over the last 100 years, heat exchangers have been studied experimentally using actual heat exchangers, full-scale models, and simplified laboratory models designed to facilitate accurate overall and local measurements. However, since the advent of high-speed digital computers and efficient numerical methods in the 1970s, computational techniques have been increasingly employed for investigating the thermofluid phenomena that occur in heat exchangers. Today, such computational investigations are used to complement and sometimes even replace laboratory experiments.

The proposed methodology for the computational optimization of the thermal performance of internally finned ducts consists of two main parts. In the first part, either control-volume-based finite difference or finite element methods (CVFDM or CVFEM) are used to solve the mathematical models of steady, laminar, fully-developed fluid flow and heat transfer phenomena in an internally finned duct with a specified geometry (the so-called *direct* problem). In the second part, an optimization algorithm, based on a

gradient approach and inputs of results from the aforementioned first part, is used to calculate a new geometry of the internally finned duct that moves it towards the optimal design. These two parts are used repeatedly until the optimal design is achieved.

In this thesis, steady, laminar, fully-developed fluid flow and heat transfer in straight internally finned ducts of rectangular, triangular, and circular cross-sections, as shown in Figure 1.3, are considered. Air is considered as the working fluid. Three different fin materials (commonly used in compact heat exchangers) are explored: stainless steel, aluminium, and copper. As was stated earlier, in the range of operating conditions considered, the average values of the thermofluid properties of the working fluid and the fin material are assumed to remain essentially constant. The fluid flow and heat transfer problems of interest are governed by the continuity, Navier-Stokes, energy, and quasi one-dimensional fin equations [White (1991); Incropera and DeWitt (2002)]. At all solid surfaces, the no-slip and impermeability conditions are imposed on the fluid flow. At symmetry surfaces, the normal fluxes of momentum and energy are set to zero. The unfinned portions of the duct walls are subjected to the following two thermal boundary conditions:

- Uniform heat input per unit axial length and uniform cross sectional temperature (indicated by H);

- Constant wall temperature (indicated by T).
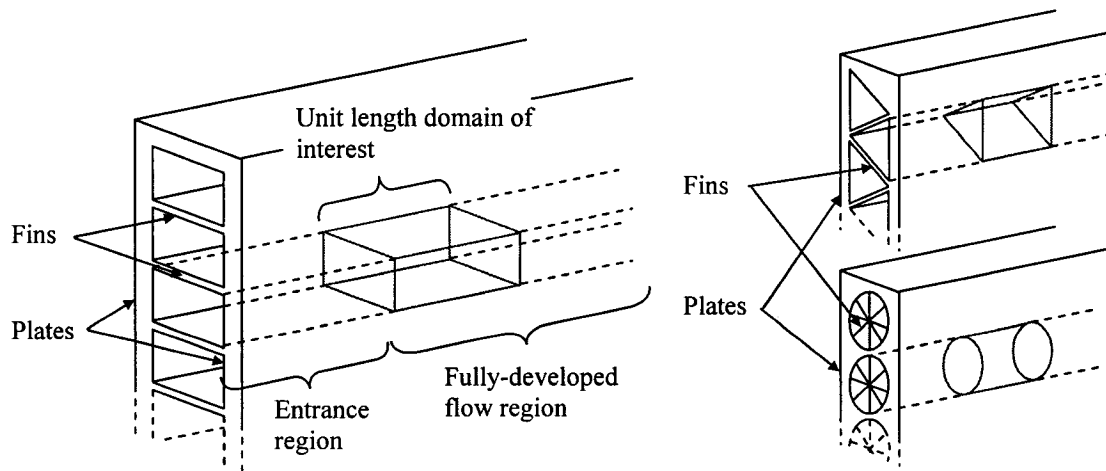
Figure 1.3 Plate Heat Exchangers: Schematic Drawing and Domains Considered

These two thermal boundary conditions were chosen because they represent extreme or bounding cases of the actual conditions in compact heat exchangers [Sparrow and Patankar (1977)]. In practice, the thermal boundary conditions encountered will lie between those two extremes [Kay and London (1984)].

1.2   SPECIFIC OBJECTIVES

The specific objectives of this investigation can be summarized as follows:

- To propose suitable criteria and constraints for thermal optimization of the aforementioned internally finned ducts. These criteria and constraints are key element of the optimization problem, as they define what is considered as thermal performance, and dictate the behaviour of the optimization algorithm;

- To propose a simple but effective methodology for achieving the above criteria for the thermal optimization of the internally finned ducts of interest, in the context of the proposed criteria and constraints;

- To demonstrate the potential of the proposed computational optimization methodology by applying it to a selection of practical cases.

1.3   LITERATURE REVIEW

An exhaustive review of the literature related to the vast subjects of fluid flow and heat transfer in ducts and compact heat exchangers is not intended in this section. Rather, this review is limited to works that are relevant or closely related to the research presented in this thesis. This section is subdivided as follows: (a) books and review articles related to fluid flow and heat transfer in ducts and heat exchangers; (b) papers related to fluid flow and heat transfer in ducts and heat exchangers; (c) books and review articles related to optimization techniques; (d) papers related to optimization techniques.

1.3.1   Books and Review Articles on Fluid Flow and Heat Transfer

There are many excellent books on the basic and more advanced aspects of fluid flow and heat transfer in ducts: examples include the works of Streeter (1962), Batchelor (1967),

Eckert and Drake (1971), Rouse (1978), Schlichting (1979), Landau and Lifshitz (1987), Churchill (1988), Kays and Crawford (1993), Bejan (1995), Panton (1996), Fox and McDonald (1998), White (1991), Wilkes (1999), Incropera and DeWitt (2002), and Cebeci (2002). The topics of laminar flow and heat transfer in ducts of various shapes have been covered comprehensively by Shah and London (1978). The *Handbook of Heat Transfer Fundamentals* edited by Rohsenow et al. (1985) is a very useful source of information on fluid flow and heat transfer in ducts. Many review articles on the recent advances in heat exchangers can be found in Afgan et al. (1996) and Kakaç et al. (1999). The book by Webb (1994) reviews the theory and applications of heat transfer enhancement devices.

The fundamentals of computational methods for the prediction of fluid flow and heat transfer in ducts are covered in books authored by Roache (1998), Patankar (1980), Reddy and Gartling (1994), and Ferziger and Peric (1999), among others. The *Handbook of Numerical Heat Transfer (2nd Edition)* edited by Minkowycz, Sparrow, and Murthy (2006) and the series *Advances in Numerical Heat Transfer (Vols. 1 and 2)* edited by Minkowycz and Sparrow (1997, 2000) provide many useful review articles on various aspects of computational fluid dynamics and heat transfer. Control-volume-based finite difference and finite element methods (CVFDMs and CVFEMs) are reviewed in Baliga and Atabaki (2006).

The work of Kays and London (1984) is one of the main references on the subject of compact heat exchangers. A recent book by Hesselgreaves (2001) provides a discussion of the basic methodology used to design compact heat exchangers and descriptions of several compact heat exchangers used in industrial applications. A review article by Shah et al. (2001) provides an excellent overview of issues related to computer simulations of fluid flow and heat transfer in the cores of compact heat exchangers. Bejan (1982) has covered the subject of entropy generation and used it in an alternative characterization of the efficiency of heat transfer in ducts.

1.3.2 Fluid Flow and Heat Transfer in Internally Finned Ducts

Masliyah and Nandkumar (1976) studied laminar, fully-developed, forced convection in an internally finned circular tube, with axially uniform heat flux and peripherally uniform temperature. The fins used were of triangular cross section. They found that for a given fin geometry, the Nusselt number based on inside tube diameter was higher than for a smooth tube. They also observed that there exists an optimum number of fins that yields the highest Nusselt number. Soliman et al. (1980) conducted numerical studies of the same type of problem, but with a uniform outside wall temperature condition, and included the fin conductance in the model as a single parameter. They observed that the local heat flux distribution at the side of the fin is strongly dependent on the fin length and number of fins. They also observed that for a large number of small fins, the fluid temperature has a single extremum value at the centre of the duct, and for a small number of long fins, this extremum was instead found between each fin. The results were compared using the Nusselt number as a criteria for thermal performance. Patankar et al. (1979) analyzed, via a mixing length model, fully-developed turbulent flow and heat transfer characteristics of tubes and annuli with longitudinal internal fins; the working fluid considered was a gas; thus, the temperature variation along the fins was considered negligible. They found that the local heat transfer coefficients exhibited a substantial variation along the fin length, with the smallest values at the base and the highest values at the tip of the fins. They also observed that as the number of fins increased, the portion of the total gas flow rate in the regions in between the fins decreased, due to the higher resistance of these inter-fin spaces. Webb and Scott (1980) have conducted a parametric analysis of forced convection in internally finned tubes. They identified key fin geometric parameters and elaborated the benefits of internal fins in circular tubes. Based on their results, they made the following observations: 1) the use of tall fins of reduced thickness is not an advantage in improving thermal efficiency, for given pumping power and heat load; 2) to obtain reduced pumping power with minimum frontal area of the fins, a small number of relatively tall axial fins are advantageous; and 3) it is possible to select internal fin geometries which provide higher thermal performance than rib-type roughness elements, again for a given pumping power. In all of the publications

mentioned in this paragraph, it is concluded that the fin surfaces transfer heat more effectively than the unfinned surfaces of the tube-wall.

Kröger (1986) has proposed an experimental method to characterize the heat transfer and pressure drop of externally finned tubes commonly used in the heat exchanger industry. Baliga and Azrak (1986) have conducted numerical studies of laminar fully-developed flow and heat transfer in plate-fin ducts of triangular cross-section. They determined the heat transfer characteristics of such ducts by analyzing the conjugate problem of quasi one-dimensional conduction in the fins and two-dimensional forced convection in the fluid region. Their results highlighted the need to consider such a conjugate problem, rather than an analysis based on standard fin theory with a computed average heat transfer coefficient as an input, as the latter can lead to significant errors. Witte (1988) has developed a method to study the performance of heat exchangers, using a criterion based on the second-law of thermodynamics rather than the first-law, which ensures that the most efficient use of available energy is being made. His method allows the determination of the number-of-heat-transfer units (NTU) at which the benefits of reduced availability losses are offset by the costs of added area, and applies to any heat exchanger whose effectiveness to NTU relation is known. Bergles (1988) has reviewed the historical background, driving trends, and the various and numerous heat transfer enhancement techniques developed over the years, and suggested that such techniques belong to the *second generation* heat transfer technology. One of his conclusions is that in order to fully understand the thermofluid phenomena present in heat exchangers, modelling using analytical or numerical prediction techniques should be used. He states that such techniques can also be used to effectively develop improved heat transfer surfaces or inserts. Cowell (1990) has proposed a family of methods for the comparison of compact heat transfer surfaces. He compared the hydraulic diameter, frontal area, total volume, pumping power, and NTU for many different surfaces. Several charts were produced which allow a wide range of easily comprehensible comparisons to be made between different heat exchangers. Zhang and Faghri (1995) have conducted a numerical study of internally finned tubes for applications in latent heat thermal energy storage systems: they found that the melting volume fraction — a key module parameter for assessing performance efficiency — can be significantly increased by increasing the

thickness, height, and number of fins. The heat transfer enhancement by fins in the microscale regime for applications in electronics has been covered by Chou et al. (1999).

Cheng and Cheng (2002) have investigated the heat transfer and pressure drop of fractal branching nets for the design of a micro heat exchanger of rectangular shape. They assumed laminar fully-developed flow, and neglected the pressure drop at the branch bifurcations. They found that the fractal net can increase the total heat transfer rate, while reducing the total pressure drop, which is surprising. As the number of branchings (levels) in the fractal increased, the heat transfer increased even more and the pressure drop decreased. It is envisaged in this paper that such devices will find a wide range of applications in the future. Vyver et al. Meyer (2003) have proposed a computational fluid dynamics (CFD) model for the fluid flow and heat transfer in a three-dimensional tube-in-tube heat exchanger. First, they validated their model by applying it to problems with available correlations and experimental results. Then, the model was used to test new duct designs: the inner tube was replaced by a quadratic Koch island fractal, which produced increases in thermal performance of up to four times that of a simple smooth tube-in-tube design. They concluded that CFD is a valuable tool in heat exchanger design.

Dul'kin and Garas'ko (2002) have published two papers (one reporting a study in two parts) on an analytical investigation of a one-dimensional heat conduction problem for a single fin with temperature dependent heat transfer coefficient, with 1) a closed-form inverse solution, and 2) a recurrent direct solution. First, an expression for the direct evaluation of the fin-tip temperature was proposed. Then, this expression was used to solve in ordinary functions the heat transfer rates yielded by each of the different fin designs considered, with a power-law-type dependence of the heat transfer coefficient on the local temperature excess.

Ko and Ting (2006), in a work that complements that of Bejan (1982), conducted a numerical investigation of entropy generation for laminar forced convection in curved rectangular ducts. The effect of the Dean number, external wall heat flux, and cross-sectional aspect ratio were investigated. Their results show that this entropy generation is

mostly governed by frictional irreversibility when the Dean number is large and the wall heat flux is small; however, for a small Dean number and large wall heat flux, it is provoked primarily by heat transfer irreversibility. Thus, they concluded that the optimal duct aspect ratio is dependent on the Dean number and the wall heat flux.

1.3.3   Books and Review Articles on Optimization Techniques

There are many books on the different optimization techniques developed and applied over the years, mainly in the vast fields of economics and engineering. The optimization techniques in engineering became increasingly well-established and used in the late 1950s, with the advent of computers, and the first complete books on this subject started to appear in the late 1960s and the early 1970s. The work of Denn (1969) covers the techniques based on the variational method and emphasizes applications in chemical engineering. A book by Converse (1970) is one of the first to present a clear and universal formulation of an optimization problem; one entire chapter in this book is solely dedicated to the formulation of the problem, and another whole chapter is devoted to the definition of the objective function. In a book by Dixon (1972), one part is devoted to static problems — it includes a historical survey of the development of optimization techniques and presents details of techniques based on the gradient search method; and in a second part, the then-new field of optimization of dynamic problems is discussed. Conley (1981) has presented optimization techniques based on sampling distributions and the Monte Carlo method, with applications to business and economics, chemical yield, pharmacology, and packaging and shipping: applications to each of these subjects are presented in a separate chapter along with a corresponding computer program.

Over the last two decades, several publications and books on optimization have focused on overall reviews, recent advances in optimization techniques, and specific applications. Pironneau (1994) has presented an in-depth review of the basic theory related to elliptic partial differential equations (PDEs), the existence of solutions, optimization based on the gradient method, optimal control theory, and the use of finite element methods. He has also demonstrated and discussed the applications of these concepts and methods for the optimal designs of airfoils and electromagnets. Seireg and Rodriguez (1997) have dedicated their book to the optimization of the shape of mechanical elements and

structures and have also presented a number of specific applications. Hernandez et al. (1999) have also published a book of review articles on computer-aided optimal designs of structures. A book by Mohammadi and Pironneau (2001) covers shape optimization of wings and nozzles using techniques that utilize finite element methods. This book also contains an overview of the concept of "optimization platforms", where an optimization algorithm controls computer-aided design (CAD) and computational fluid dynamics (CFD) software, for manipulations of complex shapes and solutions of the related fluid flow problems. The field of dynamic optimization has been reviewed and expanded in a book by Bryson (1999).

A highly valuable resource in this area is a book by Rao (1996) entitled *Engineering Optimization: Theory and Practice*. This book presents clear and concise discussions of most of the optimization techniques employed today. It was one of the key references used in the development of the optimization method proposed in this thesis. Deb (2001) has written a book on multi-objective optimization using evolutionary algorithms. In this book, a class of genetic algorithms are used for the solution of complex problems involving multiple objectives and constraints. A very powerful and useful application of optimization methods in engineering is the solution of inverse heat transfer problems, where the objective is to obtain a design that produces desired measurements or results as precisely as possible. This subject is covered in books by Kurpisz and Nowak (1995) and Özisik and Orlande (2000), among others.

Onwubolu and Babu (2004) have reviewed recent optimization techniques in engineering. The methods presented in this book represent the next, or new generation of optimization methods, based on techniques such as genetic algorithms, ant colony optimization, memetic algorithms, and self-organizing migrating algorithms. Many current applications of these methods are also presented in this book. An excellent book that complements the aforementioned books on optimization is one by Piegl and Tiller (1997) on nonuniform rational B-splines (NURBs), which covers the various ways that shapes can be effectively approximated, controlled, and modified during the design process.

1.3.4   Optimization Techniques

Mohammadi and Pironneau (2004) have surveyed some recent developments in optimal shape design for applications involving fluid flow. According to this survey, recent applications include those in which the Hemlholtz equation for waves is solved in the direct problem: examples include the design of a harbour that minimizes incoming waves, microfluidic applications, and large paper-making machines. However, this survey concludes that the biggest demand for optimization is in the airplane industry, where even a small decrease in drag translates into strong reductions of operating costs, and is thus a strong incentive for buyers. Other applications of optimization covered in this survey include weight reduction, aeroacoustic design of engines, cars, musical instruments, electromagnetics, and wave cancelling for boats. This survey also examines unsolved optimization problems: examples include shockwave minimization and shape optimization involving unsteady turbulent flows. It suggests that future optimization methods will probably involve coupling between gradient-based approaches and genetic algorithms.

The gradient method in one of the most widely used method for shape optimization, because of its simplicity, versatility, and robustness. In this context, it should be noted that the computation of the gradient may be performed by either direct numerical differentiation, which requires more computing time but is intuitive and easy to implement, or by the adjoint method, which requires relatively much less computing time but is more prone to errors and harder to implement efficiently. Shape optimization for heat conduction problems has been discussed by Dems and Mroz (1998), Meric (1998), Cheng and Wu (2000), and Lan et al. (2001). In each of these four works, the problem was to find the optimal shape that leads to a desired surface or internal temperature distribution for applications involving an internal heat source. Ashrafizadeh et al. (2002) have solved a similar problem, where the objective was to achieve a given surface temperature or heat flux. In works related to aeronautics, the efforts have been almost exclusively directed towards airfoil shape optimization: Burgreen and Baysal (1994) have focused on the optimization of airfoils in steady, two-dimensional, inviscid transonic flow at zero angle of attack; Pandya and Baysal (1997) have optimized an airfoil, but in three-dimensions, using an alternating direction implicit scheme, which breaks up the problem

into multiple sub-problems, in order to reduce the computer memory requirements, and obtains the solution to the full problem by solving the sub-problems iteratively. Soto and Löhner (2001) have optimized a hydrofoil with a method based on the adjoint formulation. Here, the Euler equation for incompressible flows was solved in the direct problem; and the shape of the hydrofoil was controlled via a pseudo-shell surface parametrization, which is similar to the use of splines and control points. They demonstrated the cost effectiveness of manipulating such surface parameters rather than multiple grid points present on the hydrofoil surface. A review of many of the methods, implementations, results, and future directions of airfoil optimization is available in a paper by Jameson (1994).

Other examples of the applications of the gradient method include the optimization of a radar cross section [Bondeson et al. (2004)], and the optimization of a shaft cross-section using an adaptive shape refinement technique akin to an automatic adjustment of the number of control points on a spline [Kohli and Carey (1993)]. An adaptive shape refinement technique, based on the gradient and the finite element methods, has been used by Schleupen et al. (2000) to optimize some mechanical objects subjected to applied stresses. A drastically new approach to shape optimization has been envisioned by Borrvall and Petersson (2003): they have proposed a method for internal or external fluid flows in the Stokes regime, in which not only the boundaries but also the topology of the whole domain of interest are optimized. Holzleitner (1997) has suggested some improvements to the way in which the objective and constraint functions are prescribed in order to facilitate the convergence of shape optimization procedures involving static stresses: he modified these functions so that high stress concentrations, which are primarily responsible for the divergence in the optimization process, are penalized. Saidi et al. (2005) have optimized the overall performance of a fuel cell, based on an exergy analysis of this device.

Optimization techniques are also widely used in inverse heat transfer investigations to obtain thermal parameters, desired fluid flow and thermal boundary conditions, and optimal shapes. Jarny, Özisik, and Bardon (1991) have presented an optimization method, based on the adjoint formulation coupled to the conjugate gradient algorithm, to

solve multidimensional inverse heat conduction problems. They demonstrated their method by solving a problem related to parameter and surface condition estimation from transient temperature measurements. Park and Chung (1999) have compared the adjoint method to the direct differentiation method for the minimization of a performance function used for the estimation of the time-varying strength of a heat source. Although each of these two methods reached the same result, they suggested a new method that is a blend of both: it avoids the increased computation cost of the direct differentiation approach (but has the same accuracy), and it is easier to implement than the adjoint formulation. Berdnik and Mukhamedyarov (2003) have used the method of neural networks to obtain solutions of inverse heat transfer problems. Their method has low computing costs and very good accuracy; thus, they suggested that it could be used in real-time applications. Dowding and Beck (1999) have used a sequential gradient method along with the adjoint formulation to solve the inverse heat conduction problem of estimating a wall heat flux distribution from temperature measurements.

Inverse methods have also been successfully used for the estimation of shapes, first with the conjugate gradient approach [Cheng and Chang (2003); Cheng et al. (2003)] and then by using truncated singular value decomposition [França et al. (2001)]. These methods have also been used successfully for the estimation of interface shape from boundary measurements [Kunisch and Pan (1994); Keanini and Desai (1995); Prabhu and Ashish (2002); Xu and Natener (2003); Cheng and Chang (2003a, 2003b, 2003c); and Cheng and Chang (2004)].

In the aeronautical industry, Zangenen et al. (1999) have successfully applied a three-dimensional inverse design method for the design of turbomachinery blades: in this method, the blade geometry is computed for a specified distribution of circulation. Huang and Hsiung (1999) have used the conjugate gradient method, along with the boundary element method, to solve the direct, sensitivity, and adjoint problems for optimize the shape of cooling passages in gas turbine blades. Shape optimization has been achieved with a gradient approach by Arkadan et al. (1996) to obtain a permanent magnet shape that minimizes the leakage flux in high-power equipment. Fic (2004) has proposed a procedure for solving the steady-state inverse convection-diffusion heat

transfer problem involving two-dimensional potential fluid flow: it employs a finite-element method and sensitivity coefficients for estimating the boundary velocity based on desired temperature measurements, or inputs.

Cingoski et al. (1999) have used a dynamically adjustable genetic algorithm to perform inverse shape optimization on a magnetic pole, where the shape of the pole was defined using several control points and ordinary spline functions. Annicchiarico and Cerrolaza (1999) have combined a finite element method, genetic algorithms, and B-splines to formulate a novel technique for shape optimization: in it, the design variables controlled by the genetic algorithm are the spline control points. Their method was successfully used to optimize the shape of a plate subjected to tension and a connecting rod.

Beliakov (2004) has investigated the sensitivity of the optimal shape with respect to the spline curve knot distribution in order to find the global minimum, which is often surrounded by local minima: he used the simplex method, together with a discrete gradient method applied to each element of the simplex procedure to improve the accuracy of the results. His algorithm also guarantees the achievement of the global minimum.

In the published literature, there are also numerous publications on the optimization of ducts and internally finned ducts. Ashrafizadeh et al. (2003) have proposed a method to optimize the shape of nozzles, diffusers, and elbows. In their method, an optimal shape is achieved by iteratively adjusting the coefficients in the discretized equations of a finite volume method (in which the coefficients depend on the dependent variable) during the overall solution process, based on the latest available distribution of the dependent variable, solving the direct fluid flow problem, and repeating the process until convergence. This proposed method is considered as an extension of the typical finite volume method for the solution of the fluid flow problem, since the coefficients of the discretized equations are adjusted as a part of the optimization process. The resulting duct shapes achieved pressure distributions along the wall exactly as prescribed.

A study by Tsukamoto and Seguchi (1984) is among the first ones in which the optimal shape of cooling fins is considered. They numerically solved a quasi one-dimensional

model of heat conduction in the fin and approximated the fin shape with a second-order polynomial, the coefficients of which were the design variables. The objective in their optimization procedure was to minimize the fin volume without any decrease in thermal efficiency or increase in pumping power. They compared the results obtained with the optimized shape to those corresponding to an initial rectangular fin (zeroth-order polynomial). Snider et al. (1990) studied analytically the effect of ripples on the surface of cooling fins, and compared the efficiencies of the such fins to those of the corresponding fins without ripples; the initial fin shape considered was the so-called "Schmidt fin" (a parabolic fin). They concluded that for the range of operating conditions considered, the addition of ripples on a given fin surface increases the corresponding heat transfer, regardless of its temperature. This work was later constructively criticized and complemented by the work of Razelos (1995). In the work of Razelos and Krikkis (2003), a procedure for the optimization of the thermal design of longitudinal rectangular fin is presented along with some results. They derived polynomial correlations for the optimal fin base and width, where the objective was to either minimize the specified weight (volume) or maximize the rate of heat transfer in the context of certain specified constraints. For the range of conditions considered in their work, they also concluded that the heat transfer from the tip of the fin could be neglected without incurring any appreciable errors.

Lorenzini, Spiga and Fabbri (1994) have proposed a method for optimizing the shape of fins attached to planar surfaces, in the context of fully-developed laminar flow: the objective function was the average Nusselt number, and the constraint was fixed fin volume. The fin surface was approximated with a polynomial, and the design variables were the polynomial coefficients. They found that the optimal fin shape included as many undulations on the side of the fins as the order of the polynomial permitted, and the increase in thermal effectiveness, presented as the ratio of the rate of heat transfer to that achieved with a reference fin of rectangular shape, reached over 300%. Following this work, Fabbri (1997) published a paper in which he validated the relation between the increase in thermal effectiveness and the order of the polynomial used to approximate the fin profile. Fabbri (1998) has also successfully used the methods developed in the aforementioned works to optimize internally finned annular ducts, used to remove heat

from a cylindrical heat source. Here again, as the order of the polynomial increased, multiple undulations were observed on the fin surface. In another paper [Fabbri (1998a)], he has presented the optimization of the shape of four internal fins in a tube, with a polynomial to approximate the fin profile and a fixed fin volume as a constraint. The resulting optimized fin shapes all had an outgrowth located approximately at half the length of the fin, regardless of the fin volume. As the order of the polynomial increased, the outgrowth became more defined and concentrated at the centre of the fin, with a corresponding noticeable increase in the Nusselt number. This outgrowth was also observed in the context of longitudinal, parallel fins on a plate dissipator [Fabbri (1998b)]. In all cases, he used a genetic algorithm for the optimization process. It should also be noted that although the resulting fin shapes increased the thermal effectiveness of the finned ducts studied, the possible fin shapes that can be obtained from a polynomial approximation are limited by the order of the polynomial.

Laor and Kalman (1995) have presented a theoretical and numerical analysis of the performance and optimum dimensions of ducts with external fins with various fin shapes: longitudinal, spine, and annular fins with rectangular, triangular, and parabolic profiles. The heat transfer coefficient at the fin surface was temperature dependent. Yeh (1994, 1996) has proposed an analytical fin shape model that depends on the heat load at the fin base, sides, and tip, and investigated its effect and the effect of the Biot number on the fin shape, with the minimum fin volume as the constraint. He observed that as the Biot number increases, the shape of the optimum fin alters from a trapezoidal to a concave profile. Kundu and Das (1999) analysed the performance and optimized the shape of eccentric annular disk fins subject to convective cooling, using a semi-analytical method. Optimization was performed with this analytical model, using the Lagrange multiplier technique, with the fin volume or the heat load as the constraint. They compared the thermal performance of concentric and eccentric fins. They came to the following conclusions: first, there is a minimum heat load over which optimal shape has an effect of the performance of the fins; second, when a space restriction is imposed on one side of the tube, optimum utilization of fin material becomes impossible above a certain heat load (higher than that for the first conclusion) by using circular fins. Under these circumstances, eccentric annular fins are better alternatives.

There are also many papers on the optimization of other types of finned surfaces, such as pin fin arrays. Examples of such papers include the works of Bejan and Morega (1993), Jubran et al. (1993), Gerencser and Razani (1995), Kacimov and Obnosov (1997), and Bonjour et al. (2003).

1.4   THESIS OVERVIEW

In earlier sections of this first chapter, the motivation for this work, its objectives, and a review of the literature directly relevant to this research were presented. In Chapter 2, relevant theoretical aspects of the fluid flow and heat transfer applicable to this work are presented and discussed concisely. The numerical methods employed for the calculation of the fluid flow and heat transfer in the internally finned ducts of interest, including conjugate heat conduction in the fins, are presented in Chapter 3. In Chapter 4, the optimization technique and related developments used in this work are described. The results of this investigation are presented and discussed in Chapter 5. Finally, in Chapter 6, the contributions of this thesis are summarized and some recommendations for extensions of this work are given.

Chapter 2. Theoretical Considerations

In this chapter, the assumptions and the equations that govern the fluid flow and heat transfer problems of interest in this work, and also the corresponding boundary conditions, are presented first. Following that, the dimensionless versions of these equations and boundary conditions are presented concisely.

2.1 LAMINAR FULLY DEVELOPED FLOW AND HEAT TRANSFER IN FINNED DUCTS

2.1.1 Overview

As was mentioned in Chapter 1, for compact heat exchangers, the values of the ratio of heat transfer area to core volume exceed 700 m^2/m^3 [Kays and London (1984)]. With these high values of this ratio, the hydraulic diameters of the plate-fin ducts of interest are usually rather small. Thus, with air as the working fluid, the Reynolds number based on the hydraulic diameter usually falls well within the laminar regime [Shah and London (1978)]. Furthermore, the entrance length of the flows in such plate-fin ducts is small compared to their total length: thus, fully-developed flow can be assumed to prevail over most of the length [Shah and London (1978)]. The cores of such heat exchangers are commonly made up of a very large matrix of similar plate-fin flow passages. Therefore, spatial edge effects, such as proximity to heat exchanger outer surfaces and corners, can be ignored: thus, for each core considered, the study can be limited to a single representative plate-fin flow passage, as illustrated in Figure 2.1.

In the present study, the proposed optimization methodology is developed and demonstrated in the context of laminar, fully-developed flow and heat transfer in straight, continuous, plate-fin ducts. However, as was mentioned in Chapter 1, the proposed optimization methodology is independent of the particular problem considered. Therefore, inclusion of phenomenon such as turbulence and the entrance flow region would only alter the optimal shape of the flow passages and the fins, and are not essential to the demonstration of the capabilities of the optimization methodology itself.

The thermal conductance of the fins is considered finite in this work: thus, the conjugate problem of forced convection in the flow and heat conduction inside the fin is solved. A quasi one-dimensional model is used for the heat conduction model inside the fins, akin to the approach adopted by Baliga and Azrak (1986) for investigating triangular plate-fin ducts.
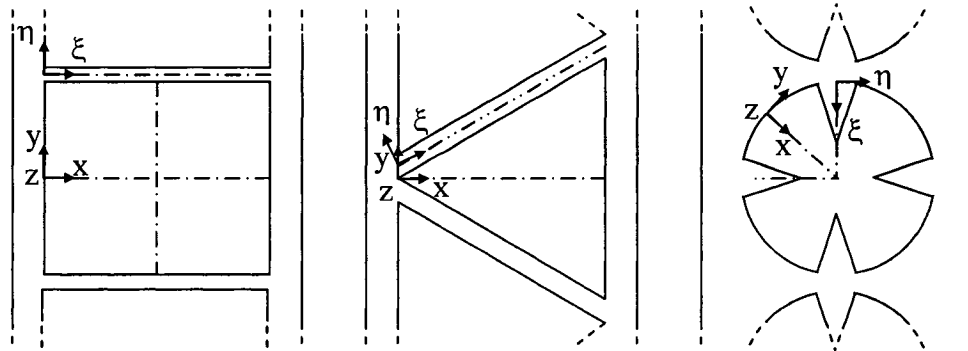
Figure 2.1 Coordinate systems used for the ducts considered

The coordinate systems used in the mathematical models of the fluid flow and heat transfer phenomena in the plate-fin ducts considered in this work are presented in Figure 2.1. In all such ducts, the z axis is parallel to the duct axis, and points in the direction of the main flow.

2.1.2 Assumptions

The assumptions presented below apply to all plate-fin ducts investigated in this work.

• The plate-fin duct is straight and non-twisted, and its inner surface is uninterrupted and smooth;

• The continuum hypothesis applies, and the working fluid is Newtonian;

- The fluid and duct material properties are considered constant: fixed at suitably averaged values, as is commonly done in heat exchanger design methods [Kays and London (1984)];

- The Reynolds number range of interest is $100 \le \text{Re} \le 1500$ and the Mach number is well less than 0.1. Therefore, the fluid flow is in the laminar regime and compressibility effects are negligible;

- The buoyancy-driven free convection effects are negligible;

- In each plate-fin duct considered in this work, the heat conduction inside the fin can be approximated as quasi one-dimensional, as is commonly done in classical fin theory: thus, the temperature inside the fin varies only in the direction along its length, and is uniform in the cross-section normal to this direction. For further details of this quasi one-dimensional assumption in fin theory and a discussion of the conditions for its validity, the reader is referred to the work of Incropera and DeWitt (2002);

- The rate of heat conduction in the axial direction (in the duct wall, the fin, and the fluid) is negligible compared to that in the cross-section of the duct;

- No heat source is present in the fluid and the viscous dissipation is negligible;

- The fluid flow and heat transfer are steady and fully-developed;

- For each of the plate-fin ducts considered, for a given pumping power, there is a unique duct-fin shape that maximizes the rate of heat transfer to or from the fluid.

These assumptions apply to all discussions in the remainder of this thesis.

2.1.3   Governing Equations

The equations that govern Newtonian fluid flows in the context of the continuum model have been well established since the second half of the 19$^{\text{th}}$ century, as discussed, for example, by Batchelor (1967), Rouse (1978), Schlichting (1979), and White (1991). They are the continuity equation, the three momentum equations (the so-called Navier-Stokes equations) and the energy equation. For details of the derivations of these equations, the reader is referred to the works of Schlichting (1979), White (1991), and

Kays and Crawford (1993). The assumptions in the previous subsection allow major simplifications of these governing equations. The simplified equations are presented in the following subsections with respect to the Cartesian coordinate systems illustrated in Figure 2.1.

2.1.3.1 Continuity equation

The general continuity equation is the following:

$$\frac{\partial \rho}{\partial t} + \frac{\partial(\rho u)}{\partial x} + \frac{\partial(\rho v)}{\partial y} + \frac{\partial(\rho w)}{\partial z} = 0 \tag{2.1}$$

In this equation, ρ is the mass density of the fluid, and in this work, as was stated earlier, it is assumed to remain constant; the velocity components in the x, y, and z directions are denoted as u, v, and w, respectively. Using the assumption that the flow is steady, $\partial \rho / \partial t = 0$ (this equation also follows from the assumption of constant density). In the fully-developed region, for laminar flow, the components of the velocity in the duct cross section, u and v, are zero, and the w remains invariant with z: thus, $\partial w / \partial z = 0$. Thus, in the context of the assumptions stated earlier, the continuity equation is satisfied.

2.1.3.2 Momentum equations

For the steady, fully-developed, laminar flows under consideration here, the x- and y-momentum equations reduce to $u = 0$ and $v = 0$, respectively. Furthermore, as was mentioned earlier, $\partial w / \partial z = 0$. The reduced pressure, P, is defined as follows:

$$P = p + \rho \tilde{g} z \tag{2.2}$$

In this equation, p is the static pressure and $\tilde{g}$ is the component of the gravitational acceleration in the z direction. In the fully-developed region, p is uniform in the duct cross-section (is not a function of x and y), and the pressure gradient in the z direction remains constant: $dp / dz = $ constant. Thus, the z-momentum equation reduces to a balance between the driving pressure force and the retarding shear forces, as follows [White (1991); Kays and Crawford (1993)]:

$$\frac{\partial p}{\partial z} = \mu(\frac{\partial^2 w}{\partial x^2} + \frac{\partial^2 w}{\partial y^2}) \tag{2.3}$$

2.1.3.3 Energy equation

In the context of the assumptions given earlier, for steady, laminar, fully-developed heat transfer, the energy equation reduces to the following form [Kays and Crawford (1993)]:

$$\rho c_p w \frac{\partial T}{\partial z} = k_f (\frac{\partial^2 T}{\partial x^2} + \frac{\partial^2 T}{\partial y^2}) \tag{2.4}$$

where c_p is the specific heat of the fluid and k_f is its thermal conductivity.

2.1.3.4 Fin heat conduction equation

Inside the fins, heat transfer occurs by conduction. In the context of the assumptions given previously, heat is first transferred from the wall of the duct into (or out of) each fin across its base, and then transferred from its other surfaces to (or from) the fluid flowing in the duct by convection. The equation that governs the quasi one-dimensional steady temperature distribution in the fin is derived by making an energy balance on a slice of the fin: this control volume is shown in Figure 2.2.
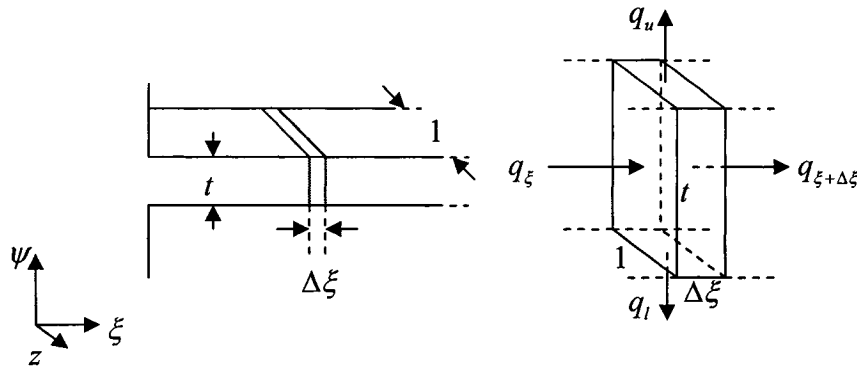
Figure 2.2 Control volume for the fin energy balance

In this figure, t is the thickness of the fin; $\Delta\xi$ is the control volume (CV) thickness (thickness of the slice of the fin); q_ξ is the rate of heat conduction into the CV across its cross-section at ξ; $q_{\xi+\Delta\xi}$ is the rate of heat conduction leaving the CV across its cross-section at $\xi + \Delta\xi$; and q_u and q_l are the rates of heat transfer from the upper and lower surfaces of the fin, respectively, to the adjoining fluid. The extent of the CV in the z direction is unity. It is assumed that the rate of heat transfer by conduction in the z

direction is insignificant in comparison with those in the ψ and ξ directions. Thus, a steady-state energy balance on the CV shown in Figure 2.2 yields the following equation:

$$q_\xi - q_{\xi+\Delta\xi} = q_u + q_l \tag{2.5}$$

For the rectangular and the circular plate-fin ducts (see Figure 2.1), the fin central surface is a symmetry surface: therefore, the rates of heat transfer leaving the fin from the top and bottom surfaces of the CV in Figure 2.2 are equal ($q_u = q_l$). For the triangular plate-fin duct, however, the fluid flows in the passages adjacent to each fin over its upper and lower surfaces are skew-symmetric: the corresponding heat fluxes, q_u'' and q_l'', reflect this skew symmetry, as shown in Figure 2.3, and the following equation applies:

$$q_u\big|_\xi = q_l\big|_{L-\xi} \tag{2.6}$$

where L is the length of the fin.

(a)   (b)
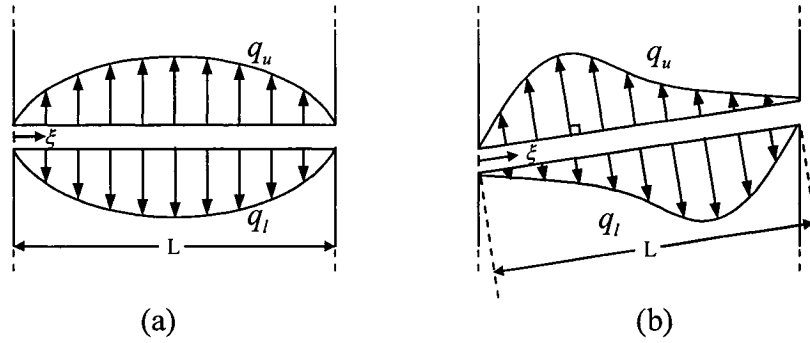
Figure 2.3 (a) Symmetric and (b) skew-symmetric distributions of heat fluxes on the upper and lower surfaces of the fin

Keeping in mind the unit extent of the fin in the z direction, q_ξ, q_l, and q_u can be expressed in terms of their respective surface heat fluxes as follows:

$$q_\xi = tq_\xi'' = t(-k_s \partial T / \partial \xi)\big|_\xi \tag{2.7}$$

$$q_l = \Delta\xi q_l'' = \Delta\xi(-k_f \partial T / \partial y)_{f,l} \tag{2.8}$$

$$q_u = \Delta\xi q_u'' = \Delta\xi\{(k_f \partial T / \partial y)_{f,u} \tag{2.9}$$

where k_s and k_f are the thermal conductivities of the solid (fin) and the fluid, respectively.

Dividing both sides of equation (2.5) by $\Delta \xi$ and taking the limit as $\Delta \xi \to 0$ on the left-hand side yield:

$$-\frac{\partial q_\xi}{\partial \xi} = q_u'' + q_l''$$

(2.10)

Combining equations (2.7) and (2.10) and rearranging leads to the following equation:

$$tk_s \frac{\partial^2 T}{\partial \xi^2} = k_f \left(-\frac{\partial T}{\partial y}\bigg|_u + \frac{\partial T}{\partial y}\bigg|_l \right)$$

(2.11)

For the rectangular and circular ducts, the top and bottom heat fluxes are symmetric and equation (2.11) reduces to:

$$tk_s \frac{\partial^2 T}{\partial \xi^2} = 2k_f \left(\frac{\partial T}{\partial y}\bigg|_l \right)$$

(2.12)

Table 2.1 presents a summary of the governing equations. The corresponding boundary conditions are presented in the following subsection.

Table 2.1 Summary of the governing equations

z-momentum	$\dfrac{\partial p}{\partial z} = \mu \left(\dfrac{\partial^2 w}{\partial x^2} + \dfrac{\partial^2 w}{\partial y^2} \right)$
Energy equation in the fluid	$\rho c_p w \dfrac{\partial T}{\partial z} = k_f \left(\dfrac{\partial^2 T}{\partial x^2} + \dfrac{\partial^2 T}{\partial y^2} \right)$
Quasi one-dimensional heat conduction in the fin	$tk_s \dfrac{\partial^2 T}{\partial \xi^2} = k_f \left(-\dfrac{\partial T}{\partial y}\bigg|_u + \dfrac{\partial T}{\partial y}\bigg|_l \right)$

2.1.4   Boundary Conditions

For the fluid flow, the boundaries conditions are:

- Along the duct wall and the fin surfaces, $w = 0$;

- Along the symmetry surfaces, $\nabla_\perp w = 0$.

where $\nabla_\perp$ is the gradient perpendicular to the symmetry plane.

As was stated earlier, for the thermal problem, along the duct wall-fluid interface, the following two boundary conditions, which represent the extremes of the conditions encountered in practice [Sparrow and Patankar (1977)], are considered:

- Uniform heat input per unit axial length (q'_{wall} = constant) and uniform cross-sectional wall temperature. Such a condition could be found, for example, in the electrical heating of duct walls having high thermal conductivity, or counter-flow exchangers with equal heat capacity rates for the hot and cold fluid streams. In this case, in the fully-developed heat transfer regime, all temperatures (in the fluid, fin, and duct wall) rise linearly with z [Kays and Crawford (1993)];

- Uniform wall temperature (T_w = constant). This condition is approximated in ducts inside the shells of condensers or boilers [Kays and Crawford (1993); Kays and London (1984)]. In this case, in the fully-developed heat transfer regime, ($T_w - T_b$) decays exponential with z [Kays and Crawford (1993)], where T_b is the bulk temperature of the fluid.

In all cases, along symmetry surfaces, $\nabla_\perp T = 0$.

2.2   DIMENSIONAL ANALYSIS

Suitable dimensionless forms of the z-momentum and the energy equations for the problems of interest are presented in this section.

2.2.1   Non-Dimensionalization of the z-momentum Equation

Following Shah and London (1978), Patankar (1980), and Kays and Crawford (1993), the following dimensionless variables are introduced:

$$X = x / D_h; Y = y / D_h; W = w\mu / \{(-dP / dz)(D_h)^2\} \tag{2.13}$$

In this equation, D_h is the hydraulic diameter, defined as follows:

$$D_h = \frac{4A_{c-s}}{Peri_{wetted}} \tag{2.14}$$

Here, A_{c-s} is the cross-sectional area for the fluid flow and $Peri_{wetted}$ is the so-called wetted perimeter of this area (total length of the solid-fluid interface portion of the bounding curve of this cross-sectional area).

Introducing these dimensionless variables in equation (2.3) and rearranging, the following dimensionless form of the z-momentum equation is obtained:

$$\frac{\partial^2 W}{\partial X^2} + \frac{\partial^2 W}{\partial Y^2} + 1 = 0 \tag{2.15}$$

Equation (2.15) is two-dimensional. The boundary conditions are the following:

- Along the duct wall and the fin surfaces, $W = 0$;

- Along the symmetry surfaces, $\nabla_{\perp} W = 0$.

A solution of equation (2.15) subject to the above-mentioned boundary conditions provides the dimensionless velocity field, W. The dimensional velocity field w can be obtained from W by using the dynamic viscosity of the fluid, the axial pressure gradient, and the duct hydraulic diameter.

There are no dimensionless parameters in equation (2.15). The only dimensionless parameters in this problem are those that characterize the duct cross-sectional geometry (they come in through the non-dimensionalization of the boundary conditions). However, as the focus here is on laminar flows, it is important to ensure that the value of the Reynolds number is less than 2000 (conservative value): here, the Reynolds number is based on the average z-direction velocity component, w_{av}, and the hydraulic diameter, D_h:

$$Re = \frac{\rho w_{av} D_h}{\mu} \tag{2.16}$$

Furthermore, the constant axial (z-direction) gradient of the reduced pressure in the fully-developed region is commonly non-dimensionalized and expressed as the Darcy friction factor, defined as follows:

$$f_D = \frac{-\frac{dP}{dz} D_h}{\frac{1}{2} \rho w_{av}^2} \tag{2.17}$$

The Darcy friction factor-Reynolds number product is:

$$f_D \cdot \text{Re} = -\frac{2}{\mu} \frac{dP}{dz} \frac{D_h^2}{w_{av}} \tag{2.18}$$

2.2.2 Non-Dimensionalization of the Energy Equation

The axial variations of the temperature for the two above-mentioned thermal boundary conditions are different. Thus, following the recommendations of Patankar (1980) and Kays and Crawford (1993), the non-dimensionalization of the energy equation for these two thermal boundary conditions is done differently, as described in the following subsections.

2.2.2.1 Thermal boundary condition H: uniform heat input per unit axial length and uniform cross sectional wall temperature

For this thermal boundary condition, in the fully-developed region, the axial gradients of all the temperatures in the duct are the same and constant [Patankar (1980); Kays and Crawford (1993)], as shown in Figure 2.4. Thus,

$$\frac{\partial T}{\partial z} = \frac{dT_b}{dz} = \frac{dT_w}{dz} = constant \tag{2.19}$$

where T_b is the bulk temperature of the fluid.
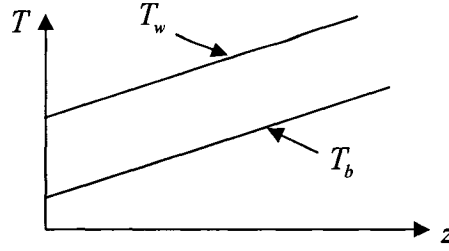
Figure 2.4 Constant increase of all temperatures in the z direction

An energy balance on a slice of the duct yields:

$$\dot{m}c_p \frac{dT_b}{dz} = q_w^{'} = Peri_{wetted}q_{w,av}^{''} \tag{2.20}$$

Knowing that $\dot{m} = \rho w_{av}A_{c-s}$ and using equation (2.20) , equation (2.4) can be rewritten as follows:

$$\frac{4}{D_h k_f}\frac{w}{w_{av}}\frac{q_w^{'}}{Peri_{wetted}} = \frac{\partial^2 T}{\partial x^2} + \frac{\partial^2 T}{\partial y^2} \tag{2.21}$$

Since the temperature variation along the duct axis is driven by the imposed heat input at the wall, the following non-dimensional temperature is used [Patankar (1980); Kays and Crawford (1993)]:

$$\theta = \frac{T_w - T}{q_w^{'}\Big/k_f} \tag{2.22}$$

In terms of X, Y, and θ, equation (2.21) can be cast in the following dimensionless form:

$$\frac{\partial^2 \theta}{\partial X^2} + \frac{\partial^2 \theta}{\partial Y^2} + 4\frac{D_h}{Peri_{wetted}}\frac{w}{w_{av}} = 0 \tag{2.23}$$

In equation (2.23), the non-dimensional temperature θ is independent of the position along the duct axis. Moreover, once the velocity field has been computed, the θ field can be readily obtained since the source term in this equation is independent of θ.

For the boundary conditions, using equation (2.22) and noting that on the duct wall, $T = T_w$, $\theta = 0$. At symmetry surfaces, $\nabla_\perp \theta = 0$. Along the fin surfaces, the following dimensionless forms of equations (2.11) and (2.12) apply:

$$\Omega \frac{\partial^2 \theta}{\partial \Xi^2} = -\frac{\partial \theta}{\partial Y}\bigg|_u + \frac{\partial \theta}{\partial Y}\bigg|_l \qquad (2.24)$$

$$\frac{\Omega}{2} \frac{\partial^2 \theta}{\partial \Xi^2} = \frac{\partial \theta}{\partial Y}\bigg|_l \qquad (2.25)$$

where $\Xi = \xi / D_h$, and Ω is the fin conductance parameter given by:

$$\Omega = \frac{t k_s}{D_h k_f} \qquad (2.26)$$

The dimensional temperature T can be retrieved from θ by using the specified wall temperature, T_w, the specified wall heat flux $q''_{w,av} = q'_w / Peri_{wetted}$, and the duct hydraulic diameter, D_h. For this boundary condition, the average Nusselt number is related to the dimensionless bulk temperature, θ_b, by the following equation:

$$Nu_{av}^H = \frac{h_{av} D_h}{k_f} = \frac{\{(q'_w / Peri_{wetted})/(T_w - T_b)\} D_h}{k_f} = \frac{D_h / Peri_{wetted}}{\dfrac{(T_w - T_b)}{(q'_w / k_f)}} = \frac{D_h / Peri_{wetted}}{\theta_b} \qquad (2.27)$$

where the superscript H refers to the current thermal boundary condition.

2.2.2.2   Thermal boundary condition T: constant duct wall temperature

For this thermal boundary condition, the wall temperature is specified and constant throughout the duct, and the following dimensionless temperature is used [Patankar (1980); Kays and Crawford (1993)]:

$$\varphi = \frac{T_w - T}{T_w - T_b} \qquad (2.28)$$

Therefore,

$$T = T_w - \varphi (T_w - T_b) \qquad (2.29)$$

In this case, in the thermally fully-developed region, all temperature differences ($T_w - T$), including ($T_w - T_b$), decay exponentially to zero at the same rate, as shown in figure 2.5;

and h (and also h_{av}), or equivalently, φ, remain invariant with z [Kays and Crawford (1993)].
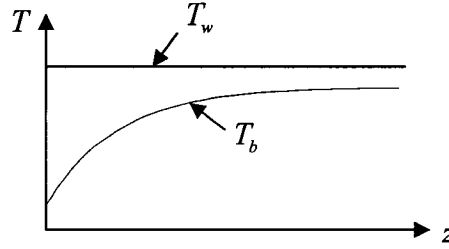
Figure 2.5 Exponential decay of $T_w - T_b$ in the z direction

In this case, following the classical analysis of Graetz, as described in Kays and Crawford (1993), the z coordinate is non-dimensionalized as follows:

$$z^* = \frac{z/D_h}{\mathrm{Re}\,\mathrm{Pr}}$$ (2.30)

Here, Pr is the Prandtl number of the fluid:

$$\mathrm{Pr} = \mu c_p / k_f$$ (2.31)

The exponential decay of $\left(T_w - T_b\right)$ is expressed as follows:

$$\left(T_w - T_b\right) = A\,\mathrm{e}^{-\lambda z^*}$$ (2.32)

where A and λ are arbitrary constants.

Differentiating equation (2.32) with respect to z^*:

$$\frac{\partial}{\partial z^*}\left(T_w - T_b\right) = -\lambda A e^{-\lambda z^*} = -\lambda\left(T_w - T_b\right)$$ (2.33)

Furthermore, in the fully-developed region $\partial T / \partial z^* = -\varphi \partial(T_w - T_b)/\partial z^*$. Therefore,

$$\frac{1}{\left(T_w - T_b\right)}\frac{\partial T}{\partial z^*} = \varphi\lambda$$ (2.34)

Noting that in the thermally fully-developed region, φ is not a function of z, and using X, Y, z^*, and equations (2.29) and (2.34), the following form of the dimensionless energy equation can be obtained [Patankar (1980); Kays and Crawford (1993)]:

$$\frac{\partial^2 \varphi}{\partial X^2} + \frac{\partial^2 \varphi}{\partial Y^2} + \varphi \lambda \frac{w}{w_{av}} = 0 \qquad (2.35)$$

Regarding the boundary conditions, on the duct wall, the temperature is T_w and $\varphi = 0$; at symmetry surfaces, $\nabla_\perp \varphi = 0$. Equation (2.35) and these boundary conditions set up an eigenvalue problem [Patankar (1980); Kays and Crawford (1993)]. An iterative method is used to solve it. First, following Sparrow and Patankar (1977) and Patankar (1980), to facilitate the iterative solution of this eigenvalue problem, a new dimensionless temperature is defined: $\varphi^* = \lambda \varphi$. In terms of φ^*, equation (2.35) becomes:

$$\frac{\partial^2 \varphi^*}{\partial X^2} + \frac{\partial^2 \varphi^*}{\partial Y^2} + \varphi^* \lambda \frac{w}{w_{av}} = 0 \qquad (2.36)$$

The dimensionless forms of the fin equations (2.11) and (2.12) are, respectively, the following:

$$\Omega \frac{\partial^2 \varphi^*}{\partial \Xi^2} = -\left.\frac{\partial \varphi^*}{\partial Y}\right|_u + \left.\frac{\partial \varphi^*}{\partial Y}\right|_l \qquad (2.37)$$

$$\frac{\Omega}{2} \frac{\partial^2 \varphi^*}{\partial \Xi^2} = \frac{\partial \varphi^*}{\partial Y} \qquad (2.38)$$

Only one combination of the eigenvalue λ and the corresponding dependent variable φ^* (the eigenfunction) satisfy these equations. First, the fluid flow problem is solved (W distribution is computed). Then, the aforementioned combination of λ and φ^* is found using the following iterative procedure [Patankar (1980)]:

1. Guess an initial φ^* field, calculate φ_b^*, and then obtain $\lambda = 1 / \varphi_b^*$;

2. Solve equations (2.36) to (2.38) and obtain φ^*; and then use this solution to obtain the corresponding value of the dimensionless bulk temperature:

$$\varphi_b^* = \frac{\int W \varphi^* \partial A_{c-s}}{\int W \partial A_{c-s}};$$

3. Knowing φ_b^*, obtain a new value for λ:

$$\lambda = 1/\varphi_b^* ;$$

4. Replace the old value of λ in equation (2.36) with the new one;

5. Return to step 2 until convergence.

Once convergence has been reached, the φ field can be retrieved using $\varphi = \varphi^* / \lambda$. The temperature field T can, in turn, be retrieved by specifying the wall and the bulk temperature in equation (2.29): the bulk temperature is a function of the position in the z direction, which, in turn, needs to be specified.

The average heat transfer coefficient is defined as follows: $h_{av} = \dfrac{q_w^{'} / Peri_{wetted}}{(T_w - T_b)}$. Then, the average Nusselt number is:

$$Nu_{av}^T = \frac{h_{av} D_h}{k_f} = \frac{D_h / Peri_{wetted}}{\dfrac{(T_w - T_b)}{q_w^{'} / k_f}} \qquad (2.39)$$

where the superscript T refers to the current boundary condition.

By performing an energy balance on a slice of the duct, in the context of the assumptions stated earlier, it can be established that $q_w^{'} = \dot{m} c_p \dfrac{\partial T_b}{\partial z}$ [Kays and Crawford (1993)], and equation (2.39) becomes:

$$Nu_{av}^T = \frac{\dot{m} c_p}{k_f (T_w - T_b)} \frac{\partial T_b}{\partial z} \frac{D_h}{Peri_{wetted}} \qquad (2.40)$$

However,

$$\frac{\partial T_b}{\partial z} = \frac{k_f}{\rho c_p w_{av} D_h^2} \frac{\partial T_b}{\partial z^*} \qquad (2.41)$$

Furthermore, $\dfrac{\partial T_b}{\partial z^*} = \varphi_b \lambda (T_w - T_b)$ and $\dot{m} = \rho w_{av} A_{c-s}$. Thus,

$$Nu_{av}^T = \frac{A_{c-s}}{Peri_{wetted} D_h} \lambda \varphi_b \qquad (2.42)$$

Finally, using the definition of the hydraulic diameter, the following convenient expression for the Nusselt number for the constant wall temperature thermal boundary condition is found:

$$Nu_{av}^T = \frac{\lambda \varphi_b}{4} \qquad (2.43)$$

2.2.2.3 Summary

Table 2.2 presents a summary of the dimensionless governing equations for the problems of interest.

Table 2.2 Summary of the dimensionless governing equations

Fluid flow	$\dfrac{\partial^2 W}{\partial X^2} + \dfrac{\partial^2 W}{\partial Y^2} + 1 = 0$
Energy equation with H boundary condition	$\dfrac{\partial^2 \theta}{\partial X^2} + \dfrac{\partial^2 \theta}{\partial Y^2} + 4 \dfrac{w}{w_{av}} \dfrac{D_h}{Peri_{wetted}} = 0$
Fin	$\Omega \dfrac{\partial^2 \theta}{\partial \Xi^2} = -\dfrac{\partial \theta}{\partial Y}\bigg|_u + \dfrac{\partial \theta}{\partial Y}\bigg|_l$
Energy equation with T boundary condition	$\dfrac{\partial^2 \varphi^*}{\partial X^2} + \dfrac{\partial^2 \varphi^*}{\partial Y^2} + \varphi^* \lambda \dfrac{w}{w_{av}} = 0$
Fin	$\Omega \dfrac{\partial^2 \varphi^*}{\partial \Xi^2} = -\dfrac{\partial \varphi^*}{\partial Y}\bigg|_u + \dfrac{\partial \varphi^*}{\partial Y}\bigg|_l$

These governing equations, subject to the corresponding boundary conditions discussed earlier, are solved using the numerical methods described in the following chapter.

Chapter 3. Overview of Numerical Methods

The two numerical methods that were used to solve the governing equations described in the previous chapter are presented in this chapter. They are a control volume finite difference method (CVFDM) and a control volume finite element method (CVFEM). In addition, a one-dimensional version of the CVFDM is described for the solution of the equation that governs quasi one-dimensional heat conduction in the fin. The formulation of the CVFDM is based on rectangular control volumes: thus, it is specially suited for the solution of problems involving the plate-fin rectangular ducts. In the CVFEM, the domain discretization is based on three-node triangular elements. Thus, it is very well suited for the solution of problems involving the triangular plate-fin ducts and also the internally finned ducts of circular cross-section. Here, it should be noted that the problems involving the rectangular plate-fin ducts could also be solved using the CVFEM, but it computationally less expensive, in terms of both storage and time, to solve such problems using the CVFDM.

3.1 GENERAL FORM OF THE GOVERNING EQUATIONS

The fully-developed fluid flow and heat transfer problems of interest are governed by partial differential equations that are akin to those that govern steady, two-dimensional, heat conduction or diffusion phenomena. The full details of these governing equations were presented in the previous chapter. With reference to the Cartesian coordinate system (x,y), these equations can be cast in the following general form [Patankar (1980)]:

$$\frac{\partial}{\partial x}\left(\Gamma_\phi \frac{\partial \phi}{\partial x}\right) + \frac{\partial}{\partial y}\left(\Gamma_\phi \frac{\partial \phi}{\partial y}\right) + S_\phi = 0 \qquad (3.1)$$

In this equation, ϕ is a general scalar dependent variable, Γ_ϕ is the corresponding diffusion coefficient, and S_ϕ is the appropriate volumetric generation rate, or source term. The CVFDM and CVFEM described in the following sections of this chapter are formulated to solve this equation subject to appropriate boundary conditions.

3.2   CONTROL VOLUME FINITE DIFFERENCE METHOD

The control volume finite difference method (CVFDM) presented in this section is based on the work of Patankar (1980). Its formulation involves the following four steps:

1. Discretization of the calculation domain into rectangular control volumes, nodes, and grid lines;

2. Prescription of appropriate interpolation functions for the dependent variable, diffusion coefficient, and source term;

3. Derivation of discretized equations, which are algebraic approximations of integral conservation equations applied to the rectangular control volumes;

4. Prescription of a procedure to solve the discretized equations.

3.2.1   Domain Discretization

The domain of interest is first discretized into a grid of rectangular control volumes following the so-called "*Practice B*" of Patankar (1980), where the control volume boundaries are first placed, and then the nodes are placed midway between the control volume boundaries. This domain discretion is schematically presented in figure 3.1.
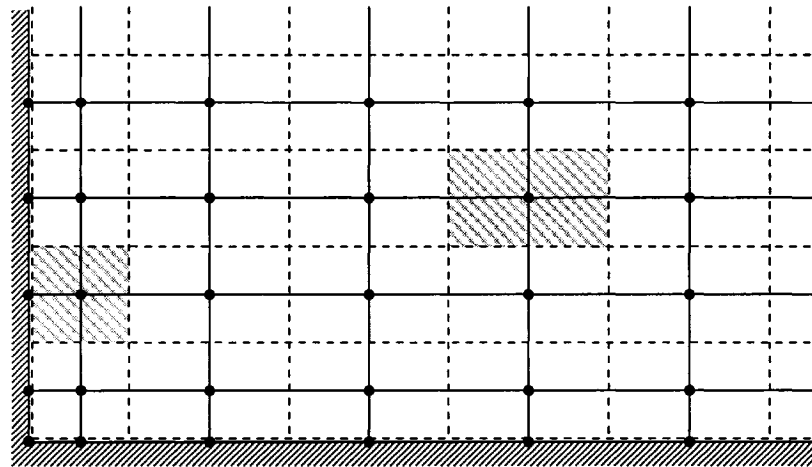
Figure 3.1 A Cartesian calculation domain and its discretization into rectangular control volumes, nodes, and grid lines

3.2.2 Profile Assumptions and Discretized Equations

The discretized equations are obtained by deriving algebraic approximations to an integral conservation equation applied to rectangular control volumes of unit depth in the z direction. With reference to the control volume and notation shown in figure 3.2, this integral conservation equation is approximated as follows:

$$\left(\Gamma_\phi \frac{\partial \phi}{\partial x}\right)_e \Delta y - \left(\Gamma_\phi \frac{\partial \phi}{\partial x}\right)_w \Delta y + \left(\Gamma_\phi \frac{\partial \phi}{\partial y}\right)_n \Delta x - \left(\Gamma_\phi \frac{\partial \phi}{\partial y}\right)_s \Delta x + \int_{CV} S_\phi dA = 0 \qquad (3.2)$$
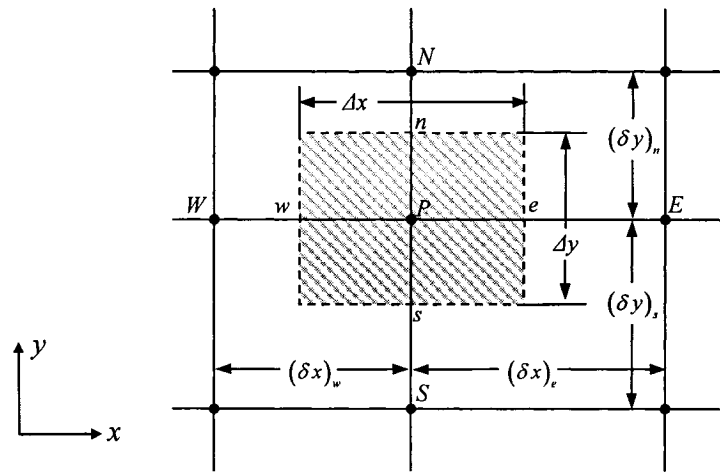
Figure 3.2 An internal control volume for the CVFDM
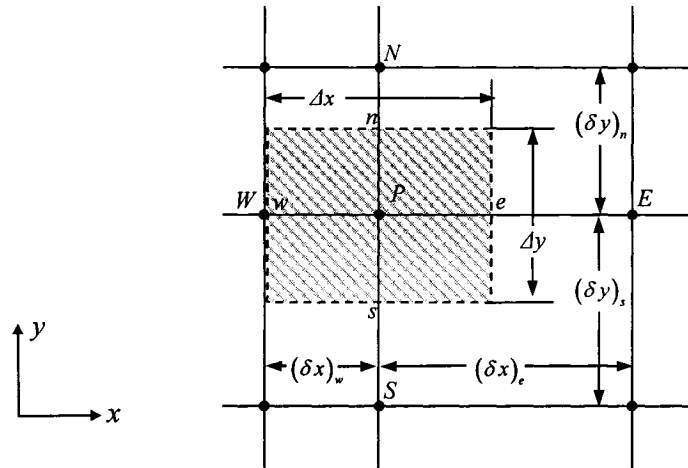
Figure 3.3 A control volume adjacent to a boundary for the CVFDM

In order to evaluate algebraic approximations to the derivatives and the integral in equation (3.2), profile assumptions (or interpolation functions) must be prescribed for the dependent variable, the diffusion coefficient, and the source term. Following Patankar (1980), the source term is first linearized, if required, as follows: $S_\phi = S_C + S_P \phi_P$. Then, in the integration of this term in equation (3.2), the nodal values of S_C, S_P, and ϕ_P are assumed to prevail over the corresponding control volumes. For the approximation of the derivatives of ϕ at the faces of the control volume, it is assumed to vary in a piecewise-linear manner along the grid lines between adjacent nodes. Again following Patankar (1980), a locally one-dimensional resistance analogy is used along the grid lines to interpolate the adjacent nodal values of the diffusion coefficient, Γ_ϕ, and obtain its values at the locations e, w, n, and s (see figures 3.2 and 3.3).

Using the above-mentioned profile assumptions, equation (3.2) can be approximated by:

$$(\Gamma_\phi)_e \frac{(\phi_E - \phi_P)}{(\delta x)_e} \Delta y - (\Gamma_\phi)_w \frac{(\phi_P - \phi_W)}{(\delta x)_w} \Delta y +$$
$$(\Gamma_\phi)_n \frac{(\phi_N - \phi_P)}{(\delta x)_n} \Delta x - (\Gamma_\phi)_s \frac{(\phi_P - \phi_S)}{(\delta x)_s} \Delta x + (S_C + S_P \phi_P)\Delta x \Delta y = 0$$

(3.3)

Equation (3.3) can be rearranged in the following convenient form:

$$a_P \phi_P = a_E \phi_E + a_W \phi_W + a_N \phi_N + a_S \phi_S + b$$

(3.4)

where

$$a_E = \frac{(\Gamma_\phi)_e \Delta y}{(\delta x)_e}$$

(3.5)

$$a_W = \frac{(\Gamma_\phi)_w \Delta y}{(\delta x)_w}$$

(3.6)

$$a_N = \frac{(\Gamma_\phi)_n \Delta x}{(\delta y)_n}$$

(3.7)

$$a_S = \frac{(\Gamma_\phi)_s \Delta x}{(\delta y)_s}$$

(3.8)

$$b = S_C \Delta x \Delta y \qquad (3.9)$$

$$a_P = a_E + a_W + a_N + a_S - S_P \Delta x \Delta y \qquad (3.10)$$

The product $\Delta x \Delta y$ is the volume of the control volume with unit depth.

3.2.2.1   Discretized equations for internal nodes

Equation (3.4) is represented in the following compact form for control volumes around the internal nodes in the calculation domain:

$$a_i \phi_i = \sum_n a_n \phi_n + b_i \qquad (3.11)$$

where the summation is taken over the n neighbour nodes (four in this case) of node i.

3.2.2.2   Discretized equations for boundary nodes

For nodes that lie on a boundary of the calculation domain, either the value of the dependent variable is given, as in equation 3.12, or the boundary is a symmetry plane.

$$\phi_i = \phi_{specified} \qquad (3.12)$$

In the latter case, a higher-order (quadratic) interpolation is used to satisfy the requirement of zero gradient of ϕ normal to symmetry boundaries, and equation (3.11) is modified accordingly. Full details of this treatment are available in Baliga and Atabaki (2006), so they are not repeated here.

At the boundaries adjacent to fins, the discretized equations presented are solved conjointly with another set of discretized equations for the quasi one-dimensional heat conduction in the fin. The derivation of those equations is presented in section 3.4. The overall steps for solving this conjugate problem are presented in section 3.5.

3.3   CONTROL VOLUME FINITE ELEMENT METHOD

The control volume finite element method (CVFEM) presented in this chapter is primarily based on the works of Baliga and Patankar (1980, 1988), LeDain-Muir and Baliga (1986), and Baliga and Atabaki (2006). The formulation of this CVFEM involves the following five steps:

1. Discretization of the calculation domain first into three-node triangular elements and then into polygonal control volumes;

2. Prescription of appropriate element-based interpolation (or shape) functions for the dependent variables;

3. Derivation of discretized equations, which are algebraic approximations of integral conservation equations, applied to the polygonal control volumes;

4. An element-by-element compilation of the discretized equations;

5. Prescription of a procedure to solve the discretized equations.

3.3.1   Domain Discretization

The calculation domains are first discretized into three-node triangular elements, as shown in figure 3.4. Then, the centroid of each triangular element is joined to the midpoints of the three element sides. Collectively, this procedure creates a polygonal control volume around each node in the domain: three such control volumes are shown as shaded areas in figure 3.5. The solid lines in figure 3.5 represent the elements boundaries and the dashed lines represent the faces of the polygonal control volumes. With this method, the curved boundary lines are represented by piecewise linear curves.

The choice of triangular elements is appropriate here as the proposed CVFEM is intended for the solution of problems involving triangular plate-fin ducts and internally finned ducts with circular cross-section (taking advantage of symmetry planes, the calculation domains for such ducts can be limited to pie-shaped portions of the cross-section). The calculation domains for such ducts do not lend themselves to discretization using quadrilateral elements.
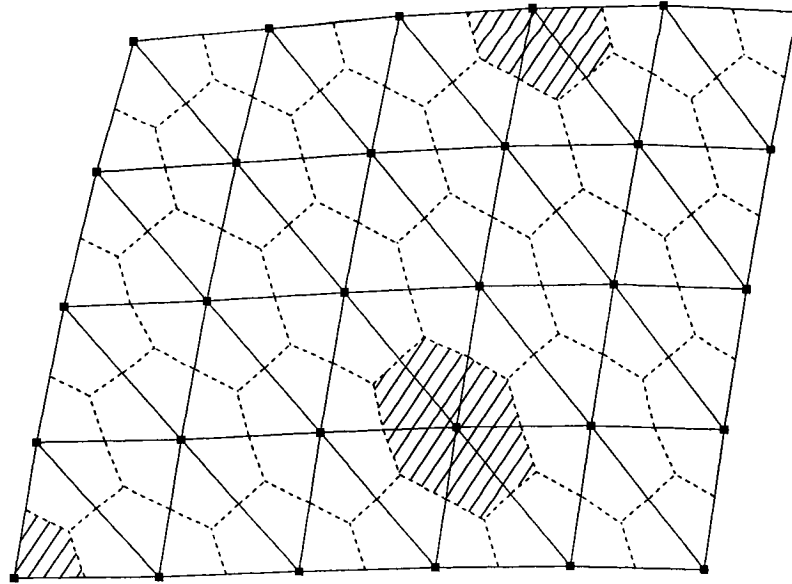
Figure 3.4 An irregularly shaped calculation domain and its discretization into three-node triangular elements and polygonal control volumes

3.3.2   Integral Conservation Equation for a Control Volume

Consider a typical node i, as shown in figure 3.5. An integral formulation corresponding to equation (3.1) can be obtained by applying the conservation principle for ϕ over the control volume surrounding such nodes in the calculation domain.

(a)   (b)   (c)
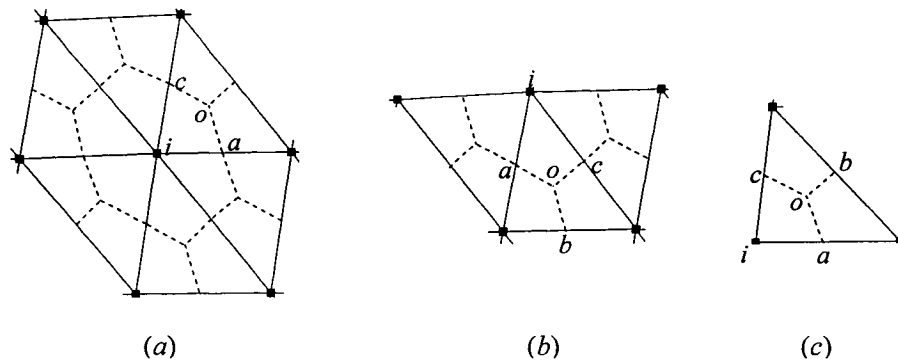
Figure 3.5 Details of the discretization in figure 3.4 and related nomenclature: (a) an internal node; (b) a boundary node with three associated elements; (c) a boundary node with one associated element

The resulting integral conservation equation can be expressed as follows:

$$\left[\int_a^o \mathbf{J} \cdot \mathbf{n} \, ds + \int_o^c \mathbf{J} \cdot \mathbf{n} \, ds - \int_{aoc} S_\phi d\vartheta \right]$$

$$+ \left[\text{similar contribution from other elements associated with node } i \right] \qquad (3.13)$$

$$+ \left[\text{boundary contributions, if applicable} \right] = 0$$

where **n** is a unit outward vector normal to the differential area element ds, and **J** is the diffusion flux of ϕ:

$$\mathbf{J} = -\Gamma_\phi \nabla \phi \qquad (3.14)$$

Equation (3.13) emphasizes that it can be assembled using an element-by-element procedure.

3.3.3   Interpolation Functions

The derivation of an algebraic approximation of equation (3.13) requires the specification of the interpolation functions for the source term, the diffusion coefficient, and the dependent variable, in every triangular element.

In each triangular element, the centroidal value of the diffusion coefficient, Γ_ϕ, is assumed to prevail. The source term is linearized, if needed, and expressed as follows [Patankar (1980)]:

$$S_\phi = S_c + S_p \phi \qquad (3.15)$$

In the integrals involving this source term, in each triangular element, the nodal values of S_C, S_P, and ϕ are assumed to prevail over the corresponding portions of the associated polygonal control volumes.

In each triangular element, the scalar dependent variable ϕ is interpolated linearly from its value at the three nodes that define an element:

$$\phi = Ax + By + C \qquad (3.16)$$

The constants A, B and C are uniquely determined in terms of the x, y coordinates of the three nodes (see figure 3.6) and their corresponding ϕ values:

$$A = [(y_2 - y_3)\phi_1 + (y_3 - y_1)\phi_2 + (y_1 - y_2)\phi_3] / DET \qquad (3.17)$$

$$B = [(x_3 - x_2)\phi_1 + (x_1 - x_3)\phi_2 + (x_2 - x_1)\phi_3]/DET \qquad (3.18)$$

$$C = [(x_2 y_3 - x_3 y_2)\phi_1 + (x_3 y_1 - x_1 y_3)\phi_2 + (x_1 y_2 - x_2 y_1)\phi_3]/DET \qquad (3.19)$$

where

$$DET = x_1 y_2 + x_2 y_3 + x_3 y_1 - y_1 x_2 - y_2 x_3 - y_3 x_1 \qquad (3.20)$$
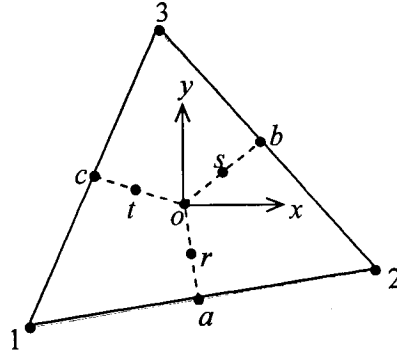
Figure 3.6 A typical three-node triangular element, the related nomenclature, and the local coordinate system (x,y)

3.3.4   Discretized Equations

The discretized equations are obtained by deriving algebraic approximations to the element contributions to the integral conservation equation (3.13), and assembling these contributions appropriately using an element-by-element procedure. Algebraic approximations of the boundary contributions are also derived and added up to the assembled element contributions, if needed. The following derivation refers to the node 1 of the element 123 shown in figure 3.6.

In each element, the diffusion flux **J** is expressed in terms of its components in the x and y directions:

$$\mathbf{J} = J_x \mathbf{i} + J_y \mathbf{j} = \left(-\Gamma_\phi \frac{\partial \phi}{\partial x}\right)\mathbf{i} + \left(-\Gamma_\phi \frac{\partial \phi}{\partial y}\right)\mathbf{j} \qquad (3.21)$$

where **i** and **j** are unit vectors in the x and y directions, respectively.

The interpolation function for the dependent variable is used to approximate J_x and J_y:

$$J_x = -A\Gamma_\phi, \qquad J_y = -B\Gamma_\phi \qquad (3.22)$$

These expressions, with reference to the element in figure 3.6, are used to approximate the integrals that represent the diffusion transport of ϕ in equation (3.13):

$$\int_a^o \mathbf{J} \cdot \mathbf{n} ds = \left(A\Gamma_\phi\right) y_a - \left(B\Gamma_\phi\right) x_a \qquad (3.23)$$

$$\int_o^c \mathbf{J} \cdot \mathbf{n} ds = -\left(A\Gamma_\phi\right) y_c + \left(B\Gamma_\phi\right) x_c \qquad (3.24)$$

The integral involving the source term is expressed as follows:

$$\int_{aoc} S_\phi d\vartheta = \frac{A_e}{3} S_c + \frac{A_e}{3} S_p \phi_1 \qquad (3.25)$$

where A_e is the area of the element 1-2-3:

$$A_e = \frac{|DET|}{2} \qquad (3.26)$$

with DET given by equation (3.20).

Substituting equations (3.17) and (3.18) into equations (3.23) and (3.24), and adding up equations (3.23)-(3.25), the total contribution of the element 1-2-3 to the conservation equation for the control volume surrounding node 1 is obtained. This total element contribution can be compactly expressed as follows [Baliga and Patankar (1988)]:

$$\int_a^o \mathbf{J} \cdot \mathbf{n} ds + \int_o^c \mathbf{J} \cdot \mathbf{n} ds - \int_{aoc} S_\phi d\vartheta = C_1 \phi_1 + C_2 \phi_2 + C_3 \phi_3 + B_1 \qquad (3.27)$$

where

$$C_1 = \frac{\Gamma_\phi}{DET}\left[(y_a - y_c)(y_2 - y_3) + (x_a - x_c)(x_2 - x_3)\right] - \frac{A_e}{3} S_p \qquad (3.28)$$

$$C_2 = \frac{\Gamma_\phi}{DET}\left[(y_a - y_c)(y_3 - y_1) + (x_a - x_c)(x_3 - x_1)\right] \qquad (3.29)$$

$$C_3 = \frac{\Gamma_\phi}{DET}\left[(y_a - y_c)(y_1 - y_2) + (x_a - x_c)(x_1 - x_2)\right] \qquad (3.30)$$

$$B_1 = -\frac{A_e}{3} S_c \qquad (3.31)$$

3.3.4.1 Discretized equations for internal nodes

Equation (3.27) accounts for the contribution of a single element to the integral conservation equation for the control volume surrounding node *I*. Such contributions from all elements associated with any internal node, *i*, are assembled appropriately, using an element-by-element procedure, to obtain the complete discretized equation. Such discretized equations for the internal nodes in the calculation domain can be expressed compactly as follows:

$$a_i \phi_i = \sum_n a_n \phi_n + b_i \qquad (3.32)$$

where the summation is taken over the *n* neighbour nodes of node *i*.

3.3.4.2 Discretization equations for boundary nodes

If the nodes lie on a boundary of the calculation domain, either the value of the dependent variable is given, as in equation (3.33), or the boundary is a symmetry plane.

$$\phi_i = \phi_{specified} \qquad (3.33)$$

In the latter case, no special boundary modifications are needed, and equation (3.32), obtained from only the assembly of the aforementioned element contributions, applies.

3.3.5 Solution of the Discretized Equations

Here again, the discretized equations derived for the CVFEM are solved conjointly with those of the fin. This solution procedure is presented in section 3.5.

3.4 CONTROL VOLUME FINITE DIFFERENCE METHOD FOR THE FIN

For the conjugate problem of heat conduction in the fin, the quasi one-dimensional model presented in section 2.1.3.4 is solved using a one-dimensional control volume finite difference method (CVFDM) akin to the one presented in section 3.2 for the solution of the thermofluid problem for rectangular plate-fin ducts. The formulation of this one-dimensional CVFDM involves the same four steps as those given in section 3.2.

3.4.1   Domain Discretization

The domain discretization scheme used for the fin depends on the duct shape. For the rectangular plate-fin ducts, the control volumes in the fluid flow region are rectangular and the nodes are placed midways between these control volume boundaries. Since the energy balance between the fin and the fluid domain is performed on a control volume basis, the faces of the corresponding adjacent control volumes must match: so for the rectangular plate-fin ducts, the domain discretization for the fin must follow "*Practice B*" of Patankar (1980). For the triangular plate-fin ducts and the internally finned circular ducts, the CVFEM is used, and the nodes in the fin are placed at the center of adjacent control-volume faces along the fin-fluid interface. Therefore, for these triangular and circular ducts, the domain discretization in the fins must follow "*Practice A*" of Patankar (1980). These fin domain discretizations are presented in figure 3.7.

(a)

Triangular duct   Circular duct

(b)
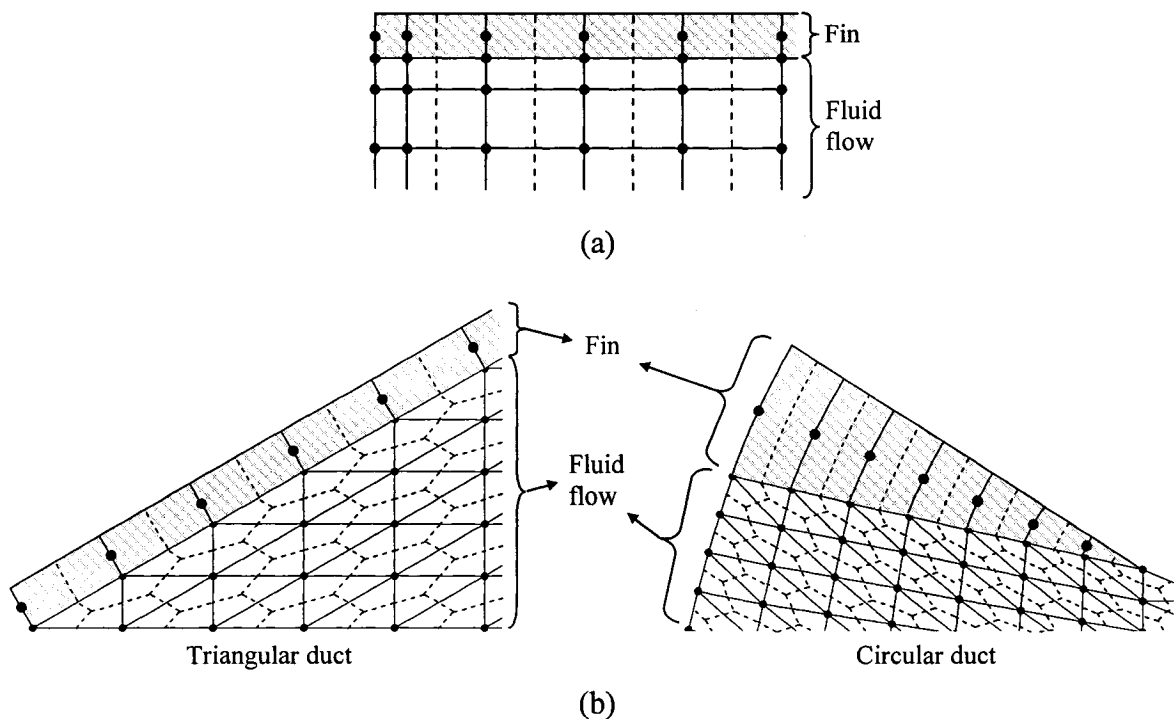
Figure 3.7 Fin domain discretization schemes (shaded regions) for (a) the rectangular plate-fin ducts and (b) the triangular plate-fin ducts and the internally finned ducts of circular cross-section

3.4.2 Profile Assumptions and Discretized Equations

The discretized equations for the fin are obtained by deriving algebraic approximations to the integral conservation equation applied to the control volumes of unit depth in the z direction (see figures 3.7 and 3.8). With reference to figure 3.8, equation (2.24) is integrated over the control volume of unit-depth and expressed as follows (here, $\eta = y$):

$$\left[\left(\Omega\frac{\partial\phi}{\partial\xi}\right)_e - \left(\Omega\frac{\partial\phi}{\partial\xi}\right)_w\right] = \int\limits_w^e\left(\frac{\partial\phi}{\partial\eta}\right)_u d\xi + \int\limits_w^e\left(\frac{\partial\phi}{\partial\eta}\right)_l d\xi \qquad (3.34)$$
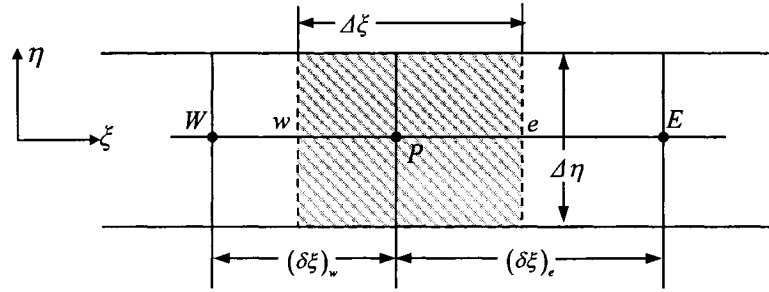
Figure 3.8 An internal control volume for the one-dimensional CVFDM

(a)   (b)
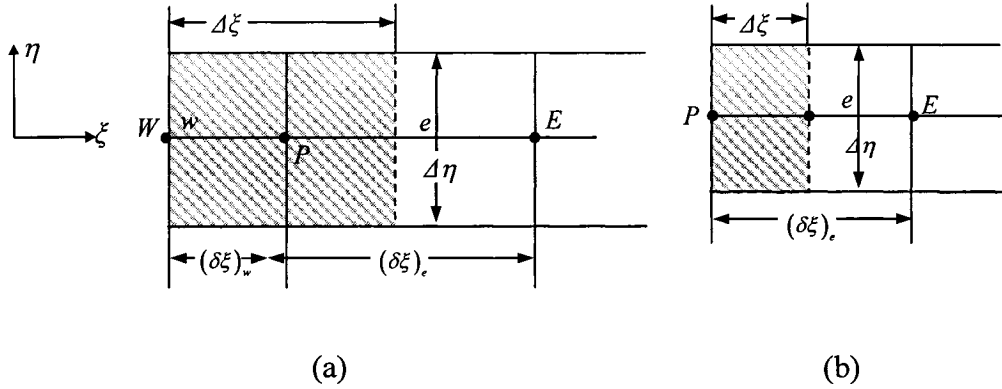
Figure 3.9 A fin control volume adjacent to a boundary for (a) Practice B and (b) Practice A

In order to evaluate the derivatives and the integrals in equation (3.34), assumptions must again be made regarding the profiles of the dependent variable, diffusion coefficient, and source terms inside the control volume. For the source term, the value at the node prevails over the control volume. The resistance analogy is used to interpolate the values of the diffusion coefficient at adjacent nodes [Patankar (1980)]. The derivatives of the

dependent variable at the faces of the control volumes are obtained by using piecewise-linear interpolation along grid lines between adjacent nodes.

Using these above-mentioned profile assumptions (interpolation functions), equation 3.34) is approximated as follows:

$$\Omega_e \frac{(\phi_E - \phi_P)}{(\delta\xi)_e} \Delta\eta - \Omega_w \frac{(\phi_P - \phi_W)}{(\delta\xi)_w} \Delta\eta + \overline{S}\Delta\xi\Delta\eta = 0 \tag{3.35}$$

Equation (3.35) can be rearranged in the following convenient form:

$$a_P \phi_P = a_E \phi_E + a_W \phi_W + b \tag{3.36}$$

where

$$a_E = \frac{\Omega_e \Delta\eta}{(\delta\xi)_e} \tag{3.37}$$

$$a_W = \frac{\Omega_w \Delta\eta}{(\delta\xi)_w} \tag{3.38}$$

$$b = \overline{S}\Delta\xi\Delta\eta \tag{3.39}$$

$$a_P = a_E + a_W \tag{3.40}$$

Here, $\overline{S}\Delta\xi\Delta\eta$ is the algebraic approximation to the right-hand side of equation (3.34).

3.4.2.1   Discretized equations for internal nodes

Equation (3.36) for the internal nodes in the fin can be expressed compactly as follows:

$$a_i \phi_i = a_{i+1}\phi_{i+1} + a_{i-1}\phi_{i-1} + b_i \tag{3.41}$$

3.4.2.2   Discretized equations for boundary nodes

If the value of the dependent variable is fixed at a boundary node, i, the discretized equation for that node becomes:

$$\phi_i = \phi_{specified} \tag{3.42}$$

3.5   SOLUTION TO THE DISCRETIZED EQUATIONS

The discretized equations derived in sections 3.2 to 3.4 were solved using the following iterative procedure:

1. Guess all unknown values of the dependent variables in the fluid flow and in the fin calculation domains;

2. Calculate the coefficients in the linearized forms of the discretized equations in the fluid flow region using the currently available values of the dependent variables;

3. Solve the resulting set of linear algebraic equations for the fluid flow;

4. Compute the heat fluxes on the upper and lower surfaces of the fin, and calculate the $\overline{S}\Delta\xi\Delta\eta$ terms in the discretized fin equations;

5. Calculate the coefficients in the linearized forms of the discretized fin equations, using the currently available values of the dependent variables;

6. Solve the resulting set of linear algebraic equations for the temperature distribution in the fin;

7. Repeat steps 2 to 6 until convergence.

The set of linear algebraic equations in steps 3 are solved using a line-Gauss-Seidel method with block correction to accelerate convergence [Patankar (1980)]. In this method and also for the solution of the linearized forms of the discretized fin equations, the tridiagonal matrix algorithm (TDMA) is used. For full details of this method, the reader is referred to the work of Sebben and Baliga (1995).

3.6   CALCULATION DOMAINS

For each of the three families of ducts considered in this work, the presence of symmetry and/or skew symmetry planes allows the restriction of the calculation domain to only one side of each of these planes. Advantage is taken of the feature of the problems of interest to decrease the number of nodes required for a desired grid density. Once the solution has been obtained for one side of these planes, it can be used, if desired, to construct it on the other side of the planes. Figure 3.10 presents the calculation domains for the three

families of ducts considered in this work. The types of grid used for each of these ducts are presented in the following subsections of this section.

For the rectangular and triangular plate-fin ducts, the calculation domain is limited to one quarter of the duct cross-sectional area between two similar fins, taking advantage of the presence of two symmetry planes for the rectangular duct, and the symmetry and the skew-symmetry planes for the triangular duct. For the circular duct with n_{fin} internal fins, there are $2n_{fin}$ symmetry planes and only a pie-like portion of the duct cross-section, with an angle of π / n_{fin}, is considered.

(a)

(b)

(c)
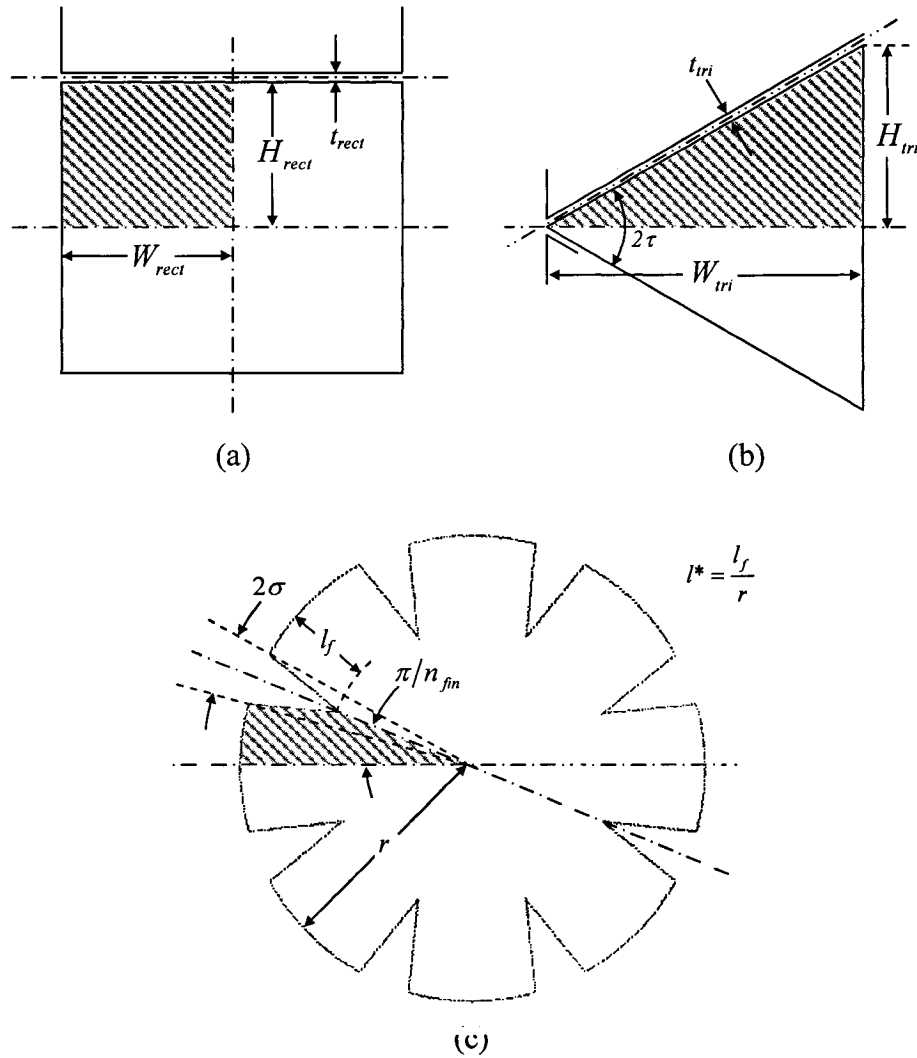
Figure 3.10 The calculation domains (indicated by shaded regions) for (a) the rectangular plate-fin ducts, (b) the triangular plate-fin ducts, and (c) the internally finned circular ducts

3.6.1 Grid for the Rectangular Plate-Fin Ducts

For the rectangular plate-fin ducts, the shaded region of figure 3.10 (a) is discretized using a uniform Type-B rectangular grid. The resulting node arrangement is presented in figure 3.11. The appropriate number of nodes in both the i_x and the i_y directions is determined in the validation of the fluid flow and heat transfer models presented in section 5.1.1.1.
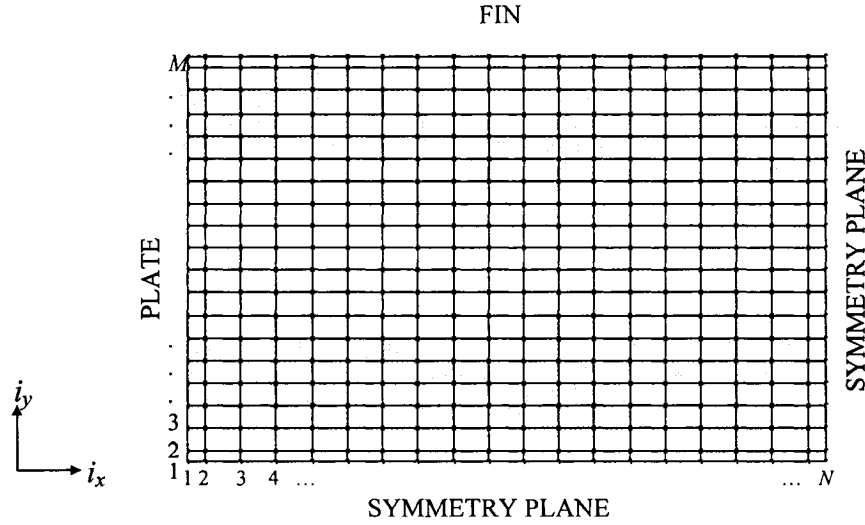
Figure 3.11 Type-B grid and nodes for the rectangular plate-fin ducts

3.6.2 Grid for the Triangular Plate-Fin Ducts

For the triangular plate-fin ducts, the shaded region of figure 3.10 (b) is discretized using three-node triangular elements, as presented in figure 3.12.
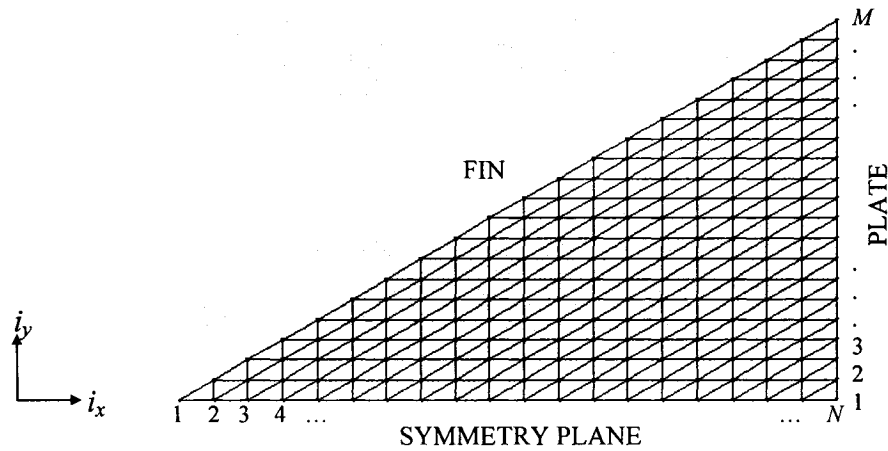
Figure 3.12 Grid and nodes for the triangular plate-fin ducts

The orientation of the triangular elements was chosen to fit the shape of the calculation domain, which has the fin boundary oriented from the bottom left to the top right corners. The number of nodes along the bottom and right boundaries in the i_x and the i_y directions, respectively, are the same; again, the appropriate number of these nodes is determined in the validation of the fluid flow and heat transfer models presented in section 5.1.1.1. The node spacing is uniform in the i_x and the i_y directions.

3.6.3   Grid for the Internally Finned Circular Ducts

For the internally finned circular ducts, two different grid configurations were used. The first configuration was designed and used for circular ducts with fins of triangular cross-section, as illustrated in figure 3.13. It was used for discretization of the calculation domains of the baseline cases, which were later optimized using the second grid configuration. Here, the angle π/n_{fin}, the radius r, the length of the fin l_f, and the base angle of the fin 2σ are specified by the user. The total number of nodes along the bottom symmetry plane, L+N, is also specified by the user. The value of L is obtained according to the following equation:

$$L = \text{Closest integer roundoff of} \left[(L + N)\frac{l_f}{r} \right]$$

N is then equal to $(L + N) - L$. The portion of the calculation domain beyond L+1 in the i_x direction is discretized into triangular elements with the longest side oriented in the top left to bottom right direction, matching the top symmetry plane; the number of nodes in the i_x and the i_y directions is the same and the node spacing is uniform. For the remaining portion of the domain, the nodes along the bottom, left, and top boundaries are initially spaced uniformly.
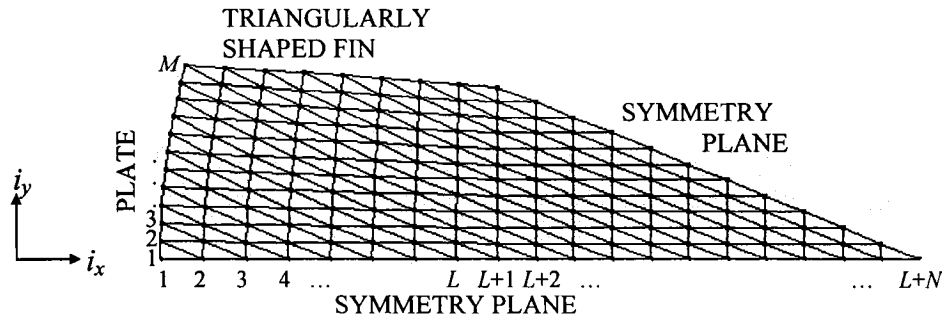
Figure 3.13 Grid and nodes for the circular ducts with triangular fins

The second configuration was used with circular ducts in which the shapes of the fins are dictated by the positions of the control points of nonuniform rational B splines (NURBS) used in the optimization procedure: the related details are elaborated in Chapter 4. An example of a computational domain for a circular duct with a control-point-shaped fin is presented in figure 3.14. For both of the aforementioned grid configurations, in the region of the calculation domain with nodes numbers less than $L+1$, the vertical positions of the nodes are first set uniformly between the top and bottom locations for each grid lines, and then the horizontal position of these same nodes are set to averages of the four surrounding nodes. This procedure creates nicely balanced domain discretizations.
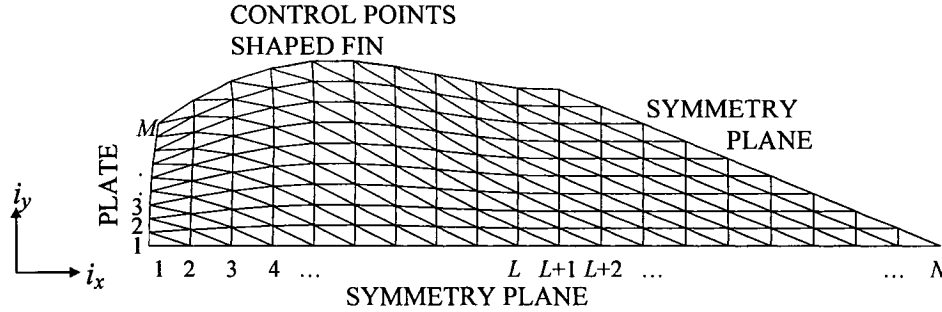
Figure 3.14 Grid and nodes for the circular duct with control-point-shaped fins

It should be noted that the above-mentioned grid generation procedure can create elements with large aspect ratios, or even overlapping elements, when the computational domain has a high angle, π / n_{fin} — that is, when the number of fins is below 4 or 5. Therefore, care should be taken to examine the generated grids, and make modifications, if needed.

Chapter 4. Optimization Methodology

In this chapter, the following topics are presented: an overview of several optimization techniques available in the literature; approximation of the fin shape using non-uniform rational B-Spline (NURS); formulation of the optimization problem, including the chosen objective functions and constraints; and the overall optimization algorithm.

4.1   OVERVIEW

The existence of optimization methods can be traced to the days of Newton, Lagrange, and Cauchy [Rao (1996)]. Research on optimization techniques intensified following the development of the simplex method by Dantzig (1947) for the solution of linear programming problems. Subsequently, most of the innovations in this area occurred in the 1950s and 1960s, with the apparition of various search methods: examples include random search methods; evolutionary algorithms; direct search methods involving the first and second derivatives of the design variables; and many variations and improvements of these methods [Converse (1970)].

Optimization problems, at the most general level, can be grouped into two main categories: static and dynamic problems [Denn (1969), Dixon (1972), Bryson (1999)]. Static problems are those where an optimal solution is obtained for a steady (non time-varying) system by means of a search method that manipulates a set of design variables. They are sometimes referred to as hill-climbing problems. Dynamic problems involve a changing optimal solution. Therefore, not only the optimal arrangement of the design variables at any particular instance is of interest, but also the variation of these variables between the various dynamic states of the system.

The optimization problem can be constrained or unconstrained [Rao (1996), Bouchard (1999)]. In unconstrained problems, the only goal is to optimize an objective, or cost, function: every value of the design variables is allowed. Such would be the case for a convex function that is known to have only one optimal state. In constrained problems, the objective is to find an optimal solution while satisfying to one or more constraints. These constraints can be equality constraints (for example, constant pumping power for

flow in a duct, or a constant fin volume), or inequality constraints (for example, minimizing the losses in a process while keeping the production above a certain value, or minimizing the drag on a wing while keeping its shape within design limits).

The problem to be optimized can also be linear or non-linear, regardless of whether it is static or dynamic. Linear optimization problems, which are often called linear programming problems, involve objective function(s) and constraint(s) that are all linearly dependent on the design variables. The solutions to such problems, with or without constraints, can be obtained by simply solving a set of coupled linear equations [Converse (1970)].

Non-linear optimization problems are more general, in the sense that the methods that are used to solve them also apply to linear problems. In these problems, the shapes of the objective and constraint functions are not known *a priori*. Most of the difficulties in solving a non-linear optimization problem arise from the unknown form, or shape, of the optimization function in the n-dimensional hyperspace spanned by the n design variables. For instance, there could be several local maxima surrounding a current state of the system, inhibiting the ability of the search algorithm to reach the hypothetical highest maximum, which could be located elsewhere.

In all static (linear or non-linear) optimization problems, the common goal is to find an optimal solution. For non-linear problems, this solution can only be reached by searching through the objective function hyperspace, while, if applicable, searching and satisfying one or more constraint function(s). This search process can be driven by direct search methods, where information from the previous solution is not used, or by guided search methods, where the search direction is intimately linked to the previous solution(s). Direct methods, often referred to as sectioning methods, include the following: the Monte Carlo method, which is based on random sampling; the Fibonacci and the Grid methods, which are based on "divide and conquer alike" schemes in the optimization space; and the Hooke and Jeeves method and the Davies, Swann and Campey method, where the search direction follows the so-called design-variables axis [Bouchard (1999)]. Guided methods are based on the evaluation of the first and, if applicable, the second derivatives

of the objective function(s). They are quite powerful, since trends in the variations of the objective and the constraint functions are extracted from knowledge of the previous states of the system. The more the information about the previous states of the system is used, the faster the optimal state can be reached. One must, however, keep in mind that the calculation of higher-order derivatives of the objective function(s) is computationally expensive, and should be used only if a significant advantage is to be gained from it.

Guided techniques in multi-dimensional problems are based on variations of a common theme: the computation of the gradient of the objective and/or the constraint function(s). The gradient of an objective function provides the direction of the steepest ascent toward increasing values of this function, ultimately reaching the maximum feasible objective function in that direction. Since the gradient vector represents the direction of steepest ascent, the negative of the gradient vector denotes the direction of steepest descent. As such, any method that makes use of the gradient vector can be expected to yield the maximum point faster than one that does not make use of this vector [Rao (1996)]. One drawback of these methods is that the gradient is a *local* property, and thus the path toward optimum is not necessarily the shortest one, but rather one that is tangent to the local gradient at each point along this path. For unconstrained problems, the simplest of such methods is the Cauchy method, where the step size is set and used to reach a minimum along the local gradient direction. Other examples of such methods include the Fletcher-Reeves, the Newton, the Marquardt, the quasi-Newton, the Davidon-Fletcher-Powell, and the Broyden-Fletcher-Goldfarb-Shanno methods [Rao (1996)]. All of these methods, however, necessitate an analytic objective function in order to obtain the optimal step length along the local gradient direction, without re-computing the function iteratively in that direction. In this work, since the objective functions of interest are based on the results of a numerical solution to a thermofluid problem, and are therefore not analytical, these methods can not be used. For constrained problems, a feasible search direction that points toward an increasing objective function while satisfying the constraint function must be resolved. Rosen's method uses the projection of the negative of the objective function gradient onto the constraint hyper-plane, ensuring that the direction is toward the optimal solution while satisfying multiple inequality constraints. However, the effectiveness of this method is confined primarily to problems in which the

constraints are all linear. The sequential quadratic programming method, which is also known as the projected Lagrangian method, is one of the most recently developed and perhaps one of the best methods in optimization. It is a generalization of Newton's method for unconstrained optimization, in that it maximizes (or minimizes) a quadratic model (sub-problem) of the problem. If the constraints are explicit functions of the design variables, it is possible to perform a transformation of the design variables such that the constraints are satisfied automatically, and the problem becomes an unconstrained one. The reader is referred to the work of Rao (1996) for more details on the methods outlined in this paragraph.

Another class of search methods is based on the genetic, or evolutionary, algorithm. It can be seen as a blend between direct and guided search techniques: akin to guided methods, the search direction is not chosen arbitrarily, and the possible movement and step sizes are restricted, as in the case of direct methods. It searches for the optimum by mimicking evolutionary principles and chromosomal processing observed in natural genetics: reproduction, crossover, and mutation toward an improved state until the optimal state is reached.

Most of the recently proposed search techniques in optimization are variations of the evolution algorithm, which are also known as *metaheuristic* methods [Onwubolu and Babu (2004)]. Among these, the self-organizing migrating algorithm is a more efficient variation of the genetic algorithm — the difference being that it considers the mutation of a group of individuals (solutions) rather than that of a single individual (solution). The memetic algorithm, developed in the late 1980s, includes the concept of competition between individuals to promote genetic improvement. Scatter search and path relinking algorithms are evolutionary methods that construct solutions by combining others by means of strategic design that exploit the knowledge of the problem considered. Other evolution algorithms include the ant colony optimization algorithm, the differential evolution algorithm, and the discrete particle swarm optimization algorithm. The reader is referred to the work of Onwubolu and Babu (2004) for more information on these techniques.

The optimization problem of interest in this work is a static problem, since the optimal duct shape is to be obtained only once for each duct. It is also non-linear, since the objective function(s) and the constraint(s) vary in a very non-linear manner with changes of each of the design variables considered. Moreover, the problem is one of constrained optimization, since an objective function is optimized while satisfying an equality constraint. Considering these characteristics of the problem, the search method adopted here is based on the gradient method with an adaptive step size. This method was chosen not only because of the nature of the problem, but also for efficiency reasons, since the computation of the objective and constraint functions requires the solution to the direct thermofluid problem, as described in Chapters 2 and 3. With the chosen method, the increase in computational cost associated with the calculation of the gradient is more than offset by the reductions in these costs provided by the knowledge of optimal direction and the use of an adaptive step size.

4.2   APPROXIMATION OF THE FIN SHAPE

In this section, the method used to approximate, control, and modify the shape of the fin is presented. This method applies to the internal fins present in the circular duct only; in the case of the rectangular and triangular plate-fin ducts, only fins of straight plate-like shape are considered.

In order to be able to modify the shape of the fin, the interface between the fin and the fluid region of the ducts must first be described mathematically, in order to attain control over its shape. A polynomial representation of this interface is often inefficient or unsuitable, as discussed in the work of Piegl and Tiller (1997), for the following reasons:

- A high-degree polynomial is required when there are many constraints: a n-1 degree polynomial is needed to pass through n points;

- A high-degree polynomial is required to accurately fit some complex shapes;

- High-degree polynomials are inefficient to process and can lead to numerical instabilities;

- Single-segment curves are not well-suited to interactive shape design.

In order to overcome such barriers, a common practice is to split the curve into multiple *piecewise polynomials* or *piecewise rational* curves. By setting rules that ensure continuity and smoothness at the location where these curves meet (such as continuity of second and third derivatives), it becomes possible, by controlling the location of these meeting points, to shape the curve as desired, with a greater control on local portions of the curve. Such curves are called *splines*. They are the mathematical equivalent of long flexible strips of wood used by ship builders, which are also called splines. On a spline curve, the locations in space where the piecewise curves meet are called the control points. The list of all the control points for a curve can be conveniently expressed in vector form as follows:

$$\mathbf{P} = \{\mathbf{P}_1, \mathbf{P}_2, ..., \mathbf{P}_i, ..., \mathbf{P}_n\} \tag{4.1}$$

The polygon whose summits are the control points is called the *control polygon* (see Figure 4.1). A useful and more commonly used variation of a spline curve is a B-spline curve, for which each control point is associated with a *basis function*. These basis functions define the portion of the curve that is affected by each control point. By setting the basis functions of each control point adequately, it becomes possible — by moving the location of a given control point — to modify the shape of the curve locally (that is, only the portion of the curve close to the control point is affected). On a B-spline curve, each control point affects a user defined portion of the curve and they all have the same weights.

4.2.1 The NURBS Curve

A generalised version of a B-spline is the so-called non-uniform rational B-spline (NURBS) curve. A NURBS curve is defined by its order, a set of weighted control points, and a knot vector. The primary difference in comparison to a B-spline is the weighting of the control points, which makes NURBS curves rational. One of the advantages of NURBS curves (and B-spline curves in general) is that they offer a way to

represent arbitrary shapes while maintaining mathematical exactness and resolution independence. Among their useful properties are the following:

- They can represent virtually any desired shape, from points, straight lines, and polylines, to conic sections (circles, ellipses, parabolas, and hyperbolas), to free-form curves with arbitrary shapes;

- They provide great control over the shape of the curve. The set of control points and knots, which guide the shape of the curve, can be directly manipulated to control its smoothness and curvature;

- They can represent very complex shapes with remarkably little data.

NURBS curves evolve along one parametric direction: u. The knot vector is a sequence of parameter values that determine where and how the control points affect the NURBS curve along its parametric length. It is defined as follows:

$$\mathbf{U} = \{u_1, u_2, ..., u_i, ..., u_n\} \qquad 0 \le u \le 1 \qquad (4.2)$$

The number of knots is always equal to the number of control points, minus the curve degree, plus one. The values of the knot vector must be in ascending order, so, for example, [0, 0, ¼, ½, ¾, 1] is valid while [0, ¼, ¾, ½, 1, 1] is not. Even if only the ratios of the difference between the knot values matter, their values are kept inclusively between 0 and 1 to be consistent with the parametric representation of the curve, which is also kept between 0 and 1. Further, no knot value is allowed to have so many duplicates that it occurs more times than the degree of the curve. Knot vectors are generally placed into one of three categories: uniform, open uniform, or non-uniform (the most general case). In a uniform knot vector, the knot spacing between every knot is uniform and $t_{i+1} - t_i = $ constant, $\forall i$. An open uniform knot vector is a uniform knot vector, but with k equal knots at both ends:

$$
\begin{aligned}
t_i &= t_1, & i \le k \\
t_{i+1} - t_i &= \text{constant}, & k \le i < n+2 \\
t_i &= t_{k+(n+1)}, & i \le n+2
\end{aligned}
\qquad (4.3)
$$

Here, the fact of having multiple identical knots at both ends of the vector ensures that the two extremities of the curves coincide with the two control points at both ends of the control polygon and tangentially to it. A non-uniform knot vector is the general case, the only constraint being $t_{i+1} \leq t_i$, $\forall i$. This type of knot vector is the most flexible, since every control point can act on a custom portion of the curve, and by adding identical knots at a given parametric location on the curve, discontinuities can be obtained. For most applications with a smooth continuous curve with no sharp corners, a uniform knot vector is adequate, since controlling the shape with the number and position of the control points and their weights can fit almost any shape. This type of knot vector is implemented to approximate the fin shape in this study.

The *order* of a NURBS curve defines the number of nearby control points that influence any given control point. The curve is represented mathematically by a polynomial having a degree one less than the order of the curve. Hence, second-order curves (which are represented by linear polynomials) are called linear curves and fourth-order curves are called cubic curves. The number of control points must be greater than or equal to the order of the curve. In practice, fourth order (cubic) NURBS curves are sufficient to fit almost any shapes and are the most commonly used. A pth degree NURBS curve is defined by:

$$\mathbf{C}(u) = \frac{\sum_{i=0}^{n} N_{i,p}(u) w_i \mathbf{P}_i}{\sum_{i=0}^{n} N_{i,p}(u) w_i} \qquad 0 \leq u \leq 1 \qquad (4.4)$$

where the $\{\mathbf{P}_i\}$ are the control points (forming a *control polygon*), the $\{w_i\}$ are the weights associated with each control points, and the $\{N_{i,p}(u)\}$ are the pth degree B-spline basis functions associated with each control point and defined on the following open uniform knot vector:

$$\mathbf{U} = \{\underbrace{a,...,a}_{p+1}, u_{p+1},...,u_{m-p-1}, \underbrace{b,...,b}_{p+1}\} \qquad (4.5)$$

where $a = 0$, $b = 1$ and $w_i > 0$ for all i. Again, the fact that the knot situated at both ends of the vector are repeated $p + 1$ times ensures that the end points of the curve falls on the end control points tangentially to the two end portions of the control polygon. Figure 4.1 shows the impact of varying the weight of a control point, while all other control points have their weights fixed at 1.0, on an open uniform third degree NURBS curve.
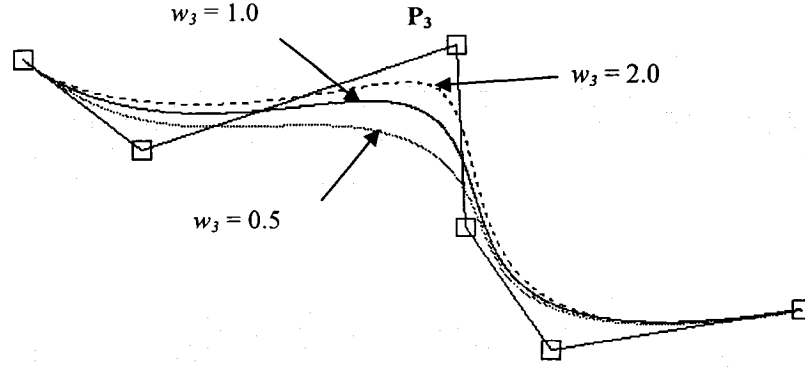
Figure 4.1 A cubic NURBS curve with w_3 varying

Setting:

$$R_{i,p}(u) = \frac{N_{i,p}(u)w_i}{\sum_{j=0}^{n} N_{j,p}(u)w_j}$$ (4.6)

allows the rewriting of equation (4.4) in the following form:

$$\mathbf{C}(u) = \sum_{i=0}^{n} R_{i,p}(u)\mathbf{P}_i$$ (4.7)

where the $\{R_{i,p}(u)\}$ are the *rational basis functions* of the NURBS curve. They are rational functions on $u \in [0,1]$. In principle, the basis functions can be defined in any way, as long as they provide the information about the type and range of influence of each control point on the curve. The next section describes the basis functions implemented in this work.

4.2.2   The Basis Functions

There are a number of ways of prescribing the basis functions needed to set the effect of each control point on the curve. Here, a recurrence formula is used, because it is convenient for computer implementation. Thus, the basis functions are defined as follows:

$$N_{i,0}(u) = \begin{cases} 0 & \text{if } u_i \leq u \leq u_{i+1} \\ 1 & \text{otherwise} \end{cases}$$

$$N_{i,p}(u) = \frac{u - u_i}{u_{i+p} - u_i} N_{i,p-1}(u) + \frac{u_{i+p+1} - u}{u_{i+p+1} - u_{i+1}} N_{i+1,p-1}(u)$$

(4.8)

Note:

- $N_{i,0}(u)$ is a step function equal to 1 on the half open interval $u \in [u_i, u_{i+1}]$;

- For $p > 0$, $N_{i,p}(u)$ is a linear combination of two $(p-1)$-degree basis functions;

- $N_{i,p}(u)$ are piecewise polynomials defined on the entire range of the parametric variable u;

- The computation of a set of basis function requires specification of the knot vector **U** and the degree p.

Figure 4.2 presents an example of the 3rd degree basis functions ($p = 3$) for 6 control points associated with the knot vector $\mathbf{U} = \{0,0,0,0,\frac{1}{3},\frac{2}{3},1,1,1,1\}$. Note that for every value of $u \in [0,1]$, the sum of every basis functions always sums up to 1, which means that every point on the curve is influenced by the corresponding fraction of the surrounding control points. Also, since there are multiple knots for the two end-control points, the basis functions $N_{1,3}$ and $N_{6,3}$ ensure that only the end control points influence the curve at its two ends.
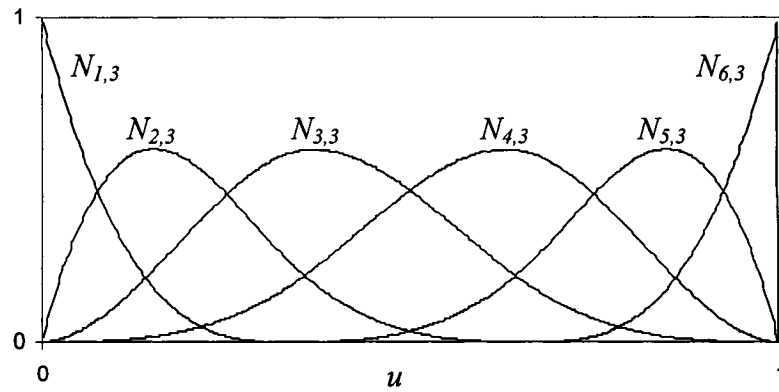
Figure 4.2 Basis functions for an open, uniform, rational curve
with 6 control points

In the next subsection, the application of a NURBS curve to obtain a conveniently modifiable fin shape is presented.

4.2.3   Approximation of the Fin Shape by a NURBS Curve

Figure 4.3 shows the control polygon and its associated open uniform rational curve that is used to approximate the shape of the fin, using 6 control points for the demonstration.
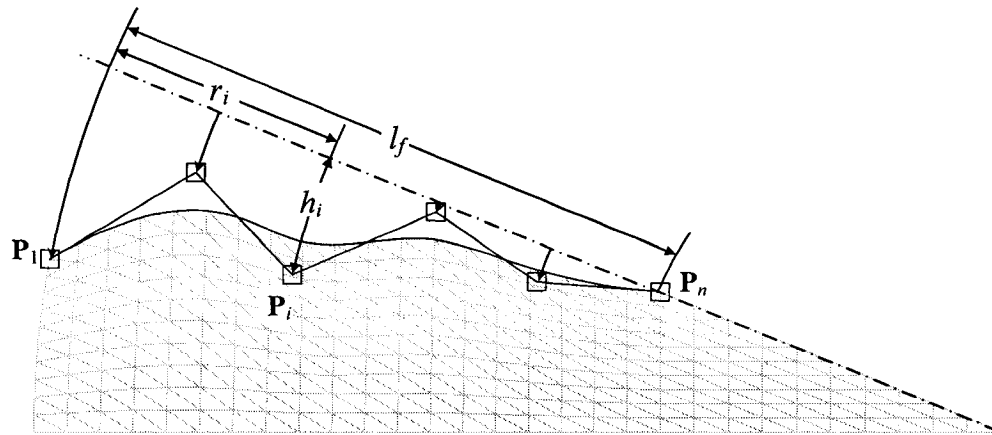
Figure 4.3 Control points approximation of the fin shape
for the circular duct

The position of each control point P_i is defined by its axial distance from the wall of the circular duct side, r_i, and its elevation above the fin central symmetry axis, h_i. The first control point, P_1, is situated directly on the duct wall and its height h_1 sets the fin width at

the base. The last control point, $\mathbf{P}_n$, is situated directly on the fin central symmetry axis so that its height h_n is 0 and its radial position, r_n, is equal to the length of the fin, l_f. The radial positions of the remaining interior control points, r_i, are set uniformly within the fin length, and the choice of their heights, h_i, depend on the desired fin shape.

Once the position of each control point is set, the NURBS curve is computed, and the position of each grid point (node) along the fin is interpolated equidistantly on the NURBS curve. Then, the nodes on the duct wall are also interpolated equidistantly between the first control point and the bottom symmetry plane. The position of the remaining interior nodes is interpolated between the surrounding bounding nodes (see section 3.6.4 for some more details).

It is possible, by changing the following parameters, to modify the shape of the fin according to the configuration presented in Figure 4.3:

- The number of control points, n;

- The height of the first $(n-1)$ control points, h_i;

- The radial position of the nth control point, r_n;

- The weight, w_i, of each control point.

The radial positions of the interior control points are kept equidistant because the same effect can be obtained by changing the quantity and/or the individual weight of the control points. The parameters presented above are the ones that are left available to the optimization algorithm, in order to search for an optimal shape, as presented in the following sections.

The number of control points that were used to optimize the fin shape in the demonstration problems is discussed and validated in Chapter 5.

4.3   FORMULATION OF THE OPTIMIZATION PROBLEM

All optimization problems have in common the goal of finding the values of a list of variables that will optimize a certain objective function. As was stated in section 4.1, the

problems to be optimized in this study are static, non-linear, multivariable problems with two different objective functions (specific to the two different thermal boundary conditions of interest), subject to an equality constraint. The mathematical formulation of such an optimization problem can be expressed in the following form:

$$\text{Find} \quad \mathbf{X} = \begin{Bmatrix} x_1 \\ x_2 \\ \vdots \\ x_n \end{Bmatrix} \quad \text{which maximizes } f(\mathbf{X}) \tag{4.9}$$

subject to the constraint:

$$g(\mathbf{X}) = \text{constant} \tag{4.10}$$

where $\mathbf{X}$ is a n-dimensional vector called the *design vector* containing the design variables, $f(\mathbf{X})$ is the *objective function*, and $g(\mathbf{X})$ is the *equality constraint function*.

Other classes of optimization problems can involve multiple objective functions, the minimization instead of the maximization of the objective function(s), multiple equality constraints, one or more inequality constraints, or the absence of any constraint (which becomes an unconstrained optimization problem). These variations of the optimization problem are not pertinent to this work and the interested reader is referred to the work of Rao (1996) for complementary information.

The designs variables, the objective functions, and the equality constraint considered in this study are presented concisely in the following subsections.

4.3.1   The Design Variables

In the process of designing an engineering system or component, there is a set of quantities that can be viewed as variables. Given a set of constraints and conditions, these quantities take on specific values that define the characteristics of the system or component in question. In general, certain quantities are fixed and can not be changed. The other quantities are treated as variables in the design process and are called the

design variables: x_i, where $i = 1, 2, ..., n$, and n is the total number of variables. These design variables are collectively represented as a design vector:

$$X = \begin{Bmatrix} x_1 \\ x_2 \\ \vdots \\ x_n \end{Bmatrix}$$

(4.11)

There are no restrictions on the number or type of variables. If an n-dimensional space with each coordinate axis representing a design variable is considered, the space is called the *design space*, and each point X in it is called a *design point* and represents each possible or impossible solution to the optimization problem. The solution to the optimization problem is expressed as an optimal value of the design vector X. For a rectangular plate-fin duct of fixed width, for example, the design variables could be the thickness of the fin and the height of the duct (see Figure 3.10), and the corresponding design vector would be:

$$X = \begin{Bmatrix} t_{rect} \\ H_{rect} \end{Bmatrix}$$

(4.12)

For an internally finned circular duct, the design variables could be the height of the first $(n-1)$ control points above the fin central axis, and the length of the fin for the nth control point ($l_f = r_n$, see Figure 4.3):

$$X = \begin{Bmatrix} h_1 \\ h_2 \\ \vdots \\ h_{n-1} \\ l_f \end{Bmatrix}$$

(4.13)

In most optimization problems, the dimensional inhomogeneity of the design variables leads to a situation of *non-Euclidian geometry* [Seireg and Rodriguez (1997)]. An example would be the optimization of the fluid bearing problem, where the design variables may be the shaft speed with magnitudes of the order of 10^3, and fluid viscosity

with magnitudes in the order of 10^{-6}. In such a case, if the variables are not properly scaled, the gradient (and thus the search direction) is distorted, and the convergence would be very slow, if not absent. In order to scale the design variables, a minimum and maximum value must be provided for each variable, and its value can only be inclusively within those two limits. They are set either by physical limits (for example, a length can not be lower than 0) or by structural integrity requirements (for example, a minimum thickness), and depend on the problem being optimized. Once the minimum and/or maximum limits are provided, the range between these two limits is scaled between 0 and 1. The transformation for this scaling is linear and is:

$$x_i^* = \left(x_{i\,max} - x_{i\,min} \right) x_i + x_{i\,min}$$

(4.14)

An example of such a scaling is presented in the following table.

Table 4.1 Example of scaling for a design variable

	x_i	x_i^*
Min	6.35E-05	0.000
Current	1.83E-03	0.478
Max	3.77E-03	1.000

Each variable in the design space is not allowed to take a value outside the range bounded by 0 and 1. If any variable in the next step in the optimization path is outside this allowed range, special care must be taken to ensure that the size and direction of the next step always lead back inside this domain. This special case of domain boundary treatment is elaborated further in section 4.4.3. This procedure is a way of indirectly taking into account the various physical constraints associated with each design variable.

The optimization algorithm only deals with non-dimensionalized design variables. Every time the algorithm needs to obtain the value of the objective function or the constraint function, the following procedure is used:

1. The dimensional versions of the design variables are computed with equation (4.14);

2. The direct thermofluid problem is solved using the CVFDM or CVFEM described in Chapter 3;

3. The objective function and the constraint function are computed using the solution from step 2;

4. The variables are nondimensionalized again, and the control is given back to the optimization algorithm.

4.3.2 Objective Functions

The goal of any design procedure is to find an acceptable or adequate design which satisfies the functional and other requirements of the problem in question. In general, there will be more than one acceptable design, and the best one must be chosen among them. Thus, a criterion has to be prescribed for comparing the different designs and choosing the best one. Such a criterion, with respect to which the design is to be optimized, is called the *objective function*. It is a function of the design variables and takes a finite value for each point in the design space. The choice of the objective function is governed by the nature of the problem. For instance, the objective is often taken as the minimization of weight in aircraft and aerospace design. In can also be the maximization of efficiency in a given mechanical or process design.

For the optimization problem studied here, the goal is to find the best plate-fin duct shape, or design, that provides the best thermal performance for a given operating condition. This thermal performance has to be maximized, and is thus the criterion with respect to which the optimal design is sought. As was stated earlier, two different thermal boundary conditions are considered in this work; thus, two distinct objective functions have to be defined and treated as two separate optimization problems. The expressions for the derivation of the objective function for the two thermal boundary conditions considered are now presented.

4.3.2.1 Objective function for the thermal boundary condition H: uniform heat input per unit axial length and uniform cross-sectional duct wall temperature

For this thermal boundary condition (of uniform heat input per unit axial length and uniform cross-sectional duct wall temperature), all temperature in a given cross section of the duct rises linearly with z, and q_w'' is constant everywhere. As a result, the average

heat transfer coefficient, $h_{av} = \dfrac{q_w{'}_{av} / Peri_{wetted}}{(T_w - T_b)}$, can only be increased by either:

decreasing the wetted perimeter; or decreasing $(T_w - T_b)$. In this sense, maximizing the average heat transfer coefficient is equivalent to minimizing $(T_w - T_b)$ — or, in other words, maximizing $1/(T_w - T_b)$. A dimensionless equivalent to this quantity must be obtained since the direct problem is solved in dimensionless form. The dimensionless bulk temperature is equal to:

$$\theta_b = \frac{(T_w - T_b)}{q_w' \Big/ k_f} \tag{4.15}$$

Since q_w' / k_f is constant throughout the duct, the objective stated above is equivalent to maximizing $q_w' / k_f / (T_w - T_b)$, or maximizing $1/\theta_b$. The average Nusselt number for this boundary condition is the following (see Chapter 2):

$$Nu_{av}^H = \frac{D_h / Peri_{wetted}}{\theta_b} \tag{4.16}$$

Thus, the objective function for this H thermal boundary condition is the following:

$$f^H(\mathbf{X}) = \frac{Nu_{av}^H}{D_H \Big/ Peri_{wetted}} \tag{4.17}$$

For a given duct shape subject to this thermal boundary condition, maximizing $f^H(\mathbf{X})$ leads to a duct shape that ensures the optimal thermal performance.

4.3.2.2 Objective function for the thermal boundary condition T: constant duct wall temperature

For this thermal boundary condition — constant duct wall temperature — the average heat flux at the wall and all temperature differences ($T_w - T$) in the fluid region decrease in exponentially along the duct axis in the thermally fully developed region. In this problem, the objective function is chosen to be $q'_w / (T_w - T_b)$, so that the optimal solution maximizes q'_w and minimizes ($T_w - T_b$). Using the definition of the average heat transfer coefficient, the Nusselt number can be expressed as follows (see Chapter 2):

$$Nu_{av}^T = \frac{D_H \Big/ Peri_{wetted}}{\dfrac{(T_w - T_b)}{q'_w / k_f}} \qquad (4.18)$$

Isolating $\dfrac{q'_w}{(T_w - T_b)}$ in equation (4.18):

$$\frac{q'_w}{(T_w - T_b)} = k_f \frac{Nu_{av}^T}{D_H \Big/ Peri_{wetted}} \qquad (4.19)$$

With the remaining terms on the right side of equation (4.19), an expression for the objective function for the T thermal boundary condition is obtained:

$$f^T(\mathbf{X}) = \frac{Nu_{av}^T}{D_H \Big/ Peri_{wetted}} \qquad (4.20)$$

k_f has been omitted from this objective function because it is constant and, therefore, has only a scaling effect on it and it does not change the location of the optimum for $f^T(\mathbf{X})$. For a given duct shape subject to this thermal boundary condition, maximizing $f^T(\mathbf{X})$ leads to a duct shape that ensures the optimal thermal performance.

Equations (4.17) and (4.20) are the objective functions for a single duct subject to the two different thermal boundary conditions considered. They are used conjointly with the appropriate constraint functions, which are presented in section 4.3.3. As dimensionless mathematical models are used in each case, the circular plate-fin duct shapes obtained by the optimization of the aforementioned objective functions are valid throughout the length of the ducts in the fully developed regions, regardless of the local bulk temperature.

For the rectangular and triangular ducts, the number of ducts in a unit height of the heat exchanger varies during the optimization process. The more duct-fin combinations are present in a unit height, the more heat can be transferred from the plates, and that must be taken into account in the objective functions. In sections 4.3.2.3 and 4.3.2.4, modified versions of the objective functions are presented, specific to rectangular and triangular plate-fin ducts, respectively.

4.3.2.3   Objective functions for the rectangular plate-fin duct

The maximization of the two objective functions given in the previous subsection is akin to the maximization of the heat transfer coefficient, h_{av}, for a single duct. For the case of rectangular plate-fin ducts, the number of ducts per unit height of the heat exchanger must be factored into the objective functions. The number of rectangular plate-fin duct combinations present in a unit height of the heat exchanger is:

$$n_{rect} = \frac{1}{\left(2H_{rect} + t_{rect}\right)} \tag{4.21}$$

where the 2 in the denominator accounts for the fact that the computational domain is limited to one quarter of the domain (half of the height by half of the length). The modified versions of the objective functions are obtained by multiplying equations (4.17) and (4.20) by equation (4.21). Thus, the resulting modified objective functions for the rectangular plate-fin ducts are the following:

$$f_{rect}^H(\mathbf{X}) = n_{rect} \cdot \frac{Nu_{av}^H}{D_H \big/ Peri_{wetted}} \tag{4.22}$$

$$f_{rect}^T(\mathbf{X}) = n_{rect} \cdot \frac{Nu_{av}^T}{D_H \big/ Peri_{wetted}} \tag{4.23}$$

4.3.2.4   Objective function for the triangular duct

For the triangular duct, the objective functions must also account for the total number of duct-fin combinations present in a unit height of heat exchanger. The component of the half-fin thickness t in the y direction is given by:

$$t_{tri\_y} = \frac{t_{tri}}{\cos\tau} \tag{4.24}$$

where τ is the half angle of the triangular duct (see Figure 3.10). The number of plate-fin ducts present in a unit height is then given by:

$$n_{tri} = \frac{1}{\left(2H_{tri} + t_{tri\_y}\right)} \tag{4.25}$$

The modified objective functions are obtained by multiplying equations (4.17) and (4.20) by equation (4.25). The resulting objective functions for the triangular duct are the following:

$$f_{tri}^H(\mathbf{X}) = n_{tri} \cdot \frac{Nu_{av}^H}{D_H \big/ Peri_{wetted}} \tag{4.26}$$

$$f_{tri}^T(\mathbf{X}) = n_{tri} \cdot \frac{Nu_{av}^T}{D_H \big/ Peri_{wetted}} \tag{4.27}$$

4.3.2.5   Objective function for the circular duct

For the circular duct, the number of ducts in a unit height of heat exchanger is invariant. Therefore, the objective functions are the following:

$$f_{circ}^{H}(\mathbf{X}) = \frac{Nu_{av}^{H}}{D_H \Big/ Peri_{wetted}}$$

(4.28)

$$f_{circ}^{T}(\mathbf{X}) = \frac{Nu_{av}^{T}}{D_H \Big/ Peri_{wetted}}$$

(4.29)

4.3.3   The Constraint Functions

In most practical problems, the design variables can not be chosen arbitrarily; rather, they have to satisfy certain specified functional and other requirements. The restrictions that must be satisfied for a certain design to be acceptable are called the *design constraints*.

In heat exchangers, the pumping power that provides the pressure needed to drive the flow through it is a crucial factor:

- Various pieces of equipment in the process rely on constant operating conditions such as flow rate and pressure distribution;

- Usually, an enhancement in thermal efficiency is desired but not at the expense of modifying the equipment that provides the fluid flow, such as fans and pumps. In other words, it is important to note that the overall efficiency of a process must also account for the total energy input.

Thus, in this work, the objective was chosen to be the following: identify a duct shape that represents the optimal thermal design for a given constant pumping power per unit length of duct. By doing so, nothing other than the thermal performance of the heat exchanger is affected in the optimizing procedure. The pumping power per unit length for the laminar fully-developed flows of interest can be expressed as follows:

$$pp = -\frac{dp}{dz} w_{av} A_{c-s}$$

(4.30)

where A_{c-s} is the total cross-sectional area of the duct(s) for the fluid flow. The constraint is that the pumping power per unit length, as given in equation (4.30), must remain constant and fixed at a constant value called pp_{target} for the solution to be acceptable. Knowing the desired pumping power per unit length provides an advantage

when choosing the appropriate constraint function. Figure 4.4 shows a function f(x) that is an inverse exponential function. In order to find the value of the x that produces a certain value of f(x) — in this case f(0.05) — three approach are possible: subtract the desired value from f(x) and use the Newton-Rhapson method to find the zero of the function; or do the same with the absolute value of this difference; or square the difference and use a gradient based method to find the zero. The last method of these three approaches is equivalent to the *least-square approximation method*. One desirable characteristic of this method is that the gradient of this function decreases continuously as the algorithm gets closer to the desired value of x; this, in turn, allows the use of a gradient-search method with a step size proportional to the gradient. Since the gradient keeps decreasing until it becomes null at the desired location, the step size also decreases continuously as the desired location is approached, akin to an adaptive step size.
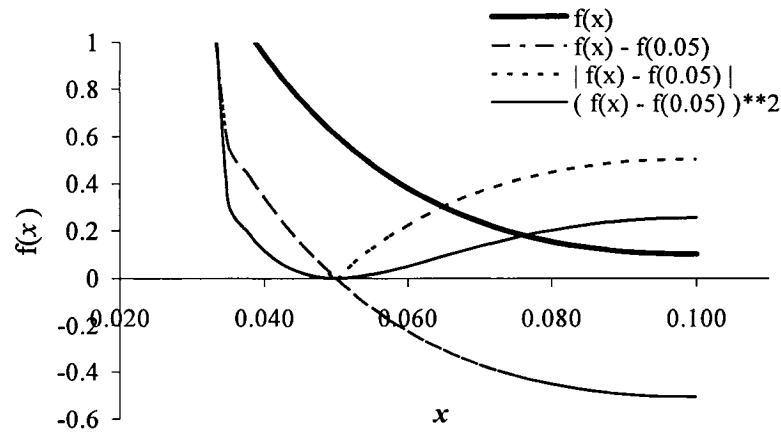
Figure 4.4 Choosing the appropriate objective function

Using the aforementioned least-square approximation, the constraint function can be expressed as follows:

$$g(\mathbf{X}) = \left(pp - pp_{target} \right)^2 \tag{4.31}$$

where pp is given by equation (4.30), and pp_{target} is the known, or desired, value of the pumping power per unit length of the duct. Thus,

$$g(\mathbf{X}) = \left(-\frac{dp}{dz} w_{av} A_{c-s} - pp_{target} \right)^2$$ (4.32)

$g(\mathbf{X})$ is a $(n-1)$-dimensional hyper-plane in the n-dimensional hyperspace spanned by the design variables. For a problem with two design variables (two-dimensional space), the constraint is a line. For a problem with three design variables, the constraint is a surface—curved or planar—located somewhere in that space, and so on. Regardless of the number of design variables, the optimum must lie on that hyper-plane in order to satisfy the constraint function.

The cross sectional area A_{c-s} in equation (4.32) depends on the problem being optimized. For the rectangular and the triangular ducts, the size of the duct is a design variable and the total number of ducts in a unit height of heat exchanger varies. As a result, specific constraints functions must be derived for each duct considered. They are presented in the following sub sections.

4.3.3.2   Constraint function for the rectangular duct

For the rectangular duct, a given height of plate-fin heat exchanger is composed of a stacked arrangement of consecutive ducts separated by fins. By varying the fin thickness and/or the height of each of the ducts, the total cross-sectional area for the flow in a unit height of the heat exchanger will vary also. Therefore, in order to force a given quantity of fluid through it, the pumping power must vary as well. Thus, the constraint of constant pumping power per unit length must take into account the presence of multiple consecutive plate-fin ducts per unit height of the heat exchanger. The number of such ducts present in a unit height is given by equation (4.21). The total cross-sectional area for fluid flow in a unit height of the heat exchanger, again considering that only one quarter of the cross section is taken as the computational domain, is given by the following expression:

$$A_{c-s} = 4 \left(W_{rect} \cdot H_{rect} \right) n_{rect}$$ (4.33)

Thus, the following constraint function is used for rectangular plate-fin ducts:

$$g_{rect}(\mathbf{X}) = \left(-\frac{dp}{dz} w_{av} 4 \left(W_{rect} \cdot H_{rect} \right) n_{rect} - pp_{target} \right)^2 = 0 \qquad (4.34)$$

4.3.3.3 Constraint function for the triangular duct

For the triangular duct, the same reasoning applies as for the rectangular duct, since the ducts are in essence the result of a zigzag-shaped fin placed between two plates. The total pumping power in a unit height of heat exchanger depends on the angle of the zigzag and the thickness of the fins. The number of plate-fin ducts present in a unit height is given by equation (4.25). The total cross-sectional area for flow in a unit height of the heat exchanger is given by the following expression:

$$A_{c-s} = \left(W_{tri} \cdot H_{tri} \right) n_{tri} \qquad (4.35)$$

Thus, the following constraint function is used for the triangular plate-fin ducts:

$$g_{tri}(\mathbf{X}) = \left(-\frac{dp}{dz} w_{av} \left(W_{tri} \cdot H_{tri} \right) n_{tri} - pp_{target} \right)^2 = 0 \qquad (4.36)$$

4.3.3.4 Constraint function for the circular duct

For the circular duct, the number of ducts in a unit height of heat exchanger is fixed: therefore, the total pumping power is only a fixed multiple of the pumping power for a single duct. Thus, the total number of ducts only has a scaling effect on the constrain function and does not change the location of the optimum. Thus, the constraint function for the circular plate-fin ducts is the following:

$$g_{circ}(\mathbf{X}) = \left(-\frac{dp}{dz} w_{av} A_{c-s} - pp_{target} \right)^2 = 0 \qquad (4.37)$$

where A_{c-s} is the cross sectional area for fluid flow in a single circular plate-fin duct.

4.4 OPTIMIZATION ALGORITHM

The proposed optimization algorithm is a variation of a simplified version of the Rosen's gradient projection method [Rao (1996)], which, in turn, is based on the more general class of gradient, or steepest descent, methods [Converse (1970), Dixon (1972), Pironneau (1994), Rao (1996), Bryson (1999), Mohammadi & Pironneau (2001)]. The

method is divided into two main parts: first, the satisfaction of the constraint function; and second, the optimization of the objective function. A distinction is made between these two parts because the corresponding search direction and step size are different. These two parts of the optimization algorithm are presented in sections 4.4.1 and 4.4.2. Then the domain boundary treatment used in cases where the next step is outside the design space is presented in section 4.4.3. Finally, the complete optimization algorithm is summarized section 4.4.4.

4.4.1 Searching for the Constraint

The initial point can be anywhere in the design space and, other than in rare cases, will not be located on the constraint hyper-plane (or constraint iso-plane). This means that before searching for the optimal design point, the constraint must be first satisfied by reaching the constraint hyper-plane. Only then is it possible to search for the optimum while staying on this hyper-plane. In that sense, the allowed design space becomes restricted to a $(n-1)$-dimensional hyper-plane located inside the n-dimensional design space, and can be visualized in Figure 4.5, where $n = 2$.
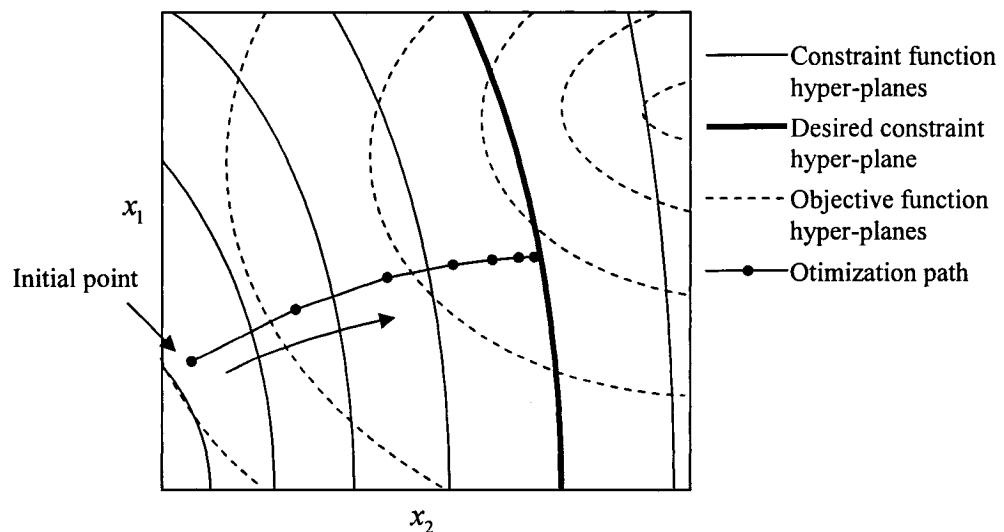
Figure 4.5 Path toward the desired constraint hyper-plane

As was stated in section 4.3.3, because of the fact that the constraint function is quadratic, the gradient decreases continuously toward the desired location, and the step size can be

set proportional to the gradient. The next step, or the design point following the current one, is defined as follows:

$$\mathbf{X}_{i+1} = \mathbf{X}_i + \lambda_i \mathbf{S}_i \qquad (4.38)$$

where $\mathbf{X}_i$ is the current design point, $\mathbf{X}_{i+1}$ is the next design point, $\mathbf{S}_i$ is the normalized search direction vector for the next design point, and λ_i it the associated step size. The gradient vector of a function, here the constraint function, is defined as:

$$\nabla g(\mathbf{X}_i) = \left[\frac{\partial g}{\partial x_1}, ..., \frac{\partial g}{\partial x_j}, ..., \frac{\partial g}{\partial x_n} \right] \qquad (4.39)$$

The norm of this vector is:

$$\left\| \nabla g(\mathbf{X}_i) \right\| = \left(\sum_{j=1}^{n} \left(\frac{\partial g}{\partial x_j} \right)^2 \right)^{\frac{1}{2}} \qquad (4.40)$$

Since the gradient is the direction of steepest ascent, its negative value must be used in order to get the direction of the steepest descent, since the constraint function is $\nabla g(\mathbf{X}_i) = 0$. The normalized gradient-based search direction is obtained with equations (4.39) and (4.40):

$$\mathbf{S}_i = -\frac{\nabla g(\mathbf{X}_i)}{\left\| \nabla g(\mathbf{X}_i) \right\|} \qquad (4.41)$$

The step size is set proportional to the norm (length of a vector) of the gradient normalized with the norm of the initial gradient, and scaled with a desired initial step size λ_{const}:

$$\lambda_i = \lambda_{const} \frac{\left\| \nabla g(\mathbf{X}_i) \right\|}{\left\| \nabla g(\mathbf{X}_1) \right\|} \qquad (4.42)$$

This approach makes it possible to start with a desired initial step size, then, for each step, the step size decreases proportionally to the gradient, which decrease as the constraint hyper-plane is approached. The resulting behaviour for this part of the

algorithm can be seen again in Figure 4.5: the search path gets closer and closer to the constant constraint hyper-plane until the following proximity criterion is satisfied:

$$g(\mathbf{X}_i) \leq \varepsilon_{const} \tag{4.43}$$

Once this criterion is satisfied, the design point is considered to have satisfied the constraint function, and the search direction can be set toward the optimum. This second part of the optimization algorithm is presented in the following section.

4.4.2   Searching for the Optimum

Once the constraint function is satisfied, efforts are directed towards finding the optimum. In order to obtain a search direction that allows an increase in the value of the objective function while at the same time satisfying constraint function, a projection of $\nabla f(\mathbf{X}_i)$ onto the constraint hyper-plane, which is normal to $\nabla g(\mathbf{X}_i)$, is applied. This projected vector is called $\nabla f_{proj}(\mathbf{X}_i)$, and is defined as:

$$\nabla f_{proj}(\mathbf{X}_i) = \mathbf{P} \nabla f(\mathbf{X}_i) \tag{4.44}$$

where $\mathbf{P}$ is the projection matrix, defined as:

$$\mathbf{P} = \mathbf{A}\left(\mathbf{A}^T \mathbf{A}\right)^{-1} \mathbf{A}^T \tag{4.45}$$

$\mathbf{A}$ in equation (4.45) is the basis that defines the constraint hyper-plane. This basis is a $(n-1) \times n$ matrix composed of the $(n-1)$ vectors which lie on the surface of the constraint hyper-plane. This projection matrix does not require the basis vectors to be orthogonal. Therefore, they are obtained from the vector normal to the hyper-plane, $\nabla g(\mathbf{X}_i)$, which equally defines the hyper-plane in question. If the components of this normal vector are taken to be individual vectors — each being in the direction of their corresponding design space axis — then the vector resulting from the subtraction of any of these component vectors will lie on the surface of the constraint hyper-plane, and, therefore, is a candidate for a basis vector. These $(n-1)$ basis vectors are given by the following equation:

$$V_j = \frac{\partial g}{\partial x_1}\mathbf{i}_{x_1} - \frac{\partial g}{\partial x_{j+1}}\mathbf{i}_{x_{j+1}} \qquad 1 \le j \le n-1 \qquad (4.46)$$

The basis matrix that is composed of these vectors is then defined as follows:

$$\mathbf{A} = \begin{bmatrix} \mathbf{V}_1 & \cdots & \mathbf{V}_j & \cdots & \mathbf{V}_{n-1} \end{bmatrix} \qquad (4.47)$$

This projection scheme is graphically presented in a convenient three-dimensional view ($n = 3$) in Figure 4.6.
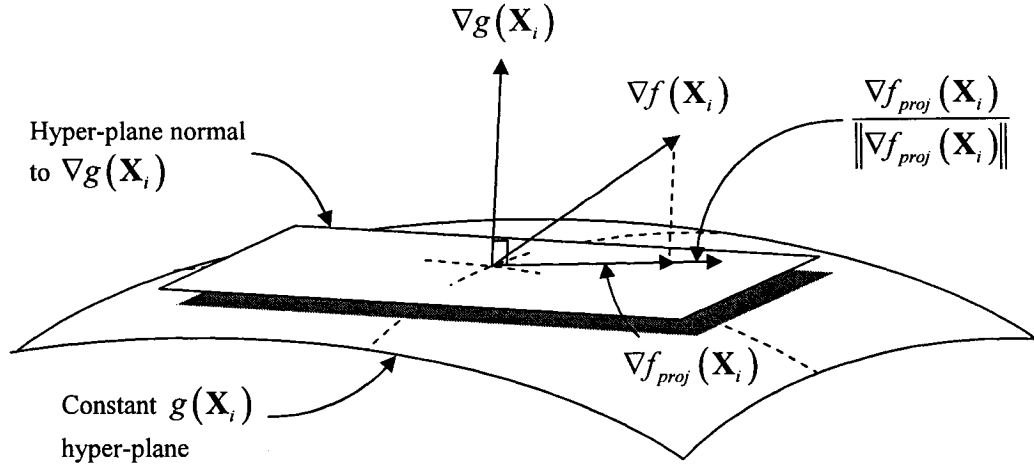
Figure 4.6 Projection of $\nabla f(\mathbf{X}_i)$ on the hyper-plane normal to $\nabla g(\mathbf{X}_i)$ for $n = 3$

Once the gradient vector has been projected on the constraint hyper-plane, its length is normalized and scaled to λ_{obj}. Therefore, the search direction is:

$$\mathbf{S}_i = \frac{\nabla f_{proj}(\mathbf{X}_i)}{\left\| \nabla f_{proj}(\mathbf{X}_i) \right\|} \qquad (4.48)$$

and the step size is:

$$\lambda_i = \lambda_{obj} \qquad (4.49)$$

The resulting search direction satisfies the constraint function (that is, the design point is located within the specified tolerance, ε_{const}, of the constraint hyper-plane), and it also guarantees an increase in the objective function at the next step or design point. Figure 4.7 shows the behaviour of a sample optimization path in a two-dimensional view, where the two main parts of the algorithm can be seen: first, the path is set toward the constraint hyper-plane; and once it is close enough to this constraint hyper-plane, it switches toward the optimum by performing the projection of the objective function gradient onto the hyper-plane.
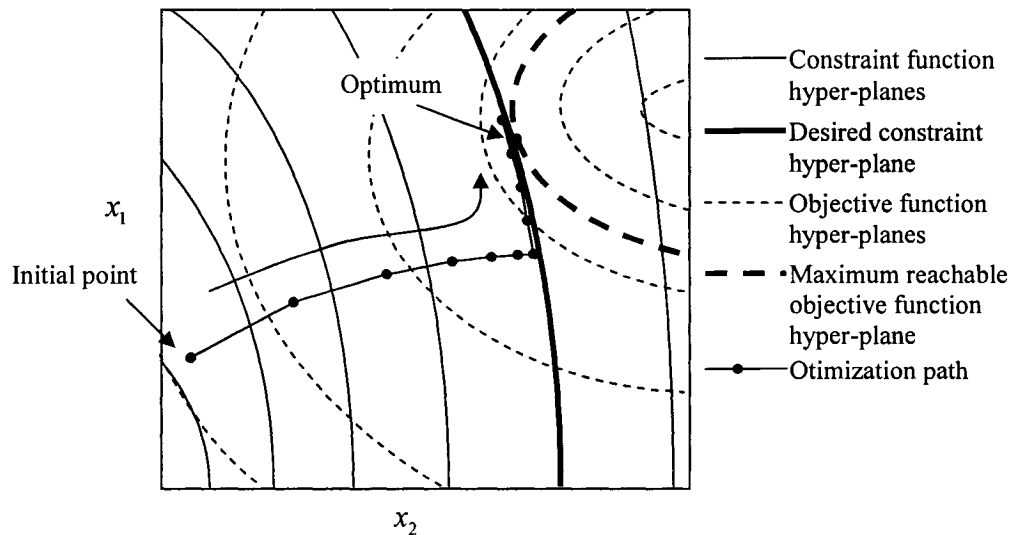
Figure 4.7 Path toward the optimum

4.4.3   Design-Space Boundary Treatment

The optimization path, as seen Figure 4.7, can sometimes lead outside the design space. This would be the case if the desired constraint hyper-plane were to be close to a limit, that is, $x_i = 0$ or 1, or if the initial point is close to such a limit. There is always a possibility of this situation occurring. Thus, it is important that the proposed optimization algorithm be able handle this situation adequately. If the next design point

falls outside the design space, it direction of the optimization path must be corrected so that this next design point lies within the design space. Moreover, the corrected direction must take into account the current state of the optimization procedure: that is, whether it is moving towards the constraint hyper-plane or towards the optimum.

If the current state of the optimization procedure is moving towards the constraint hyper-plane, the algorithm is navigating freely in the design space: that is, it is not following a constraint hyper-plane. Thus, if a design-space boundary is encountered, the step size, λ_{const}, is conserved, but the search direction, S_i, is projected onto the limiting hyper-plane being crossed $x_j = (0 \text{ or } 1)$ using equation (4.45), as follows:

$$S_{i\ corrected} = \frac{\mathbf{P} \cdot \mathbf{S}_i}{\|\mathbf{P} \cdot \mathbf{S}_i\|} \tag{4.50}$$

In this case, the vector needed to get the basis vectors in $\mathbf{A}$ has all of its components set to 0 except the component of the limiting hyper-plane being crossed.

If the current state of the optimizing procedure is moving toward the optimum, not only must the corrected vector be tangent to the limiting hyper-plane being crossed, but also it must lie on the constraint hyper-plane. This is achieved by first setting the components of S_i and $\nabla g(\mathbf{X}_i)$ normal to the limiting hyper-plane being crossed to 0. This has the effect of making these two vectors tangent to the limiting hyper-plane being crossed. Then, the tangent version of S_i is projected onto the hyper-plane normal to the tangent version of $\nabla g(\mathbf{X}_i)$, again using equation (4.45). This proposed design-space boundary treatment ensures that no matter what the current and the next design points are, the algorithm searches only inside the design space — thus, constraining the design variables within their individual allowable limits.

4.4.4   Proposed Optimization Algorithm

The proposed optimization algorithm first aims at satisfying equation (4.43) using the method outlined in section 4.4.1. Once this condition is satisfied, the algorithm moves

the design point in order to maximize the objective function, using the method outlined in section 4.4.2. The initial values for the step sizes and the tolerances are the following:

$$\lambda_{const} = 0.1$$
$$\lambda_{obj} = \frac{\lambda_{const}}{2}$$
$$\varepsilon_{const} = 0.02$$
$$\varepsilon_{final} = 10^{-5}$$

(4.51)

Up to this point, the tolerance, ε_{const}, and the reference step sizes, λ_{const} and λ_{obj}, remain constant. If the condition $f(\mathbf{X}_i) < f(\mathbf{X}_{i-1})$ has been satisfied four times in a row (that is, in four consecutive iterations), it is assumed that the optimum is somewhere in the vicinity of these last four design points. As a consequence, the step sizes λ_{const} and λ_{obj} are reduced by a factor of three, and the tolerance ε_{const} is reduced by a factor of five. This has the effect of searching more accurately in the region of the design space suspected to contain the optimum, and closer to the constraint hyper-plane. These reduction factors were chosen because in numerous preliminary computations they allowed the optimum to be reached in a relatively small number of iterations. This step-size and tolerance reduction process is repeated until the overall tolerance is satisfied, that is $\varepsilon_{const} \leq \varepsilon_{final}$: in this case, the algorithm has reached an acceptable solution. Every time the design point of the next iteration is determined to be outside the design space, that is, $0 < x_j > 1$ where $1 \leq j \leq n$, the design-space boundary treatment outlined in section 4.4.3 is used.

The overall optimization algorithm can be summarized by the following steps:

1. Start with an initial point $\mathbf{X}_1$, set the initial step sizes λ_{const} and λ_{obj}, and set the iteration number as 1;

2. Calculate the constraint function gradient $\nabla g(\mathbf{X}_i)$;

3. Test whether or not $g(\mathbf{X}_i) \leq \varepsilon_{const}$. If yes, the constraint function is satisfied and the search direction can be set toward the projected objective function gradient:

move to step 4. If no, the constraint is not satisfied and the search direction must be set toward the satisfaction of the constraint: go to step 6;

4. Calculate the objective function gradient $\nabla f(\mathbf{X}_i)$;

5. Calculate the basis $\mathbf{A}$ of the constraint hyper-plane defined by its normal vector, $\nabla g(\mathbf{X}_i)$, the projection matrix, $\mathbf{P} = \mathbf{A}(\mathbf{A}^T\mathbf{A})^{-1}\mathbf{A}^T$, and the normalized projected search direction, $\nabla f_{proj}(\mathbf{X}_i) = \dfrac{\mathbf{P}\nabla f(\mathbf{X}_i)}{\|\mathbf{P}\nabla f(\mathbf{X}_i)\|}$. Set $\mathbf{S}_i = \nabla f_{proj}(\mathbf{X}_i)$ and $\lambda_i = \lambda_{obj}$. Go to step 7;

6. Set the normalized search direction, $\mathbf{S}_i = -\dfrac{\nabla g(\mathbf{X}_i)}{\|\nabla g(\mathbf{X}_i)\|}$, and the step size proportional to the gradient and normalized with the initial step size $\lambda_i = \lambda_{const}\dfrac{\|\nabla g(\mathbf{X}_i)\|}{\|\nabla g(\mathbf{X}_1)\|}$;

7. Test whether or not $0 < \mathbf{X}_i + \lambda_i\mathbf{S}_i > 1$. If yes, the new location is outside the design hyperspace, and the direction must be adjusted so that the next step will be inside the domain, go to 8. If no, the next step is within the allowed region, go to 9;

8. The next step direction vector $\mathbf{S}_i$ must be projected back into the domain. If the current state is towards the constraint hyper-plane, the component of $\mathbf{S}_i$ that crosses the boundary is set to 0, the base matrix $\mathbf{A}$ of the hyper-plane defined by the vector normal to $x_j = (0 \text{ or } 1)$ is calculated, and the new $\mathbf{S}_i$ is projected onto it. If the current state is toward the optimum, the base matrix $\mathbf{A}$ of the constant constraint hyper-plane is calculated, and the new $\mathbf{S}_i$ is projected onto it. In both cases, the projection is computed using the matrix $\mathbf{P} = \mathbf{A}(\mathbf{A}^T\mathbf{A})^{-1}\mathbf{A}^T$ and the new normalized projected search direction $\mathbf{S}_i = \dfrac{\mathbf{P}\cdot\mathbf{S}_i}{\|\mathbf{P}\cdot\mathbf{S}_i\|}$ is obtained. Then, go to step 9;

9. Find the new design variables location as $\mathbf{X}_{i+1} = \mathbf{X}_i + \lambda_i\mathbf{S}_i$;

10. Test if $f(\mathbf{X}_i) < f(\mathbf{X}_{i-1})$. If this condition has been satisfied four times in a row, the search region is refined, by decreasing the step sizes λ_{obj} and λ_{const}, and also the tolerance ε_{const}, all by a factor of three. If $\varepsilon_{const} \leq \varepsilon_{final}$ the optimum has been reached: stop. Else, increment the iteration number and go to step 2.

It is worth mentioning that the condition $f(\mathbf{X}_i) < f(\mathbf{X}_{i-1})$ in step 10 ensures that the search order can only be decreased once a maximum for the objective function has been found.

The optimization algorithm described above is presented as a flow chart in Figure 4.8.

Initialization

Compute $\nabla g(\mathbf{X}_i)$

Compute $\nabla f(\mathbf{X}_i)$

Does $g(\mathbf{X}_i) \le \varepsilon_{const}$?

no / yes

Compute
$$\mathbf{P} = \mathbf{A}\left(\mathbf{A}^T\mathbf{A}\right)^{-1}\mathbf{A}^T$$
and set
$$\mathbf{S}_i = \frac{\mathbf{P}\nabla f(\mathbf{X}_i)}{\left\|\mathbf{P}\nabla f(\mathbf{X}_i)\right\|}$$
$$\lambda_i = \lambda_{obj}$$

Set
$$\mathbf{S}_i = -\frac{\nabla g(\mathbf{X}_i)}{\left\|\nabla g(\mathbf{X}_i)\right\|}$$
$$\lambda_i = \lambda_{const}\frac{\left\|\nabla g(\mathbf{X}_i)\right\|}{\left\|\nabla g(\mathbf{X}_1)\right\|}$$

Has $f(\mathbf{X}_i) < f(\mathbf{X}_{i-1})$ been satisfied 4 times in a row?

no / yes

Decrease order of magnitude for the tolerances and the step sizes

Does $0 < \mathbf{X}_i + \lambda_i\mathbf{S}_i > 1$?

no / yes

Compute
$$\mathbf{S}_{i\ corrected} = \frac{\mathbf{P}\cdot\mathbf{S}_i}{\left\|\mathbf{P}\cdot\mathbf{S}_i\right\|}$$

$$\mathbf{X}_{i+1} = \mathbf{X}_i + \lambda_i\mathbf{S}_i$$

Does:
- $\varepsilon_{const} \le \varepsilon_{final}$
- Toward objective
- Obj. has been topped 4 times in a row

no / yes

Stop

Figure 4.8 Flow chart representation of the proposed optimization algorithm

Chapter 5. Results and Discussions

In this chapter, notes on the computational grids used and the validation of the control-volume finite difference and the control-volume finite element methods (CVFDM and CVFEM, respectively) described in Chapter 3 are presented first. Following that, the proposed optimization methodology is demonstrated in the context of four practical cases: a heat exchanger with rectangular plate-fin ducts; a heat exchanger with triangular plate-fin ducts; and two different internally finned circular ducts. The results for each of these four demonstration problems are presented and discussed concisely in this chapter.

5.1 VALIDATION OF THE CVFDM AND CVFEM

Numerous preliminary investigations were done with the CVFDM and CVFEM described in Chapter 3 in order to establish suitable computational grids and also validate the formulations and computer implementations of these numerical methods. Overview of these preliminary investigations and their results are presented in this section.

5.1.1 Selection of Computational Grids

The proposed CVFDM and CVFEM were first used to solve steady, laminar, fully-developed flow and heat transfer problems in a variety of plate-fin ducts: all cases considered in these investigations were governed by the mathematical models discussed in Chapter 2. The duct shapes and problem parameters investigated were similar to those used for the practical cases (demonstration problems) discussed later in this chapter. Based on these preliminary investigations, computational grids that provide a good balance between accuracy of the results and the associated computational costs were established. In particular, successively finer uniform grids were used with the CVFDM and the CVFEM: both these methods are second-order accurate with uniform grids [Baliga and Atabaki (2006)]. The results of these grid-refinement exercises were used in the well-know Richardson extrapolation scheme to obtain essentially grid-independent solutions to the problems investigated. Following that, it was established that the following relatively modest computational grids (see Figures 3.11 – 3.14 for the corresponding patterns) give results that are within 0.05% of the aforementioned extrapolated grid-independent solutions:

- For the rectangular plate-fin ducts (see Figure 3.11), 20 uniformly spaced nodes along the x axis and 20 uniformly spaced nodes along the y axis;

- For the triangular plate-fin ducts (see Figure 3.12), 40 uniformly spaced nodes along the bottom symmetry plane, and also 40 uniformly spaced nodes along the plate;

- For the circular plate-fin ducts with triangular fins (see Figure 3.13), 50 uniformly spaced nodes the along the bottom symmetry plane, and the corresponding number of nodes in the other directions, calculated in accordance with the discussion presented in Section 3.6.4.

5.1.2   Applications to Test Problems and Results

In order to establish the validity of the formulations and computer implementations of the proposed CVFDM and CVFEM, they were used to solve several test problems and the computed results were checked against those available in the published literature. In all cases the above-mentioned computational grids were used.

The CVFDM was applied to laminar fully-developed flow and heat transfer in straight rectangular plate-fin ducts, with aspect ratios of Ar = 0.5, 0.75, and 1.0, and a constant-property Newtonian fluid. The fins were assigned infinite conductance in these tests, so they had the same temperature as the duct walls. The following results were computed: $f_D \cdot \mathrm{Re}$, Nu_{av}^H and Nu_{av}^T. These results were then checked against the corresponding results available in the work of Shah and London (1978). The results and the comparisons are in Tables A.1 and A.2 of Appendix A. They show that the aforementioned overall fluid flow and heat transfer results provided by the CVFDM agree very well with the benchmark values available in Shah and London (1978): the absolute percentages differences between the corresponding results are all well below 0.5%.

The CVFEM was applied to laminar fully-developed flow and heat transfer in straight triangular plate-fin ducts with the following angles between the fins (see Figure 3.12): $10°$, $30°$, $60°$, $90°$, and $120°$. A constant-property Newtonian fluid was considered in these tests. In all cases, the fins were assigned an infinite conductance. The results

obtained for $f_D \cdot \text{Re}$ and Nu_{av}^H were compared to those of Shah (1975) and Baliga & Arzak (1986). The results for Nu_{av}^T were compared to those of Schmidt and Newell, as found in Shah & London (1978), and Baliga & Arzak (1986). These results and comparisons are presented in Tables A.3 and A.4 of Appendix A. Here again, the results agree very well with the aforementioned benchmark solutions: in all cases, the absolute percentage differences between the corresponding results were all less than 2.5%.

Laminar fully-developed flow and heat transfer in triangular plate-fin ducts with finite values of the fin conductance parameter (Ω) were investigated using the CVFEM. The fluid was Newtonian and was assumed to have constant properties. The results were compared to corresponding results of Baliga and Azrak (1986) for Ω = 1, 2, 5, 10, 25, and ∞. The results and comparisons are presented in Table A.5 of Appendix A. Again, the results agree very well with the benchmark values: in all cases, the absolute differences between corresponding results were all less than 2%.

The CVFEM was also applied to laminar fully-developed fluid flow and heat transfer in straight internally finned ducts of circular cross-section; the longitudinal fins were of triangular cross-section. Again, a constant-property Newtonian fluid was considered in these tests. The CVFEM results for $\left(Nu_{av}^H \right)_d$, $\left(Nu_{av}^T \right)_d$, and $\left(f_D \cdot \text{Re} \right)_d$ were compared to those of Masliyah, as found in Shah and London (1978). The results and comparisons are given in Tables A-6, A-7, A-8, and A-9, and also Figures A-1, A-2, A-3, and A-4 in Appendix A. Again, the results yielded by the CVFEM agree very well with the aforementioned benchmark results: in most cases, the absolute differences between corresponding results were all less than 10%.

5.2　PRACTICAL CASE 1: OPTIMIZATION OF A HEAT EXCHANGER WITH RECTANGULAR PLATE-FIN DUCTS

This first practical case is used to demonstrate the following capabilities of the proposed optimization methodology:

- Optimization of a heat exchanger with rectangular plate-fin ducts, for three different fin materials;

- Ability to handle a problem with two design variables.

First, the solution for the selected baseline problem is presented in section 5.2.1. Then, the optimization of this baseline problem is presented in section 5.2.2.

5.2.1   Baseline Problem

The characteristics of the baseline problem in this case are presented in Table 5.1 (see Figure 3.10 for related geometric details and notation). The fin thickness in the baseline problem was deliberately chosen to be large with respect to the height of the duct in order to allow the optimization procedure to achieve appreciable relative increases of the objective function.

Table 5.1 Geometric dimensions of the baseline problem for Case 1

$2W_{rect}$	1 in (25.4 mm)
$2H_{rect}$	0.5 in (12.7 mm)
t_{rect}	0.25 in (6.35 mm)
n_{rect}	52.5 ducts / m

The three fin materials considered were stainless steel (AISI 302), pure aluminium, and pure copper. The corresponding values of the fin conductance, Ω, for the baseline problem, are presented in Table 5.2.

Table 5.2 Fin conductances for the baseline problem in Case 1

Material	Ω
Stainless steel	101.08
Aluminium	1586.49
Copper	2684.31

In all cases, the Reynolds number was fixed at 100. The corresponding pumping power per unit length of duct and a unit height of heat exchanger for the baseline problem was computed to be 4.07×10^{-4} W/m. This value was maintained constant (as the constraint) during the optimization procedure.

5.2.2   Optimization

Two design variables were considered in this optimization exercise: the height of the plate-fin ducts, H_{rect}; and the thickness of the fins, t_{rect}. The width of the ducts was considered fixed at the baseline value. The statements of the optimization problems for this case are the following:

$$\text{Find}\quad \mathbf{X} = \left\{ \begin{matrix} t_{rect} \\ H_{rect} \end{matrix} \right\}\quad \text{which maximizes}\quad f_{rect}^{H}(\mathbf{X}) = n_{rect} \cdot \frac{Nu_{av}^{H}}{D_H \Big/ Peri_{wetted}} \tag{5.1}$$

and

$$\text{Find}\quad \mathbf{X} = \left\{ \begin{matrix} t_{rect} \\ H_{rect} \end{matrix} \right\}\quad \text{which maximizes}\quad f_{rect}^{T}(\mathbf{X}) = n_{rect} \cdot \frac{Nu_{av}^{T}}{D_H \Big/ Peri_{wetted}} \tag{5.2}$$

Both the optimizations were subjected to the following constraint:

$$g_{rect}(\mathbf{X}) = \left(-\frac{dp}{dz} w_{av} 4 \left(W_{rect} \cdot H_{rect} \right) n_{rect} - pp_{target} \right)^2 = 0 \tag{5.3}$$

The limits for each of the two aforementioned design variables and also their initial values are presented in Table 5.3:

Table 5.3 Limits and initial values of the design variables in Case 1

Design variable	Dimensions [mm]		
	Min	Max	Init. value
H_{rect}	0.0	127.0	63.5
t_{rect}	0.0254	2.54	1.283

The proposed optimization methodology was applied to this case for the two thermal boundary conditions (H and T) discussed in Chapter 2. The relative improvements in the thermal performance are represented by the ratio of the value of the objective function calculated for the baseline problem to that achieved in the optimized plate-fin duct:

$$\eta_{rect}^{H} = \frac{\left[f_{rect}^{H}(\mathbf{X})\right]_{\text{Base line case}}}{\left[f_{rect}^{H}(\mathbf{X})\right]_{\text{Optimized}}} \tag{5.4}$$

$$\eta_{rect}^{T} = \frac{\left[f_{rect}^{T}(\mathbf{X})\right]_{\text{Base line case}}}{\left[f_{rect}^{T}(\mathbf{X})\right]_{\text{Optimized}}} \tag{5.5}$$

The results are presented in Table 5.4.

Table 5.4 Optimization results for Case 1

Material	pp [W/m]	Ω [-]	H_{rect} [mm]	t_{rect} [mm]	n_{rect} [ducts/m]	η_{rect}^{H} [-]
Thermal boundary condition H						
Stainless steel	4.08×10^{-4}	4.534	14.551	0.3112	67.29	1.1736
Aluminium	4.08×10^{-4}	31.14	14.612	0.1366	67.80	1.1829
Copper	4.08×10^{-4}	58.04	14.602	0.1503	67.79	1.1834
Thermal boundary condition T						
Stainless steel	4.08×10^{-4}	3.920	14.570	0.2693	67.39	1.1759
Aluminium	4.08×10^{-4}	26.35	14.626	0.1156	67.84	1.1839
Copper	4.08×10^{-4}	47.24	14.610	0.1224	67.88	1.1855

In all cases, the pumping power is the same as that in the baseline case (constraint), which ensures that only the thermal performance of the heat exchanger is affected.

The best improvement in the thermal performance was obtained with the copper fins for both of the thermal boundary conditions, H and T: with relative increases of 18.34% and 18.55%, respectively. These results can be explained by noting that copper has the highest thermal conductivity of the three fin material considered; for copper, the fin thickness could be significantly lowered before there were noticeable decreases in the temperature along its length. Not surprisingly, the optimized ducts with fins made of stainless steel, which has the lowest thermal conductivity of the three materials

considered, yielded the lowest relative increases in thermal performance: 17.36% and 17.59% for the H and T boundary conditions, respectively. These improvements show that the design of the baseline problem was not optimal. In all cases, the optimal duct height H_{rect} turned out to be approximately 14.6 mm. The relative invariance of this height with respect to the fin material used and also to the thermal boundary conditions is because H_{rect} is much greater than t_{rect}, and, therefore, it has a significantly greater impact on the variation of the pumping power in the optimization process: thus, the optimal value of H_{rect} is mostly governed by the constant-pumping-power constraint and has relatively little effect on the thermal performance, as opposed to t_{rect} which has only very limited effect on the pumping power but greatly affects the thermal performance. The optimized dimensionless fin temperature distributions for each optimized solutions are presented in Figure 5.2: the fin temperature varies the most along its length for stainless steel (the material with the lowest thermal conductivity) and the least for copper (the material with the highest thermal conductivity).
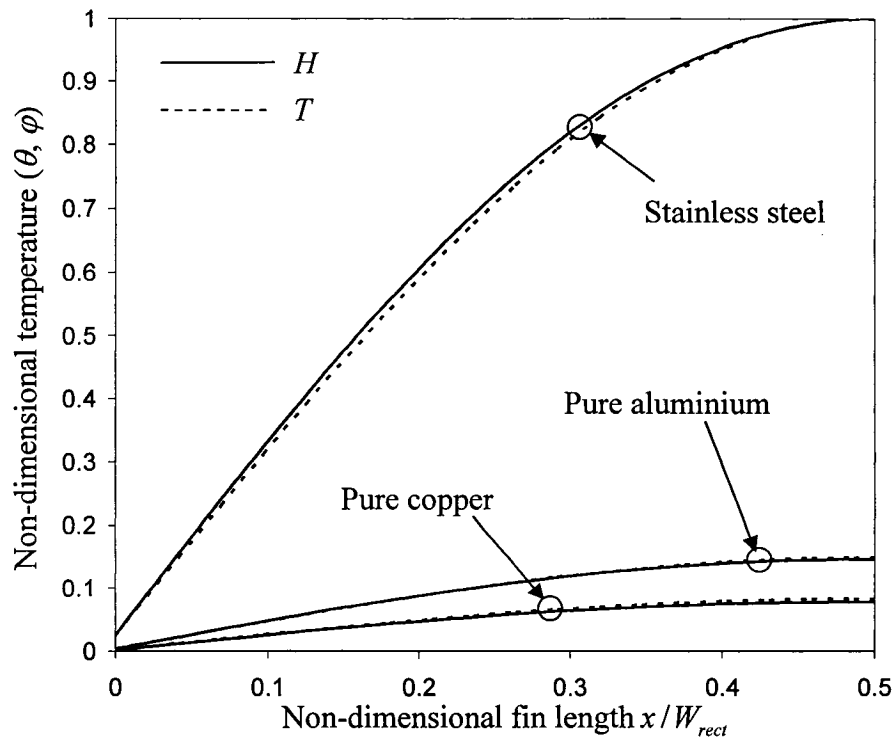
Figure 5.1 Optimized dimensionless fin temperature distributions for Case 1

5.3 PRACTICAL CASE 2: OPTIMIZATION OF A HEAT EXCHANGER WITH TRIANGULAR PLATE-FIN DUCTS

This second practical case is used to demonstrate the following capabilities of the proposed optimization methodology:

- Optimization of heat exchangers with triangular plate-fin ducts, for three different fin materials;

- Achieve the same optimal solution using different, but essentially equivalent, design variables.

First, the baseline problem for this case is presented in section 5.3.1. Then, the optimization of this baseline problem is presented in section 5.3.2.

5.3.1 Baseline Problem

The characteristics of the baseline problem in this case are presented in Table 5.5 (see Figure 3.10 for related geometric details and notation). For the preceding case, the baseline fin thickness was deliberately chosen to be quite large so that an appreciable improvement of the thermal performance could be observed in the optimized solutions. For the current practical case, the fin thickness was chosen to be much smaller, such that for a given pumping power, the baseline problem was already quite well designed. Therefore, the improvements in the relative thermal performance of the optimized solutions for this case were expected to be smaller than those achieved in the previous case.

Table 5.5 Geometric dimensions of the baseline problem for Case 2

W_{rect}	1 in (25.4 mm)
2τ	60°
t_{rect}	0.0787 in (2.0 mm)
n_{rect}	31.61 ducts / m

The three fin materials considered are again stainless steel (AISI 302), pure aluminium, and pure copper. The corresponding values of Ω for the baseline problem are presented in Table 5.6.

Table 5.6 Fin conductances for the baseline problem in Case 2

Material	Ω
Stainless steel	42.45
Aluminium	666.24
Copper	1127.27

In all cases, the Reynolds number was fixed at 100 and the corresponding pumping power per unit length of the duct and for a unit height of heat exchanger for the baseline problem was computed to be 2.433×10^{-4} W/m. This was kept the same during the optimization procedure (constraint).

5.3.2   Optimization

The design variables chosen for the optimization of the baseline problem in this case were the aperture angle between the fins of the triangular plate-fin ducts, 2τ, and the fin thickness, t_{tri}. Again, the distance between the plates, W_{tri}, was kept constant at its value in the baseline problem. The statements of the optimization problems in this case are the following:

$$\text{Find} \quad \mathbf{X} = \begin{Bmatrix} t_{tri} \\ 2\tau \end{Bmatrix} \quad \text{which maximizes} \quad f_{tri}^H(\mathbf{X}) = n_{tri} \cdot \frac{Nu_{av}^H}{D_H / Peri_{wetted}} \tag{5.6}$$

and

$$\text{Find} \quad \mathbf{X} = \begin{Bmatrix} t_{tri} \\ 2\tau \end{Bmatrix} \quad \text{which maximizes} \quad f_{tri}^T(\mathbf{X}) = n_{tri} \cdot \frac{Nu_{av}^T}{D_H / Peri_{wetted}} \tag{5.7}$$

Both these optimizations are subjected to the following constraint:

$$g_{tri}(\mathbf{X}) = \left(-\frac{dp}{dz} w_{av} \left(W_{tri} \cdot H_{tri} \right) n_{tri} - pp_{target} \right)^2 = 0 \qquad (5.8)$$

The limits for each design variable and also their initial values are presented in Table 5.7.

Table 5.7 Limits and initial values of the design variables in Case 2

| Design variables | Dimensions (2τ [°], t_{rect} [mm]) | | |
	Min	Max	Init. value
2τ	20.0	120.0	70.0
t_{tri}	0.1	5.08	3.04

The proposed optimization method was applied to the two thermal boundary conditions (H and T) discussed in Chapter 2. The relative improvements in the thermal performance of the optimized solutions are again represented by the ratios of the value of objective function calculated for the baseline problem to that achieved in the optimized plate-fin ducts:

$$\eta_{tri}^H = \frac{\left[f_{tri}^H(\mathbf{X}) \right]_{\text{Base line case}}}{\left[f_{tri}^H(\mathbf{X}) \right]_{\text{Optimized}}} \qquad (5.9)$$

$$\eta_{tri}^T = \frac{\left[f_{tri}^T(\mathbf{X}) \right]_{\text{Base line case}}}{\left[f_{tri}^T(\mathbf{X}) \right]_{\text{Optimized}}} \qquad (5.10)$$

The results of this optimization exercise are presented in Table 5.8.

As was expected, the relative improvements in the thermal performance of the optimized plate-fin ducts are much smaller than those achieved in Case 1: the best improvement is 3.23% for this case. In the optimized solutions, the number of ducts per unit height of the heat exchanger was increased by an average of 3.22%. Other characteristics of the optimized solutions for this case can be explained in a similar manner to that for Case 1.

Table 5.8 Optimization results for Case 2

Thermal boundary condition H					
Material	pp [W/m]	Ω [-]	2τ [°]	t_{tri} [mm]	n_{tri} [ducts/m]	η_{tri}^{H} [-]
Stainless steel	2.434×10^{-4}	7.7276	61.556	0.7282	32.60	1.0282
Aluminium	2.434×10^{-4}	100.63	61.615	0.6042	32.63	1.0324
Copper	2.434×10^{-4}	170.26	61.615	0.6042	32.63	1.0325
Thermal boundary condition T					
Material	pp [W/m]	Ω [-]	2τ [°]	t_{tri} [mm]	n_{tri} [ducts/m]	η_{tri}^{H} [-]
Stainless steel	2.434×10^{-4}	6.1646	61.628	0.5809	32.64	1.0298
Aluminium	2.434×10^{-4}	100.63	61.615	0.6042	32.63	1.0322
Copper	2.434×10^{-4}	170.26	61.615	0.6042	32.63	1.0322
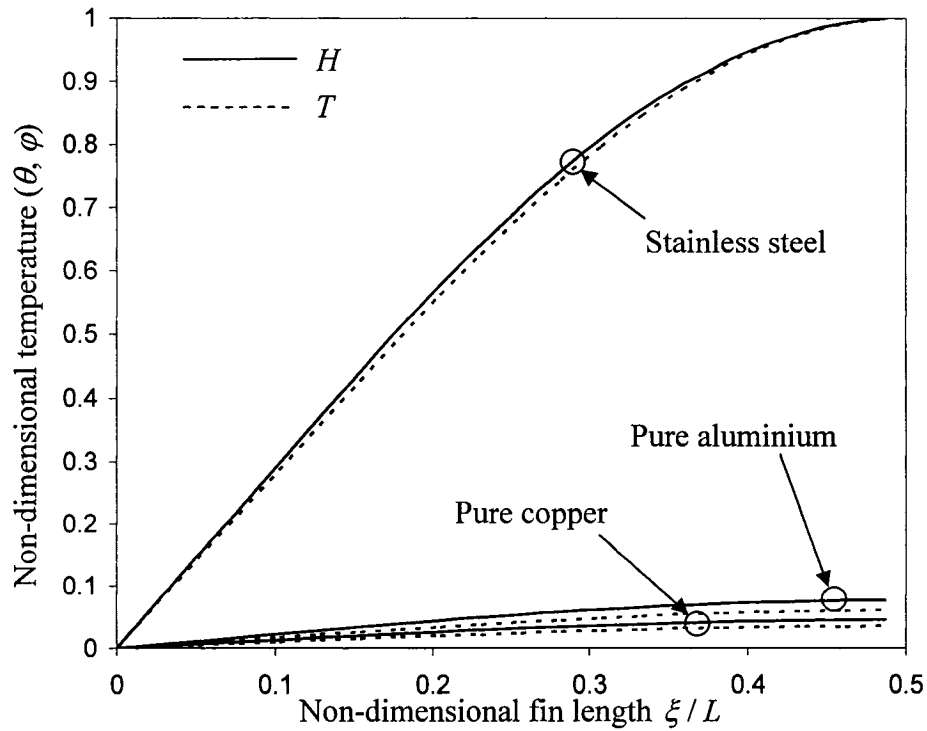
Figure 5.2 Optimized dimensionless fin temperature profiles for Case 2

The optimal duct aperture, 2τ, is almost identical in all cases with an average value of 61.61°: again, this is because the impact of 2τ on the pumping power per unit length of the duct (the constraint) is much greater than that of t_{tri}.

The optimized dimensionless fin temperature profiles for this case are presented in Figure 5.3. Again, as expected, the temperature variation along the fin length is the most for stainless steel and the least for copper.

The optimization in this case was also performed with a different, but equivalent, set of design variables, for stainless steel and the thermal boundary condition H, in order to establish the consistency of the proposed optimization methodology and its implementation in this work. In this exercise, the fin thickness was kept the same, but the aperture of the duct, 2τ, was replaced by the half-height of the triangular duct, H_{tri}. The same optimal solution should be obtained with this alternative, but equivalent, set of design variables, since it is possible to attain same the plate-fin duct shape by adjusting H_{tri} rather than 2τ. The results of these optimization runs are presented in Table 5.9.

Table 5.9 Optimization results for Case 2 achieved with equivalent design variables

Design var.	pp [W/m]	Ω [-]	2τ [°]	H_{tri} [mm]	t_{tri} [mm]	n_{tri} [ducts/m]	η_{tri}^{H} [-]
$(t_{tri}, 2\tau)$	2.434×10^{-4}	7.728	61.556	0.0151	0.7282	32.60	1.0282
(t_{tri}, H_{tri})	2.434×10^{-4}	7.719	61.557	0.0151	0.7274	32.59	1.0282

The results presented in Table 5.9 show that with t_{tri} and H_{tri} as the design variables, the optimized shape is almost identical to the shape obtained when with the original design variables, t_{tri} and 2τ. In fact, the largest difference is between the values of fin conductances obtained with these two sets of design variables, and even this difference is only 0.116%, which is negligible for all practical purposes.

5.4 PRACTICAL CASE 3: OPTIMIZATION OF A HEAT EXCHANGER WITH INTERNALLY FINNED CIRCULAR DUCTS

This third practical case is used to demonstrate and explore the following aspects of the proposed optimization methodology:

- Its use with non-uniform rational B-splines (NURBS) and its control points to approximate the fin shape;

- Its use with a large number of design variables;

- Determination of the minimum number of control points of the NURBS that ensure the resulting optimized fin shape is essentially independent of this parameter;

- Determination of the effect of the control point weights on the fin shape;

- Determination of the effect of the initial values of the design variables (initial design point) on the optimal solution;

- Determination of the effect of the number of fins on the optimal fin profile;

- Optimization of a plate-fin heat exchanger with internally finned circular ducts, for three different plate-fin materials, and for a baseline duct having eight internal fins of triangular cross-section;

- Establishing that the optimal shape of the fin, in the context of the dimensionless formulation of the problem, is independent of the Reynolds number and the duct size.

The selected baseline problem for this case is presented in section 5.4.1. Then, the optimization of the baseline problem and the other aforementioned aspects of this case are presented in section 5.4.2.

5.4.1 Baseline Problem

For this case, the baseline problem is a circular duct with eight internal fins of triangular cross-section. The cross-section of the duct for this base line case is presented in figure 5.3. The dimensionless length of the fin, $l^* = l_f / r$, is 0.6; the number of fins, n_{fin}, is 8;

and the angle of the fins at the base, 2σ, is 6° (see Figure 3.10 for details). The materials considered for the fins are again stainless steel (AISI 302), pure aluminium, and pure copper. Since the fin shapes can take various forms in this case, the fin thickness is not constant, but varies along its length. As a result, the fin conductance Ω also varies along its length: thus, is not being presented in tabular form in the results.
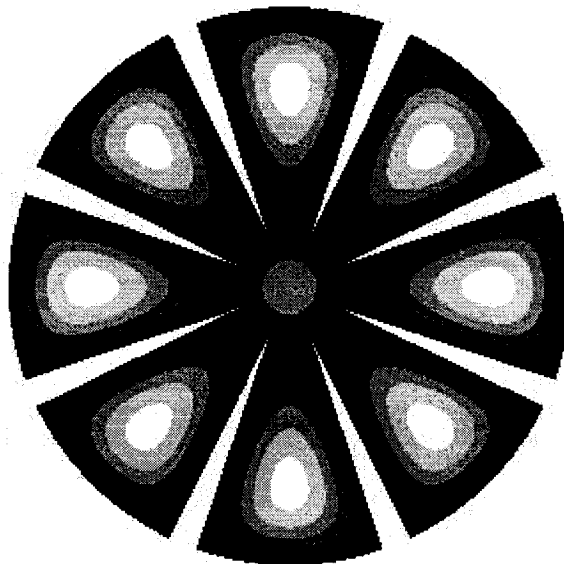
Figure 5.3 Duct cross-section for the baseline problem in Case 3, with equally-spaced axial velocity contours

Various runs were undertaken in order to obtain the objective functions values and pumping power for the Reynolds numbers 10, 100, 200, 500, and 1000 (the laminar flow regime), for two commonly used duct sizes: diameters of one-half (½) inch (r = 6.35mm), and one-and-a-half (1½) inches (r = 19.05mm). The fluid flow results for this baseline problem are presented in Table 5.10; the overall thermal results are presented in the next subsection. For each combination or Reynolds number and duct size, the dimensionless friction-Reynolds number product $\left(f_D \cdot \mathrm{Re} \right)_d$ remains constant. The corresponding values of the pumping power per unit length of the duct are given in Table 5.10, and used as the constraints for the optimization of the corresponding versions of the baseline problem for this case.

Table 5.10 Overall fluid flow results for the baseline problem in Case 3

Re [-]	$\varnothing$ [mm]	pp [W/m]	$(f_D \cdot Re)_d$ [-]
10	6.35	1.1414×10^{-5}	218.35
100	6.35	1.1414×10^{-3}	218.35
200	6.35	4.5657×10^{-3}	218.35
500	6.35	2.8535×10^{-2}	218.35
1000	6.35	1.1414×10^{-1}	218.35
10	19.05	1.2682×10^{-6}	218.35
1000	19.05	1.2682×10^{-2}	218.35

5.4.2 Optimization

The statements of the optimization problems for this case are the following:

$$\text{Find} \quad \mathbf{X} = \begin{Bmatrix} h_1 \\ h_2 \\ \vdots \\ h_{n-1} \\ l* \end{Bmatrix} \quad \text{which maximizes} \quad f_{circ}^H(\mathbf{X}) = \frac{Nu_{av}^H}{D_H \big/ Peri_{wetted}} \tag{5.11}$$

and

$$\text{Find} \quad \mathbf{X} = \begin{Bmatrix} h_1 \\ h_2 \\ \vdots \\ h_{n-1} \\ l* \end{Bmatrix} \quad \text{which maximizes} \quad f_{circ}^T(\mathbf{X}) = \frac{Nu_{av}^T}{D_H \big/ Peri_{wetted}} \tag{5.12}$$

both subject to the following constraint:

$$g_{circ}(\mathbf{X}) = \left(-\frac{dp}{dz} w_{av} A_{c-s} - pp_{target} \right)^2 = 0 \tag{5.13}$$

where n in the design vector is the number of control points, or design variables, that defines the fin shape. The relative improvements in the thermal performance of the

optimized solutions are again represented by the ratios of the value of objective function calculated for the baseline problem to that achieved in the optimized plate-fin ducts:

$$\eta_{circ}^{H} = \frac{\left[f_{circ}^{H}(\mathbf{X})\right]_{\text{Base line case}}}{\left[f_{circ}^{H}(\mathbf{X})\right]_{\text{Optimized}}} \tag{5.14}$$

$$\eta_{circ}^{T} = \frac{\left[f_{circ}^{T}(\mathbf{X})\right]_{\text{Base line case}}}{\left[f_{circ}^{T}(\mathbf{X})\right]_{\text{Optimized}}} \tag{5.15}$$

The limits for each design variable and their initial values are presented in Table 5.11. The minimum values of h_i are the minimum thickness of the fins relative to the radius, and the maximum values are set as bounding triangular fins with coinciding bases and same length as the actual fin.

Table 5.11 Limits and initial values of the design variables in Case 3

Design variables	Dimension	
	Min	Max
h_i $1 \leq i \leq (n\text{-}1)$	$\dfrac{r}{100}$	$\pi \dfrac{r}{n_{fin}} \left(1 - \dfrac{n-i}{n-1}\right)$
$l*$	0.2	0.9

The initial design point varies depending on the number of fins present in the duct: in order to decrease the number of iterations needed to reach an optimum, the fin is assigned an initial length and initial thickness similar to the expected optimized shape. Before optimizing the baseline problem, the determination of effect of the number of control points and the effect of the initial design point are presented in the subsections 5.4.2.1 and 5.4.2.2.

5.4.2.1 Effect of the number of control points and their weights on the optimal shape of the fin

The effect of the number of control points on the fin shape must be determined first in order to use the appropriate number of control points, or design variables, which ensure

that the final optimal shape is essentially independent of this parameter in the optimization process.

Table 5.12 Optimized results obtained with different number of control points in Case 3

Number of control points	$(f_D \cdot \mathrm{Re})_d$	η_{circ}^{H}
4	213.635	1.0517
6	215.640	1.0626
9	227.343	1.0660
12	232.621	1.0510
15	240.548	1.0252

(a) 4 control points

(b) 6 control points

(c) 9 control points

(d) 12 control points
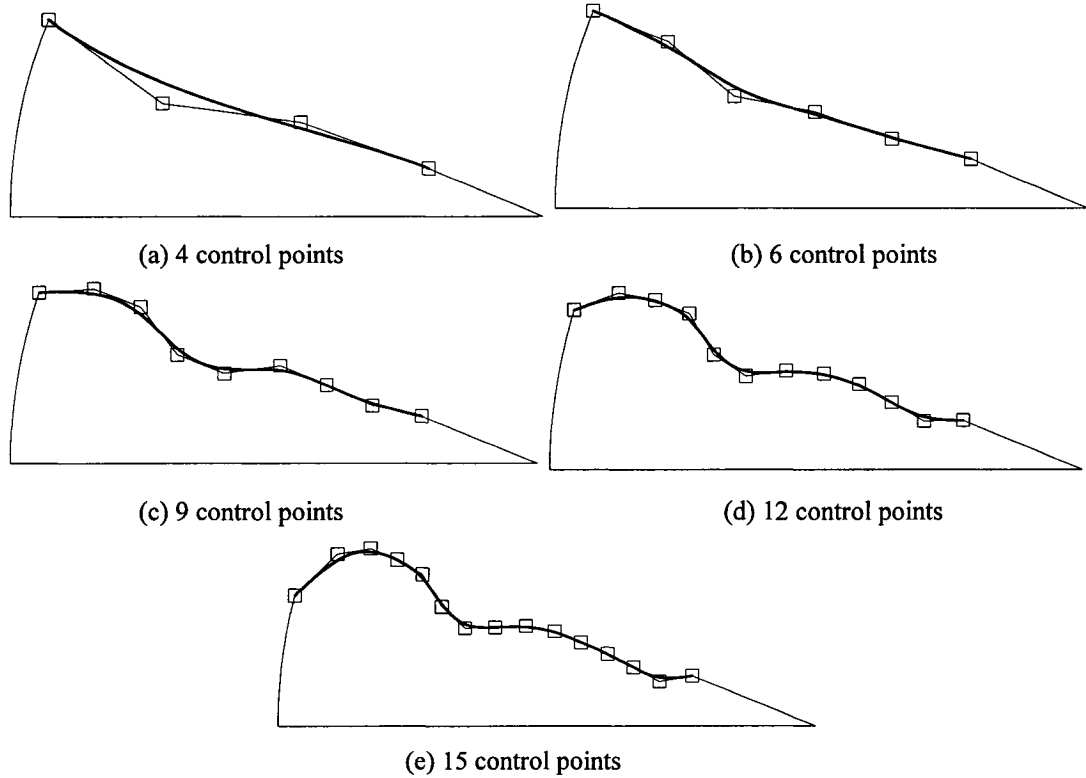
(e) 15 control points

Figure 5.4 Effect of the number of control points on the optimized fin shape in Case 3

Runs of the optimization procedure were performed, with n = 4, 6, 9, 12, and 15. The results are presented in Table 5.12, and the corresponding optimized fin shapes are

presented in Figure 5.4. In all optimization runs, the pumping power per unit length of the duct was maintained at the value calculated for the baseline problem (constraint).

The following conclusions can be arrived at by examining Figures 5.4 (a) to (e): first, it appears as if the optimal fin shape has a bulge (a larger thickness) in the middle — as the number of control points increases, those located in the middle region of the fin along its length tend to pull the fin surface outward from its central axis. This bulge, or outgrowth, starts to be captured with nine control points. However, with 12 and 15 control points, the fin shapes obtained are very similar and capture the bulge entirely, and the only difference between these two solutions is that the width of the optimized fin at its base is slightly larger for the 15 than the 12 control-points solutions. Therefore, it is assumed from this point on that the 12 control points provide results that are adequate for the demonstration of the capabilities of the proposed optimization methodology, and it provides a good compromise between the cost of the computations and the accuracy the optimal fin shape.

The effect of the weights of the control points must also be determined. In order to do this, the proposed optimization method was used for the optimization of the baseline problem with 12 control points, and their weights were included as design variables. The total number of design variables was then 22, since the NURBS curve falls on the two end points, and the weight of each of these end points was fixed at unity (1). The resulting shape of the fin is presented in Figure 5.5.
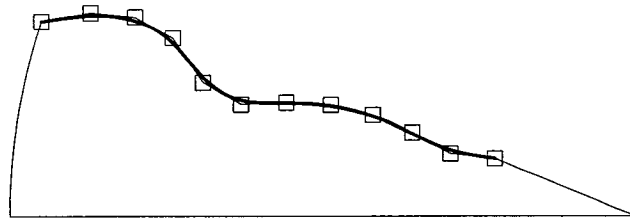
Figure 5.5 Optimal fin shape obtained with the weights of 12 control points as design variables

The differences between the values of $\left(f_D \cdot \mathrm{Re}\right)_d$ and η_{circ}^H results for the optimal shapes with and without the weights of the 12 control points as design variables are 0.51% and 0.95%, respectively. Moreover, with 12 control points, the local variation of the fin

shape generated by the variation of the weights is negligible, as the obtained shapes (Figure 5.4 (d) and Figure 5.5) are almost identical. The effect of the weights on the local shape would be greater with a small number of control points due to the larger distances between adjacent control points. For an equal number of design variables, using a large number of control points without their weights as design variables allows more localized flexibility in the calculation of the fin shape than using a small number of control points with their weights as the design variables. With 12 control points, the increase in the cost of the computations created by the addition of their weights as design variables is much greater than the difference generated in the optimal fin shape: thus, it was decided to use 12 control points but not to include their weights as design variables from this point on.

5.4.2.2   Effect of the initial design point on the optimal design

The n-dimensional design space spanned by the design variables can present multiple local maximums and minimums. These local optima can sometimes prevent the algorithm from reaching the absolute maximum in the design space if they are located between the current design point and this absolute maximum. In these cases, one must either take the obtained solution as a satisfying optimal solution, or repeat the optimization process with a different initial design point, so that there is a path for which the objective function keeps increasing until the true summit is reached. Since the proposed method is gradient-based, the effect of the initial design point on the optimal design must be determined. Table 5.13 presents the results of the optimization of the baseline problem in this case for the thermal boundary condition H, with 10 different initial design points, which were chosen arbitrarily, while not making them too far apart from each other (because of grid generation limits). The design vector in each case is presented in Table B.1 of Appendix B. The fin material used in these tests was stainless steel.

Table 5.13 Optimization results obtained with different initial design points in Case 3

Run No.	1	2	3	4	5	6	7	8	9	10
η_{circ}^{H}	1.0593	1.0148	0.9826	1.0772	0.9961	1.0080	1.0791	1.0361	1.0340	0.9943
$(f_D \cdot \text{Re})_d$	226.9	244.3	262.8	214.0	259.8	215.9	212.8	228.8	227.6	241.8

The corresponding optimized fin shapes for each of these runs are presented in Appendix B. The standard deviation of the results presented in Table 5.11 is 7.76% for $(f_D \cdot \text{Re})_d$, and is 3.38% for η_{circ}^{H}. Even if the pumping power is maintained the same (constant) in all these runs, the resulting shapes show a variation with differences in the initial design point. Also, they all show the same bulge on the side of the fin, as seen in Figures 5.4 and 5.5. Thus, the space spanned by the design variables must present many local minima and maxima. At this point, it is worth mentioning that since the average increase in thermal performance is quite small in these runs, as the baseline problem for this case was already well designed, and the bulk of the increase is obtained with the growth of the bulge on the side of the fin, once this bulge is captured by the optimization procedure, details such as the fin widths closer to its base and its tip affect the thermal performance on a smaller scale.

For the remainder of the computations, the initial design point was chosen so that the initial fin shape was as close as possible to that of the baseline problem being optimized, and with a smooth surface (that is, with the control points aligned). This way, the constraint of constant pumping power per unit length of the duct could be satisfied in a limited number of iterations, and the likelihood of obtaining a smooth optimal fin shape was increased. In this context, it should also be noted that a smoothly varying fin surface has the advantage of being easier to manufacture than one with sudden changes in shape.

5.4.2.3   Optimization

In order to optimize the baseline problem, it is necessary to determine the effect of the Reynolds number and duct size on the optimal solution. To do so, the proposed optimization method was applied to every version of the baseline problem presented in Table 5.10, with the corresponding values of Re and duct diameter, and with stainless

steel as the fin material. The results are presented in Table 5.14, and the corresponding fin shapes are presented in Figure 5.6.

Table 5.14 Effects of Reynolds number and duct diameter on the optimal solutions in Case 3

Re [-]	r [mm]	pp [W/m]	η_{circ}^{H} [-]	η_{circ}^{T} [-]
10	6.35	1.1414×10^{-5}	1.0509	1.1041
100	6.35	1.1414×10^{-3}	1.0593	1.1082
200	6.35	4.5657×10^{-3}	1.0438	1.1059
500	6.35	2.8535×10^{-2}	1.0402	1.0217
1000	6.35	1.1414×10^{-1}	1.0504	1.0942
10	19.05	1.2682×10^{-6}	1.0590	1.1059
1000	19.05	1.2682×10^{-2}	1.0580	1.1104

The optimal fin shapes obtained are almost identical in all these tests, except for a slight variation of the thickness of the fin at the base: however, these variations have only very limited impact on the improvements in the thermal performance.

r = 19.05 mm

r = 6.35 mm
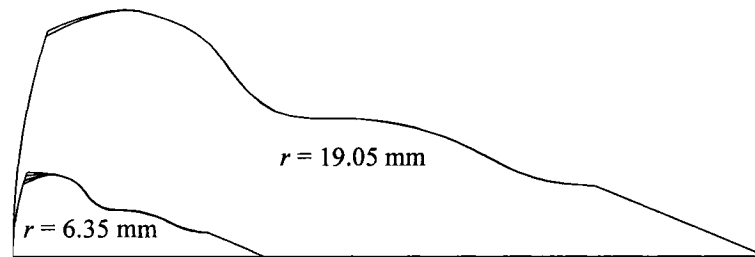
Figure 5.6 Optimized shapes for various Reynolds numbers and duct sizes

This independence of the optimal shape with regard to the Reynolds number and the duct diameter is keeping with the fact that the objective function is based on the Nusselt number, which is independent of the Reynolds number and the duct diameter. Moreover, the ratio of the hydraulic diameter to the wetted perimeter — which is present in the objective functions — is also independent of the duct diameter. The constant pumping

power constraint is different for different values of Reynolds number and duct diameter. However, in the design space unique to each optimization problem, these different pumping power hyper-planes are all equivalent, in terms of the ensemble of design points that defines each of them. It is, therefore, assumed from this point forward that the optimal solution is independent of the Reynolds number and the duct diameter, and the following results are presented for Re = 100 and r = 6.35 mm.

Table 5.15 Optimization results for the boundary condition H in Case 3

n_{fin}	Stainless steel		Aluminium		Copper	
	$(f_D \cdot Re)_d$	η_{circ}^H	$(f_D \cdot Re)_d$	η_{circ}^H	$(f_D \cdot Re)_d$	η_{circ}^H
5	393.34	1.1850	404.95	1.1711	669.11	0.8374
6	250.13	1.2547	247.15	1.3206	258.53	1.2221
7	243.26	1.1578	244.59	1.1652	242.41	1.1560
8	226.93	1.0593	233.24	1.0459	232.73	1.0452
9	235.48	0.9132	236.39	0.9121	218.97	0.9622
10	233.11	0.6253	235.02	0.6206	234.01	0.6255
11	217.57	0.3676	219.95	0.3948	221.59	0.3823

Table 5.16 Optimization results for the boundary condition T in Case 3

n_{fin}	Stainless steel		Aluminium		Copper	
	$(f_D \cdot Re)_d$	η_{circ}^T	$(f_D \cdot Re)_d$	η_{circ}^T	$(f_D \cdot Re)_d$	η_{circ}^T
5	683.76	0.9284	-	-	-	-
6	396.21	1.0921	393.01	1.0879	395.00	1.0822
7	248.38	1.2192	277.22	1.1532	261.07	1.1784
8	228.74	1.1082	233.56	1.1017	227.49	1.1092
9	240.73	0.7661	241.80	0.7477	241.24	0.7602
10	228.67	0.3336	227.86	0.3278	225.23	0.3407
11	203.51	0.2234	205.67	0.2147	205.10	0.2158

The proposed optimization method was applied to the baseline problem, with stainless steel, aluminium, and copper as the fin materials, and with number of fins between 5 and 11 (inclusive). The purpose of optimizing with different number of fins is to determine the optimal value of this variable too. The results are presented in Tables 5.15 and 5.16, for the two thermal boundary conditions considered, H and T, respectively. In all runs, the pumping power was kept constant at 1.1414×10^{-3} W/m. In all figures showing the optimal ducts, the contour lines represent constant values of the axial velocity.

The relative increases in thermal performance presented in Tables 5.15 and 5.16 are presented graphically in Figure 5.7. For a fixed number of fins, the increase in thermal performance relative to that of the objective functions for the baseline problem, for the thermal boundary condition H, are 5.9% for stainless steel, 4.6% for aluminium, and 4.5% for copper. The corresponding fin shapes, as presented in Figure 5.8, are very similar, except for a slightly smaller fin base width for stainless steel. If the number of fins in the duct is left unspecified, the thermal performance improves even more than when the number of fins is fixed; and the optimal number of fins (six), again for the H boundary condition, is the same for all fin materials considered. The increases in relative thermal performance are 25.47% for stainless steel, 32.06% for aluminium, and 22.21% for copper. The corresponding fin shapes are presented in Figure 5.9.
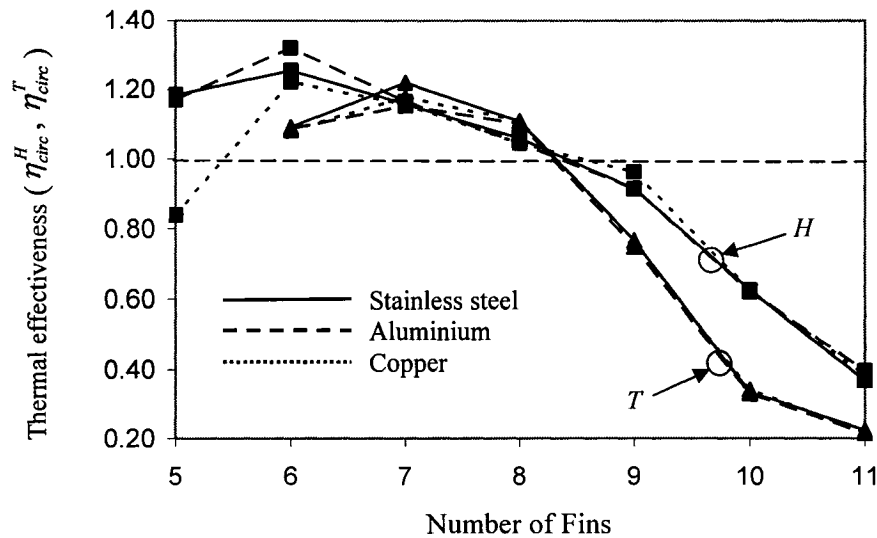
Figure 5.7 Effect of the number of fins on η_{circ}^{H} and η_{circ}^{H} in Case 3
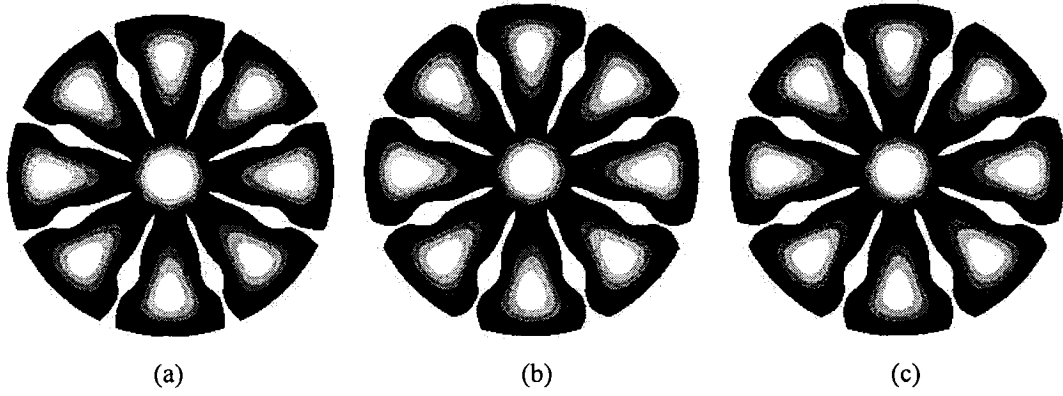
Figure 5.8 Optimal designs with $n_{fin} = 8$, thermal boundary condition H, and the following fin materials for Case 3: (a) stainless steel, (b) aluminium, and (c) copper
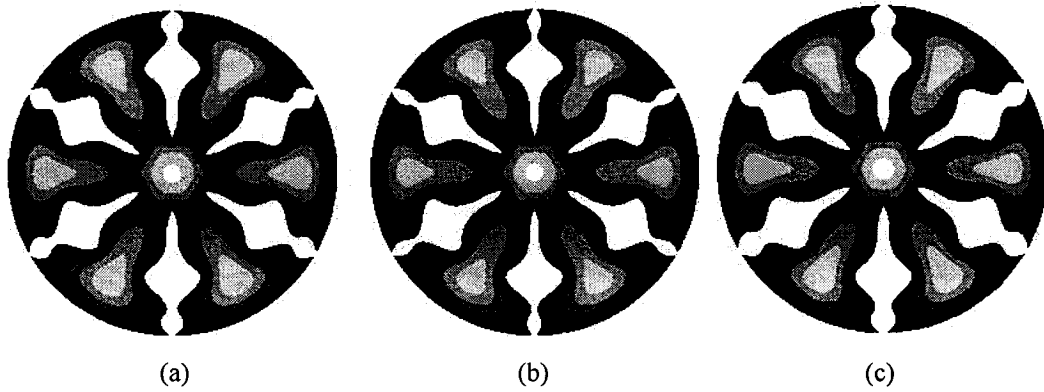
Figure 5.9 Optimal designs with n_{fin} variable, thermal boundary condition H, and three fin materials for Case 3: (a) stainless steel, (b) aluminium, and (c) copper

Qualitatively, the optimal fin shapes presented in Figures 5.8 and 5.9 have in common the presence of a bulge on the side of the fins, located approximately at 43% of the length of the fin, when measured from the base to the top. The axial velocity profiles achieved with the optimized fin shapes exhibit $(n_{fin} + 1)$ local maxima, one of them being located at the centre of the duct and the others in the spaces in between adjacent fins. For the baseline problem, the flow also shows such local maxima, but the difference is that the optimized shapes distribute this flow more evenly in the spaces in between adjacent fins. When the number of fins decreases, the space between adjacent fins increases, and the size of the bulge on the side of the fin also increases in order achieve the aforementioned even distribution of the flow in the duct cross-section.

When the number of fins in the duct is five or six, the bulges on the sides of the fin dominate the overall shape of flow passage. However, when the number of fins increases, the space in between adjacent fins decreases and the bulges on the sides of the fins also decrease. This pattern continues until the point where there is not enough space between the fins for the bulge to exist, and the distribution of the flow is controlled by adjustments of the length of the fin and increasing the base of the fins.

The choice of material for the fins does not have much of an influence on their optimal shape in this case: this is because the conductance of all the fins is quite high, so the temperature does not vary much along the length of the fin. The choice of the fin material may have had more of an effect on the optimal fin shapes if a fluid with a higher thermal conductivity than air (for example, water) were used in these tests.

(a)   (b)   (c)
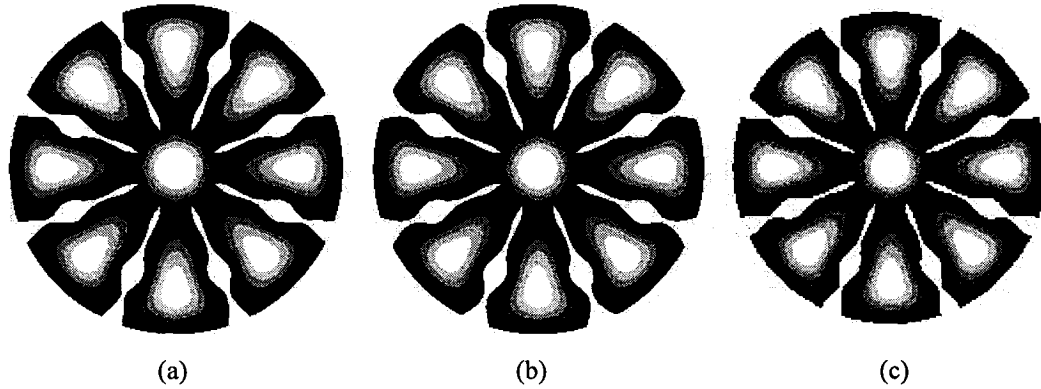
Figure 5.10 Optimal designs with $n_{fin} = 8$, thermal boundary condition T, and three fin materials for Case 3: (a) stainless steel, (b) aluminium, and (c) copper

For the thermal boundary condition T, the increases in relative thermal performance after optimization are 10.8% for stainless steel, 10.2% for aluminium, and 10.9% for copper, when the number of fins is fixed at eight. The corresponding optimized fin shapes are presented in Figure 5.10. If the number of fins is undetermined, the optimal solution is achieved with seven fins for each material, and the increases in relative thermal performance are 21.9% for stainless steel, 15.3% for aluminium, and 17.9% for copper: the corresponding optimal fin shapes are illustrated in Figure 5.11.
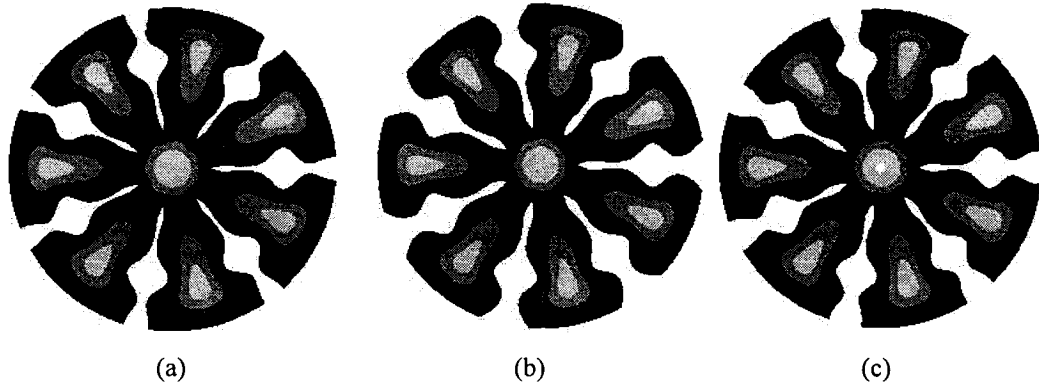
Figure 5.11 Optimal designs with n_{fin} variable, thermal boundary condition T, and the following fin materials for Case 3: (a) stainless steel, (b) aluminium, and (c) copper

The explanations of the results shown in Figures 5.10 and 5.11, which pertain to the T thermal boundary condition, are similar to those presented earlier for the results pertaining to the H boundary condition (Figures 5.8 and 5.9).

5.5 PRACTICAL CASE 4: OPTIMIZATION OF A HEAT EXCHANGER WITH INTERNALLY FINNED CIRCULAR DUCTS

The purpose of this fourth practical case is to demonstrate that the proposed optimization methodology can produce dramatic increases in relative thermal performance if the chosen baseline problem is poorly designed. The chosen baseline problem for this case is presented in section 5.5.1. The optimization results are presented in section 5.5.2.

5.5.1 Baseline Problem

In order to provide a contrast with the previous case, the baseline problem chosen here has twice the number of fins, and thus is a rather poor initial design. The dimensionless length of the fin, $l^* = l_f / r$, is 0.6; the number of fins, n_{fin}, is 16; and the angle of the fins at the base, 2σ, is 3° (see Figure 3.10 for details). The materials considered for the fins are again stainless steel (AISI 302), pure aluminium, and pure copper. The cross-section of the duct for this case is presented in Figure 5.12.

Since it has been determined in the previous case that the Reynolds number and duct size have no effect on the final optimal design, the results for the baseline problem for this case were obtained only for Re = 100 and a duct diameter of 0.5 inches (r = 6.35 mm): the corresponding fluid flow results are presented in Table 5.17. The heat transfer results for this baseline problem are included along with the optimization results in the next subsection.

Table 5.17 Overall fluid flow results for the baseline problem in Case 4

Re [-]	$\varnothing$ [mm]	pp [W/m]	$(f_D \cdot \mathrm{Re})_d$ [-]
100	6.35	2.4616×10^{-3}	258.08
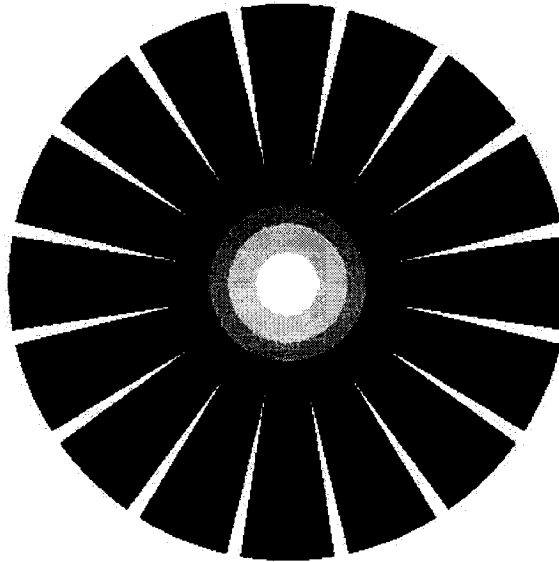
Figure 5.12 Duct cross-section for the baseline problem in Case 4

5.5.2 Optimization

The statements of the optimization problem for this case are identical to those presented for Case 3, so they are not repeated here. The results of this optimization exercise are presented in Tables 5.18 and 5.19, and also graphically in Figure 5.13. In all these runs, the pumping power per unit length of the duct (the constraint) was kept constant at the value calculated for the baseline problem, 2.4616×10^{-3} W/m.

Table 5.18 Optimization results for the boundary condition H in Case 4

n_{fin}	Stainless steel		Aluminium		Copper	
	$(f_D \cdot Re)_d$	η_{circ}^{H}	$(f_D \cdot Re)_d$	η_{circ}^{H}	$(f_D \cdot Re)_d$	η_{circ}^{H}
7	596.97	7.0655	543.57	7.4590	538.00	7.4877
8	420.77	7.6800	426.59	7.5813	424.97	7.6325
9	379.36	7.1425	379.60	7.1011	383.32	7.0760
10	368.46	6.2510	349.62	6.4299	352.53	6.4631
12	338.36	4.3496	337.65	4.3766	338.11	4.3676
14	288.25	1.8662	288.12	1.8572	288.23	1.8563
16	256.90	1.0284	256.92	1.0237	256.92	1.0235

Table 5.19 Optimization results for the boundary condition T in Case 4

n_{fin}	Stainless steel		Aluminium		Copper	
	$(f_D \cdot Re)_d$	η_{circ}^{T}	$(f_D \cdot Re)_d$	η_{circ}^{T}	$(f_D \cdot Re)_d$	η_{circ}^{T}
7	742.71	8.9105	873.00	6.7556	676.85	8.2802
8	569.31	8.7990	568.03	8.7996	584.40	8.1858
9	383.70	10.681	399.72	10.496	395.77	10.614
10	361.77	9.5603	350.58	9.5827	359.58	9.5480
12	339.57	2.9840	337.02	3.0626	338.05	3.0671
14	284.44	1.4303	285.32	1.4369	283.60	1.4217
16	253.57	1.0135	252.22	1.0104	252.93	1.0168
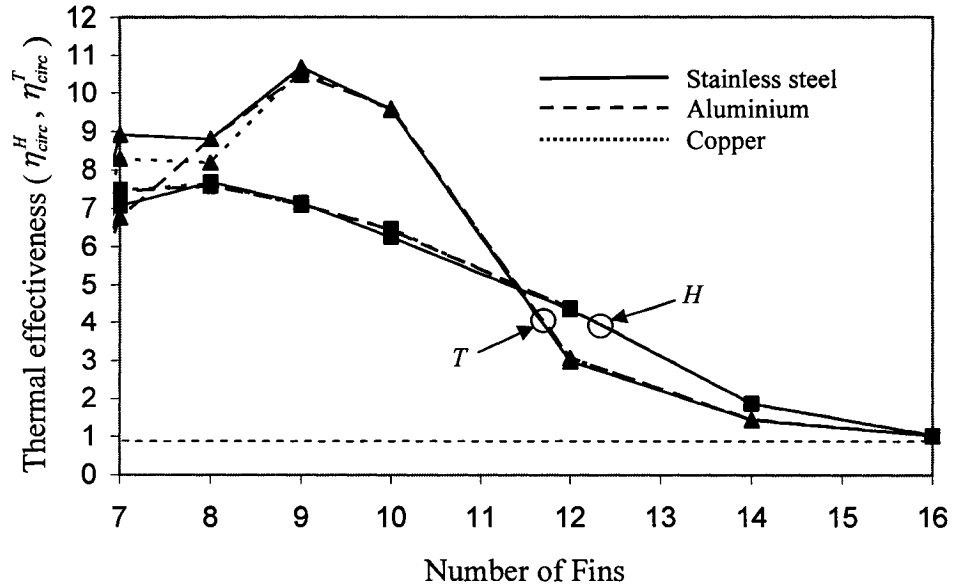
Figure 5.13 Effect of the number of fins on η_{circ}^{H} and η_{circ}^{T} in Case 4

For a fixed number of fins, the increase in relative thermal performance with respect to the objective functions for the baseline problem for H thermal boundary condition are 2.8% for stainless steel, 2.4% for aluminium, and 2.4% for copper. The corresponding fin shapes are presented in Figure 5.14. Again, the optimized shapes are virtually identical for the three fins material considered here. With the number of fins kept the same as in the baseline problem, only these small improvements in thermal performance are possible.

(a)   (b)   (c)
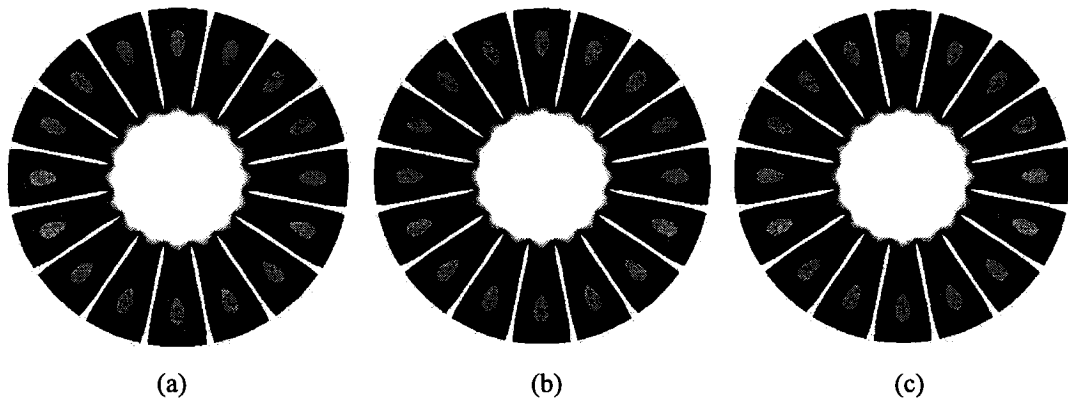
Figure 5.14 Optimal designs with $n_{fin} = 16$, thermal boundary condition H, and three fin materials for Case 4: (a) stainless steel, (b) aluminium, and (c) copper

When the number of fins is allowed to vary, the optimal shapes generated by proposed method produce dramatic increases in relative thermal performance: 7.58 for stainless steel, 7.68 for aluminium, and 7.63 for copper. The corresponding optimal shapes are illustrated in Figure 5.15.

| (a) | (b) | (c) |
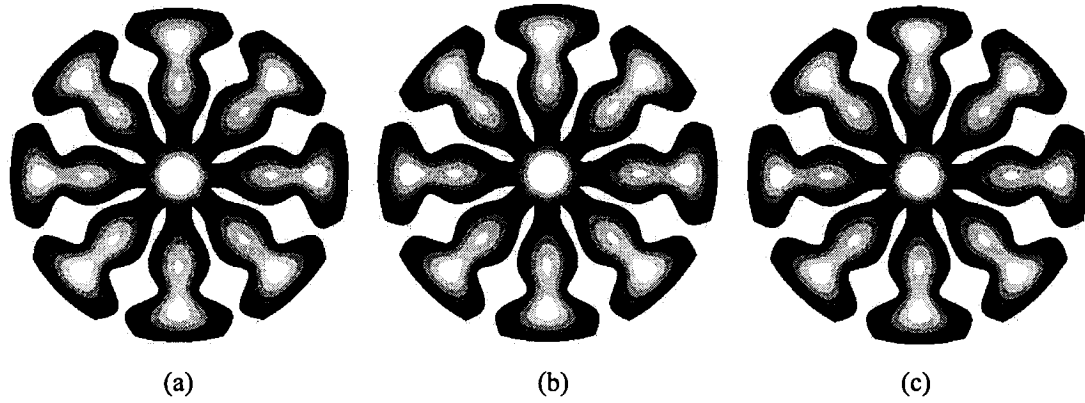
Figure 5.15 Optimal designs with n_{fin} variable, thermal boundary condition H, and three fin material for Case 4: (a) stainless steel, (b) aluminium, and (c) copper

For the thermal boundary condition T, the increases in relative thermal performance with the number of fins fixed at 16 are 1.35% for stainless steel, 1.04% for aluminium, and 1.68% for copper. The corresponding optimal shapes are presented in Figure 5.16. However, if the number of fins is allowed to vary, again dramatic increases in relative thermal performance are achieved by the proposed optimization method: 10.68 for stainless steel, 10.50 for aluminium, and 10.61 for copper. The corresponding optimal shapes are illustrated in Figure 5.17.

| (a) | (b) | (c) |
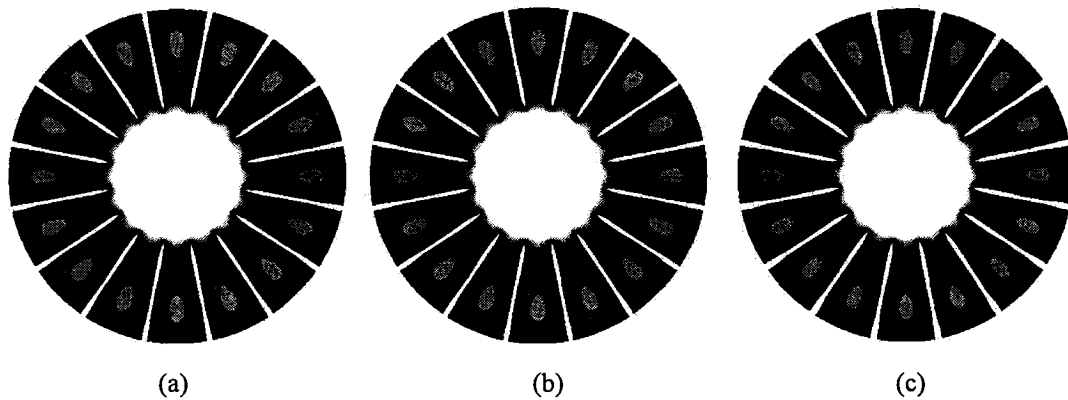
Figure 5.16 Optimal designs with n_{fin} = 16, thermal boundary condition T, and three fin materials for Case 4: (a) stainless steel, (b) aluminium, and (c) copper

Figure 5.17 Optimal designs with n_{fin} variable, thermal boundary condition T, and three fin materials for Case 4: (a) stainless steel, (b) aluminium, and (c) copper

Chapter 6. Conclusion

This final chapter presents a review of the contents of the thesis and its contributions, and concludes with a list of recommendations for extensions of this work. The contributions of the thesis are highlighted in the text by presenting them in *italics*.
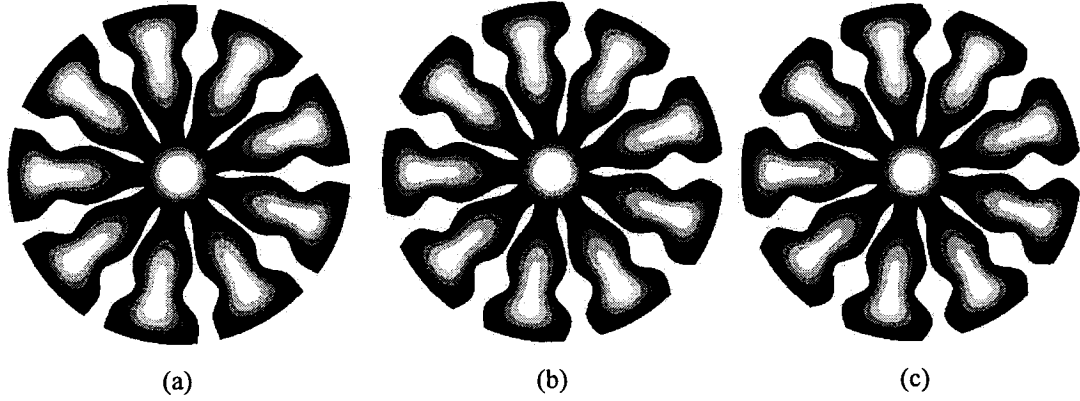
6.1 REVIEW OF THE THESIS AND ITS CONTRIBUTIONS

In Chapter 1, the motivation, context, overall goals, and specific objectives of the thesis were discussed. A review of the pertinent published literature was also presented. An overview of the organization of this thesis was presented at the end of the chapter.

Chapter 2 was devoted to the presentation of the theoretical considerations related to the problems studied in this work. These problems involve fully-developed laminar fluid flow and heat transfer in straight ducts, with the conjugate problem of quasi one-dimensional heat conduction in the fins. The assumptions employed were presented and justified. The equations that govern the fluid flow and heat transfer phenomena were then presented, along with the quasi one-dimensional mathematical model of heat conduction in the fins. Following that, the two thermal boundary conditions used in this work were put forward and discussed. Dimensionless formulations of these mathematical models of the problems of interest were also presented in this chapter.

In Chapter 3, the numerical techniques that were formulated, implemented, tested, and used to solve the mathematical models presented in Chapter 2 were presented. For the plate-fin heat exchangers with rectangular flow passages, a control-volume finite difference method (CVFDM) was used. For the plate-fin heat exchangers with triangular flow passages and for the internally finned circular tubes, a control-volume finite element method (CVFEM) was used. For the fin, the quasi one-dimensional model was solved using a CVFDM. The validity of the formulations and implementations of the aforementioned CVFDMs and CVFEM was established by applying them to well-established test problems and comparing the solutions with those in the published literature [Shah and London (1971, 1978), Shah (1975), Baliga and Azrak (1986)].

The bulk of this research was devoted to the formulation, implementation, and application of a methodology for optimizing the thermal performance of plate fin ducts. The proposed optimization techniques were presented in Chapter 4. First, an overview of the available optimization techniques was presented. Then, the technique used to approximate and control the fin shape, using non-uniform rational B-spline (NURBS) curves, was described in detail. This was followed by the formulation of the optimization problem, in which the design variables, the objective functions, and the constraint function were formulated and discussed. While many others have used the Nusselt number as the objective function to be maximized, in this work a rational derivation of the objective functions has been provided: for the H thermal boundary condition (uniform heat input per unit length and uniform duct wall temperature in the cross-section), the objective function is related to the minimization of $(T_w - T_b)$; for the T thermal boundary condition (specified constant duct wall temperature), the objective function is based on a maximization of the rate of heat transfer per unit length of the duct, q_w'. For these two cases, it was shown that the dimensionless forms of the objective function is the Nusselt number divided by the ratio of the hydraulic diameter to the wetted perimeter; these objective functions take into account the effect of the variation of the available surface area for heat transfer on the optimized thermal performance of the ducts. In both cases, the constraint function was the pumping power per unit axial length of the duct. *The formulations of the objective and constraint functions are considered to be one of the important contributions of this thesis.*

Following this, the proposed optimization algorithm was introduced. In this algorithm, the first goal is to satisfy the constraint function by moving the being-optimized-design, or current design point, on to the constraint hyper-plane. Then it seeks the maximization of the objective function by projecting the gradient of the objective function onto the constraint hyper-plane, and then setting the search direction toward the optimum. Techniques to correct inadvertent excursions outside the permitted design space were also proposed. *This proposed optimization algorithm is considered to be the main contribution of this thesis.*

The applications of the proposed optimization method to four practical cases were presented in Chapter 5. In all cases, three different fin materials (commonly used in the construction of compact heat exchangers) were considered: stainless steel (AISI 302), pure aluminum, and pure copper. Air was the working fluid in all these cases. Case 1 involved a plate-fin heat exchanger with rectangular flow passages. Here, the method was demonstrated in the context of two design variables, and an average increase of 18.1% in the relative thermal effectiveness with respect to the chosen the baseline problem was observed. In Case 2, the proposed method was applied to a plate-fin heat exchanger with triangular flow passages. This case was used to demonstrate that the proposed method reaches the same optimal design using different, but essentially equivalent sets of design variables. In this case, the optimization yielded an average increase of 3.1% in the relative thermal performance with respect to the chosen baseline problem; this number is lower than that for the first case because the design for the baseline problem was already close to the optimum.

The third and the fourth cases involved internally finned circular tubes. Case 3 was used to: 1) demonstrate the effect of the number of control points in the NURBS curves on the final optimal design, 2) demonstrate the effect of the initial design point on the final optimized design, and 3) verify that the effects of the duct diameter and the Reynolds number on the optimal design were negligible. The number of control points that provided a good balance between the increase in cost of computing the gradient of the objective function and accuracy in the approximation of the fin shape was found to be 12 for this case. It was also observed that the optimal design is sensitive to the initial design point, although the final shapes were qualitatively similar, for most cases. The best results were obtained when the initial fin shape was smooth, that is, without sudden changes or big differences in initial values of adjacent control points. For this Case 3, the baseline problem had eight fins, and the average increases in the relative thermal performance of the optimized design with respect to the base line case were 26.6% for the thermal boundary condition H and 18.4% for the thermal boundary condition T, with six and seven fins, respectively.

The baseline problem for Case 4 was deliberately chosen to be far from the optimum design, so that a large increase in the relative thermal performance could be observed. The baseline problem had 16 fins, and the average increase in relative thermal performance of the optimized designs with respect to the baseline problem reached rather the dramatic figures: 763% and 1060% for the thermal boundary conditions H and T, respectively.

The optimized shapes for Cases 3 and 4 all presented very similar bulges on the side of the fins, the size of which depends on the pumping power of the baseline problem and also the number of fins. Since the fin thickness and thermal conductivity was, in these cases, always much higher than that required to observe any appreciable variations of the fin temperature along its length, the optimal designs were essentially independent of the fin material used. Moreover, the qualitative differences between the optimal designs for the two thermal boundary conditions considered were small enough that it would be acceptable to propose a single optimized shape for both these conditions. *These demonstrations of the proposed optimization methodology, the use of the relative thermal performance with respect to a chosen baseline problem to quantify the benefits provided by the optimal designs, and all of the related discussions are together considered as another major contribution of this work.*

6.2   RECOMMENDATIONS FOR EXTENSIONS OF THIS WORK

It would be natural to conduct an experimental validation of the shapes obtained in the optimization of the baseline problems for the four cases presented in Chapter 5. Such an experimental exercise would not only provide a validation of the proposed optimization method and approaches, but give valuable insights into the manufacturing implications of the optimized fin shapes.

In the industry, heat exchanger design is often governed by other constraints than the one applied in this work (fixed pumping power per unit length). For example, other constraints could include fixed fin volume, for weight and cost reasons, and minimum fin

base width, for structural integrity and maintenance reasons. Thus, it would be desirable to test the effects of these other constraints on the optimal design of plate-fin ducts, either independently or conjointly with the one used in this work.

It would also be desirable to test the effect of using different fluids, such as water, on the optimal designs. With water, since it has a thermal conductivity that is about 20 times larger than that of air, the fin material would be expected to have a significant effect on the optimal designs of the plate-fin ducts.

It would be desirable to extend the applications studied in this thesis to turbulent flow and heat transfer. Since turbulence tends to flatten the axial velocity profile in the duct cross-section, the optimal shape, which depends partially on the velocity profile, would surely be affected.

It would be interesting and useful to consider other practical fin patterns in the optimization exercise: examples include helical twisted fins and interrupted-surface fins.

It would also be highly desirable to implement the adjoint formulation for the calculation of the gradient of the objective function in the proposed optimization algorithm. In the adjoint formulation, the direct problem is not solved for the dependent variables, but rather their sensitivities to slight perturbation of the design variables are directly solved. As a result, the solutions of the adjoint problem provide the gradients of the dependent variables. The implication of this approach is that the costs of computing the gradients are greatly decreased, and thus much more complex applications could be optimized using the method proposed in this work. Such applications could potentially include three-dimensional problems involving phenomenon such as turbulent flow, combustion, and phase change.

Finally, the author hopes that the work presented in this thesis will help in the global efforts directed towards the improvement of heat transfer enhancement devices. He also hopes that this work will encourage others to pursue some of the aforementioned extensions.

References

Afgan, N., Carvalho, M. da G., Bar-Cohen, A. and Butterworth, D., (1996), "New Developments in Heat Exchangers", *Gordon and Breach Science Publishers SA.*, The Netherlands

Annicchiarico, W. and Cerrolaza, M., (1999), "Finite Element, Genetic Algorithms and b-Splines: a Combined Technique for Shape Optimization", *Finite Elements in Analysis and Design*, Vol. 33, pp. 125-141

Arkadan, A. A., Subramaniam-Sivanesan, S. and Demerdash, N. A. O., (1996), "Shape Optimization of PM Devices Using Constrained Gradient Based Inverse Problem Methodology", *IEEE Transactions on Magnetics*, Vol. 32, No. 3, pp. 1222-1225

Ashrafizadeh, A., Raithby, G. D. and Stubley, G. D., (2002), "Direct Design of Shape", *Numerical Heat Transfer*, Part B, 41, pp. 501-520

Ashrafizadeh, A., Raithby, G. D. and Stubley, G. D., (2003), "Direct Design of Ducts", *Transactions of the ASME*, Vol. 125, pp. 158-165

Baliga, B. R. and Azrak, R. R., (1986), "Laminar Fully Developed Flow and Heat Transfer in Triangular Plate-Fin Ducts", *Transactions of the ASME*, Vol. 108, pp. 24-32

Baliga, B. R. and Patankar, S. V., (1980), "A New Finite-Element Formulation for Convection-Diffusion Problems", *Numerical Heat Transfer*, Vol. 3, pp. 393-409

Baliga, B.R. and Patankar, S.V., (1988), "Elliptic Systems: Finite-Element Method II", Chapter 11, *Handbook of Numerical Heat Transfer* (Eds. W.J. Minkowycz, E.M. Sparrow, G.E. Schneider and R.H. Plether), John Wiley & Sons, Inc., pp. 421-461

Baliga, B.R. and Atabaki, N., (2006), "Control-Volume-Based Finite-Difference and Finite-Element Methods", Chapter 6, *Handbook of Numerical Heat Transfer, 2nd Edition*, (Eds. W.J. Minkowycz, E.M. Sparrow, and J.Y. Murthy), John Wiley & Sons, Inc., pp. 191-224

Batchelor, G.K. (1967), *An Introduction to Fluid Dynamics*, Cambridge University Press, Cambridge, U.K.

Bejan, A. (1982), *Entropy generation through heat and fluid flow*, , J. Wiley, New York

Bejan, A. (1984), *Convection Heat Transfer*, J. Wiley, New York (Second Edition, 1995).

Bejan, A. and Morega, A. M., (1993), "Optimal Arrays of Pin Fins and Plate Fins in Laminar Forced Convection", *Journal of Heat Transfer*, Vol. 115, pp. 75-81

Beliakov, G., (2004), "Least Squares Splines with Free Knot: Global Optimization Approach", *Applied Mathematics and Computation*, Vol. 149, No. 3, pp. 783-798

Berdnik, V. V. and Mukhamedyarov, R. D., (2003), "Application of the Method of Neural Networks to Solution of the Inverse Problem of Heat Transfer", *High Temperature*, Vol. 41, No. 6, pp. 839-843

Bergles, A. E., (1988), "Some Perspectives on Enhanced Heat Transfer – Second-Generation Heat Transfer Technology", *Journal of Heat Transfer*, Vol. 110, pp. 1082-1096

Bondeson, A., Yang, Y. and Weinerfelt, P., (2004), "Shape Optimization for Radar Cross Sections by a Gradient Method", *International Journal for Numerical Methods in Engineering*, Vol. 61, pp. 687-715

Bonjour, J., Rocha, L. A. O., Bejan, A. and Meunier, F., (2003), "Dendritic Fins Optimization for a Coaxial Two-Stream Heat Exchanger", *International Journal of Heat and Mass Transfer*, Vol. 47, pp. 111-124

Borrvall, T. and Petersson, J., (2003), "Topology Optimization of Fluids in Stokes Flow", *International Journal for Numerical Methods in Fluids*, Vol. 41, pp. 77-107

Bryson, A. E. Jr., (1999), "Dynamic Optimization", Addison Wesley Longman, Inc., Menlo Park

Burgreen, G. W. and Baysal, O., (1994), "Aerodynamic Shape Optimization Using Preconditioned Conjugate Gradient Methods", *AIAA Journal*, Vol. 32, No. 11, pp. 2145-2152

Cebeci, T. (2002), *Convective Heat Transfer*, Horizons Publications, New York.

Chen, Y. and Cheng, P., (2002), "Heat Transfer and Pressure Drop in Fractal Tree-Like Microchanel Nets", *International Journal of Heat and Mass Transfer*, Vol. 45, pp. 2643-2648

Cheng, C.-H. and Chang, M.-H., (2003), "Shape Design for a Cylinder with uniform Temperature Distribution on the Outer Surface by Inverse Heat Transfer Method", *International Journal of Heat and Mass Transfer*, Vol. 46, pp. 101-111

Cheng, C.-H. and Chang, M.-H., (2003a), "Shape Identification for Water-Ice Interface Within the Cylindrical Capsule in Cold Storage System by Inverse Heat Transfer Method", *International Journal of Refrigeration*, Vol. 26, pp. 543-550

Cheng, C-H. and Chang, M-H, (2003b), "A Simplified Conjugate-Gradient Method for Shape Identification Based on Thermal Data", *Numerical Heat Transfer*, Part B 43, pp. 489-507

Cheng, C-H. and Chang, M-H., (2003c), "Shape Identification by Inverse Heat Transfer Method", *Transactions of the ASME*, Vol. 125, pp. 224-231

Cheng, C.-H. and Chang, M.-H., (2004), "Shape Design for Surface of a Slider by Inverse Method", *Journal of Tribology*, Vol. 126, pp. 519-526

Cheng, C.-H., Lin, H.-H. and Aung, W, (2003), "Optimal Shape Design for Packaging Containing Heating Elements by Inverse Heat Transfer Method", *Heat and Mass Transfer*, Vol. 39, pp. 687-692

Cheng, C-H. and Wu, C-Y, (2000), "An Approach Combining Body-Fitted Grid Generation and Conjugate Gradient Methods for Shape Design in Heat Conduction Problems", *Numerical Heat Transfer*, Part B 37, pp. 69-83

Chou F.C., Lukes J. R. and Tien C.L. (1999), "Heat Transfer Enhancement by Fins in the Microscale Regime", *Journal of Heat Transfer – Transactions of the ASME*, 121 (4), pp. 972-977

Churchill, S.W. (1988), *Viscous Flows: the Practical Use of Theory*, Butterworths, Boston.

Cingoski, V., Kaneda, K., Yamashita, H. and Kowata, N., (1999), "Inverse Shape Optimization Using Dynamically Adjustable Genetic Algorithms", *IEEE Transactions on Energy Conversion*, Vol. 14, No. 3, pp. 661, 666

Conley, W., (1981), "Optimization: A Simplified Approach", Petrocelli Books, Inc, New York

Converse, A. O., (1970), *Optimization*, Thayer School of Engineering, Dartmouth College, Holt, Rinehart and Winston Inc.

Cowell, T. A., (1990), "A General-Method for the Comparison of Compact Heat-Transfer Surfaces", *Journal of Heat Transfer – Transactions of the ASME*, 112 (2), pp. 288-294

Deb, K, (2001), "Multi-Objective Optimization using Evolutionary Algorithms", John Wiley & Sons, Ltd, West Sussex, England

Dems, K. and Mroz, Z., (1998), "Sensitivity Analysis and Optimal Design of External Boundaries and Interfaces for Heat Conduction Systems", *Journal of Thermal Stresses*, Vol. 21, pp. 461-488

Denn, M. M., (1969), "Optimization by Variational Methods", McGraw-Hill Book Company, New York

Dixon, L. C. W., (1972), "Nonlinear Optimization", The English Universities Press Ltd., London

Dowding, K. J. and Beck, J. V., (1999), "A Sequential Gradient Method for the Inverse Heat Conduction Problem (IHCP)", *Journal of Heat Transfer (ASME)*, Vol. 121, pp. 300-306

Dul'kin, I. N. and Garas'ko, G. I. (2002), "Analytical Solutions of the 1-D Heat Conduction Problem for a Single Fin with Temperature Dependent Heat Transfer Coefficient – I. Colsed-Form Inverse Solution", *International Journal of Heat and Mass Transfer*, Vol. 45, pp. 1895-1903

Eckert, E.R.G. and Drake, R.M. (1971), *Analysis of Heat and Mass Transfer*, McGraw-Hill, New York.

Fabbri, G., (1997), "A Genetic Algorithm for Fin Profile Optimization", *International Journal of Heat and Mass Transfer*, Vol. 40, no. 9, pp. 2165-2172

Fabbri, G., (1998), "Heat Transfer Optimization in Finned Annular Ducts under Laminar-Flow Conditions", *Heat Transfer Engineering*, Vol. 19, no. 4, pp. 42-54

Fabbri, G., (1998a), "Heat Transfer Optimization in Internally Finned Tubes under Laminar Flow Conditions", *International Journal of Heat and Mass Transfer*, Vol. 41, no. 10, pp. 1243-1253

Fabbri, G., (1998b), "Optimization of Heat Transfer through Finned Dissipators Cooled by Laminar Flow", *International Journal of Heat and Fluid Flow*, Vol. 19, pp. 644-654

Ferziger, J.H. and Peric, M. (1996), *Computational Methods for Fluid Dynamics*, Springer, New York (Second Edition, 1999).

Fic, A., (2004), "A Study of the Steady-State Inverse Heat Transfer Problem of Estimating the Boundary Velocity", *Numerical Heat Transfer*, Part A, 45, pp. 153-170

Fox, R.F. and McDonald, A. (1985), *Introduction to Fluid Mechanics*, Third Edition, Wiley and Sons, New York (Fifth Edition, 1998).

França, F. H. R., Ezekoye, O. A. and Howell, J. R., (2001), "Inverse Boundary Design Combining Radiation and Convection Heat Transfer", *Transactions of the ASME – C – Journal of Heat Transfer*, Vol. 123, pp. 884-891

Gerencser, D. S. and Razani, A., (1995), "Optimization of Radiative-Convective Arrays of Pin Fins Including Mutual Irradiation Between Fins", *International Journal of Heat and Mass Transfer*, Vol. 38, no. 5, pp. 899-907

Hernandez, S., Kassab, A. J. and Brebbia, C. A., (1999), "Computer Aided Optimum Design of Structures VI", WIT Press, Southampton, Boston

Hesselgreaves, J.E. (2001), *Compact Heat Exchangers: Selection, Design, and Operation*, Pergamon, New York.

Holzleitner, L., (1997), "Improvements on Objective and Constraint Functions in Domain Optimization", *Computer Methods in Applied Mechanics and Engineering*, No. 163, pp. 271-291

Hookey, N. A. Baliga, B. R. and Prakash, C., (1988), "Evaluation and Enhancement of Some Control Volume Finite-Element Methods 1: Convection-Diffusion Problems", *Numerical Heat Transfer* 14 (3), pp. 255-272

Huang, C.-H. and Hsiung, T.-Y., (1999), "An Inverse Design Problem of Estimating Optimal Shape of Cooling Passages in Turbine Blades", *International Journal of Heat and Mass Transfer*, Vol. 42, pp. 4307-4319

Incropera, F. P. and DeWitt, D. P., (2002), "Introduction to Heat Transfer", 4th Edition, John Wiley & Sons, Inc., New York

Jameson, A., (1994), "Optimum Aerodynamic Design via Boundary Control", *Optimum Design Methods for Aerodynamics*, AGARD Report, No. R-803, pp. 3.1-3.33

Jarny, Y., Özisik, M. N. and Bardon, J. P., (1991), "A General Optimization Method Using Adjoint Equation for Solving Multidimensional Inverse Heat Conduction", *International Journal of Heat and Mass Transfer*, Vol. 34, no. 11, pp. 2911-2919

Jubran, B. A., Hamdan, M. A. and Abdualh, R. M., (1993), "Enhanced Heat Transfer, Missing Pin, and Optimization for Cylindrical Pin Fin Arrays", *Transaction of the ASME*, Vol. 115, pp. 576-583

Kacimov, A. R. and Obnosov, Y. V., (1997), "Explicit, Rigorous Solutions to Two-Dimensional Heat Transfer: Two-Component Media and Optimization of Cooling Fins", *International Journal of Heat and Mass Transfer*, Vol. 40, No. 5, pp. 1191-1196

Kakaç, S., Bergles, A. E., Mayinger, F. and Yüncü, H., (1999), "Heat Transfer Enhancement of Heat Exchangers", *NATO ASI Series*, Serie E: Applied Sciences, Vol. 355

Kakac, S. and Liu, H. (2002), *Heat Exchangers: Selection, Rating, and Thermal Design*, CRC Press, Boca Ratón, Florida, Second Edition.

Kays, W.M. (1972), "Compact Heat Exchangers", *AGARD Lecture Series*, No.57 on Heat Exchangers, AGARD-LS-57-72, NATO, pp. 1-22.

Kays, W.M. and London, A.L. (1964), *Compact Heat Exchangers*, First Edition, McGraw-Hill, New York.

Kays, W.M. and London, A.L. (1984), *Compact Heat Exchangers*, Third Edition, McGraw-Hill, New York.

Kays, W.M. and Crawford, M.E. (1993), *Convective Heat and Mass Transfer*, McGraw-Hill, New York, Third Edition.

Keanini, R. G. and Desai, N. N., (1996), "Inverse Finite Element Reduced Mesh Method for Predicting Multi-Dimensional Phase Change Boundaries and Nonlinear Solid Phase Heat Transfer", *International Journal of Heat and Mass Transfer*, Vol. 39, No. 5, pp. 1039-1049

Ko, T. H., and Ting, K., (2006), "Entropy Generation and Optimal Analysis for Laminar Forced Convection in Curved Rectangular Ducts: A Numerical Study", *International Journal of Thermal Sciences*, 45, pp. 138-150

Kohli, H. S. and Carey, G. F., (1993), "Shape Optimization Using Adaptative Shape Refinement", *International Journal for Numerical Methods in Engineering*, Vol. 36, pp. 2435-2451

Kröger, D. G., (1986), "Performance Characteristics of Industrial Finned Tubes Presented in Dimensional Form", *International Journal of Heat and Mass Transfer*, Vol. 29, No. 8, pp. 1119-1125

Kundu, B. and Das, P. K., (1999), "Performance Analysis and Optimization of Eccentric Annular Disk Fins", *Journal of Heat Transfer (ASME)*, Vol. 121, pp. 128-135

Kunisch, K. and Pan, X., (1994), "Estimation of Interfaces from Boundary Measurements", *SIAM Journal on Control and Optimization*, Vol. 32, No. 6, pp.1643-1674

Kurpisz, K. and Nowak, A. J., (1995), "Inverse Thermal Problems", *International Series on Computational Engineering*, Computational Mechanics Publications, Billerica, MA, US

Lan, C.-H., Cheng, C.-H. and Wu, C.-Y., (2001), "Shape Design for Heat Conduction Problems Using Curvilinear Grid Generation, Conjugate Gradient, and Redistribution Methods", *Numerical Heat Transfer*, Part A, 39, pp. 487-510

Landau, L.D. and Lifshitz, E.M. (1959), "Fluid Mechanics", translated from the Russian by J.B. Sykes and W.H. Reid, Pergamon Press, Oxford (Second Edition, 1987)

Laor, K. and Kalman, H., (1995), "Performance and Optimum Dimensions of Different Cooling Fins with a Temperature-Dependent Heat Transfer Coefficient", *International Journal of Heat and Mass Transfer*, Vol. 39, No. 9, pp. 1993-2003

LeDain-Muir, B. and Baliga, B.R., (1986), "Solution of three-dimensional convection-diffusion problems, using tetrahedral elements and flow-oriented upwind interpolation functions", *Numerical Heat Transfer*, Vol. 9, pp. 143-162

Lorenzini, E., Spiga, M. and Fabbri, G., (1994), "A Polynomial Fin Profile Optimization", *Int. J. Heat and Technology*, Vol. 12, No. 1-2, pp. 137-144

Masliyah, J. H. and Nandkumar, K., (1976), "Heat Transfer in Internally Finned Tubes", *Journal of Heat Transfer*, May 1976, pp. 257-261

Meissner, L. P. and Organick, E. I., (1892), "Fortran 77: Featuring Structured Programming", Addison-Wesley Series in Computer Science, Addison-Wesley Publishing Company, Menlo Park

Meric, R. A., (1998), "Shape Design Sensitivity Analysis and Optimization for Nonlinear Heat and Electric Conduction Problems", *Numerical Heat Transfer*, Part A, 34, pp. 185-203

Minkowycz, W.J. and Sparrow, E.M., editors (1997), *Advances in Numerical Heat Transfer, Vol. 1*, Taylor and Francis, Washington D.C.

Minkowycz, W.J. and Sparrow, E.M., editors (2000), *Advances in Numerical Heat Transfer, Vol. 2*, Taylor and Francis, Washington D.C.

Minkowycz, W.J., Sparrow, E.M. and Murthy, J.Y., (2006), *Handbook of numerical heat transfer*, J. Wiley, Hoboken, N.J.

Mohammadi, B. and Pironneau, O., (2001), "Applied Shape Optimization for Fluids", Oxford Science Publications, Oxford

Mohammadi, B. and Pironneau, O., (2004), "Shape Optimization in Fluid Mechanics", *Annu. Rev. Fluid Mech.*, Vol. 36, pp. 255-279

Onwubolu, G. C. and Babu, B. V., (2004), "New Optimization Techniques in Engineering", *Studies in Fuzziness and Soft Computing*, Volume 141, Springer-Verlag, Berlin

Özisik, M. N. and Orlande, H. R. B., (2000), "Inverse Heat Transfer – Fundamentals and Applications", Taylor & Francis, New York

Page, C. G., (1995), "Professional Programmer's Guide to Fortran 77", University of Leicester, U.K.

Pandya, M. J. and Baysal, O., (1997), "Gradient-Based Aerodynamic Shape Optimization Using Alternating Direction Implicit Method", *Journal of Aircraft*, Vol. 34, No. 3, pp. 346-352

Panton, R.L. (1996), *Incompressible Flow*, Second Edition, J. Wiley, New York.

Park, H. M. and Chung, O. Y., (1999), "Comparison of Various Conjugate Gradient Methods for Inverse Heat Transfer Problems", *Chemical Engineering Communications*, Vol. 176, pp. 201-228

Patankar, S. V., Ivanovic, M. and Sparrow, E. M., (1979), "Analysis of Turbulent Flow and Heat Transfer in Internally Finned Tubes and Annuli", *Journal of Heat Transfer*, Vol. 101, pp. 29-37

Patankar, S.V., (1980), "Numerical Heat Transfer and Fluid Flow", Taylor & Francis, Delhi

Piegl, L. and Tiller, W., (1997), "The NURBS Book", 2nd Edition, Monographs in Visual Communication, Springer-Verlag, Berlin

Pironneau, O., (1994), "Optimal Shape Design for Elliptic Systems", Springer Series in Computational Physics, Springer-Verlag, New York

Prabhu, K. N. and Ashish, A. A., (2002), "Inverse Modeling of Heat Transfer with Application to Solidification and Quenching", *Materials and Manufacturing Processes*, Vol. 17, No. 4, pp. 469-481

Rao, S. S., (1996), "Engineering Optimization: Theory and Practice", 3rd Edition, John Wiley & Sons, Inc., New York

Razelos, P. and Krikkis, R. N., (2003), "On the Optimum Thermal Design of Individual Longitudinal Fins with Rectangular Profile", *International Communications in Heat and Mass Transfer*, Vol. 30, pp. 349-358.

Razelos, P., (1995), "The Quest for the Optimum Longitudinal Fin Profile", *Heat Transfer Engineering*, Vol. 16, No. 3, pp. 19-29

Reddy, J.N. and Gartling, D.K. (1994), *The Finite Element Method in Heat Transfer and Fluid Dynamics*, CRC Press, Boca Ratón, Florida.

Roache, P.J., (1998), *Fundamentals of Computational Fluid Dynamics*, Hermosa Publishers, Albuquerque, New Mexico.

Rohsenow, W.M., Harnett, J.P. and Ganic, E.M., editors (1985), *Handbook of Heat Transfer Fundamentals*, Second Edition, McGraw-Hill, Toronto.

Rouse, H. (1978), *Elementary Mechanics of Fluids*, Second Edition, Dover Publications Inc., New York

Saidi, M. H., Ehyaei, M. A. and Abbasi, A., (2005), "Optimization of a Combined Heat and Power PEFC by Exergy Analysis", *Journal of Power Sources*, Vol. 143, pp. 179-184

Schleupen, A., Maute, K. and Ramm, E., (2000), "Adaptive FE-procedures in Shape Optimization", *Struct. Multidisc. Optim.*, Vol. 19, pp. 282-302

Schlichting, H. (1979), *Boundary Layer Theory*, Third Edition, McGraw Hill, New York

Sebben, S. and Baliga, B. R., (1995), "Some Extension of Tridiagonal and Pentadiagonal Matrix Algorithms", *Numerical Heat Transfer*, Part B, 28, pp. 323-351

Seireg, A. A. and Rodriguez, J., (1997), "Optimizing the Shape of Mechanical Elements and Structures", Marcel Dekker, Inc., New York

Shah, R.K., Heikal, M.R., Thonon, B. and Tochon P. (2001), "Progress in the Numerical Analysis of Compact Heat Exchanger Surfaces", *Advances in Heat Transfer*, Vol. 34, pp. 363-443.

Shah, R. K. and London, A. L., (1978), "Laminar Flow Forced Convection in Ducts", *Supplement 1, Advances in Heat Transfer*, Academic Press, New York

Snider, A. D., Kraus, A. D., Graff, S., Rodriguez, M. and Kusmierczyk, A. G., (1990), "Optimal Fin Profiles – Classical and Modern", *Proceedings of the 9th International Heat Transfer Conference*, Vol. 4, pp. 15-19

Soliman, H. M., Chau, T. S. and Trupp, A. C., (1980), "Analysis of Laminar Heat Transfer in Internally Finned Tubes with uniform Outside Wall Temperature", *Transactions of the ASME*, Vol. 102, pp. 598-604

Soto, O. and Löhner, R., (2001), "CFD Shape Optimization Using an Incomplete-Gradient Adjoint Formulation", *International Journal for Numerical Methods in Engineering*, Vol. 51, pp. 735-753

Sparrow, E.M. and Patankar, S.V. (1977), "Relationships among boundary conditions and Nusselt numbers for thermally developed duct flows", *ASME J Heat Transfer*, Vol. 99, pp. 483-485

Streeter, V.L (1951), *Fluid mechanics*, McGraw Hill, Boston (Third Edition, 1962).

Tsukamoto, Y. and Seguchi, Y., (1984), "Shape Optimization Problem for Minimum Volume Fin", *Heat Transfer – Japanese Research*, 13, pp. 1-19

Vyver, H. V. D., Driker, J. and Meyer, J. P., (2003), "Validation of a CFD Model of a Three-Dimensional Tube-in-Tube Heat Exchanger", *Third International Conference on CFD in the Minerals and Process Industries (CSIRO), pp. 235-240*

Webb, R. L., (1994), "Principles of enhanced heat transfer", Wiley Interscience, New York

Webb, R. L. and Scott, M. J., (1980), "A Parametric Analysis of the Performance if Internally Finned Tubes for Heat Exchanger Application", *Journal of Heat Transfer*, Vol. 102, pp. 38-43

White, F.M. (1991), *Viscous Fluid Flow*, Second Edition, McGraw-Hill, New York

Wilkes, J.O. (1999), *Fluid Mechanics for Chemical Engineers*, Prentice Hall, Upper Saddle River, New Jersey.

Witte, L. C., (1988), "The Influence of Availability Costs on Optimal Heat Exchanger Design", *Transactions of the ASME*, Vol. 110, pp. 830-835

Xu, R. and Naterer, G. F., (2003), "Controlling Phase Interface Motion in Inverse Heat Transfer Problems with Solidification", *Journal of Thermophysics and Heat Transfer*, Vol. 17, no. 4, pp. 488-497

Yeh, R.-H., (1994), "Optimization of Longitudinal Fins with Temperature Dependent Thermal Parameters", *Heat Transfer Engineering*, Vol. 15, No. 3, pp. 25-34

Yeh, R.-H., (1996), "Technical Notes – Errors in One-Dimensional Fin Optimization Problem for Convective Heat Transfer", *International Journal of Heat and Mass Transfer*, Vol. 39, pp. 3075-3078

Zangenen, M., Goto, A. and Harada, H., (1999), "On the Role of Three-Dimensional Inverse Design Methods in Turbomachinery Shape Optimization", *Proceedings of the Institution of Mechanical Engineers*, Vol. 213, Part C, pp. 27-42

Zhang, Y. and Faghri, A., (1996), "Heat Transfer Enhancement in Latent Heat Thermal Energy Storage System by Using the Internally Finned Tube", *International Journal of Heat and Mass Transfer*, Vol. 39, No. 15, pp. 3165-3173

Appendix A. Validation of the CVFDM and CVFEM

Table A.1 Overall fluid flow results for the rectangular ducts

Ar	$f_D \cdot \text{Re}$ [CVFDM]	$f_D \cdot \text{Re}$ [*]
1.0	56.8717	56.9083
0.75	57.8636	57.9028
0.50	62.1402	62.1922

* Shah & London (1971)

Table A.2 Average Nusselt numbers with $\Omega = \infty$ for the rectangular ducts

Ar	Nu_{av}^H [CVFDM]	Nu_{av}^H [*]	Nu_{av}^T [CVFDM]	Nu_{av}^T [*]
1.0	3.61713	3.60795	2.97846	2.976
0.75	3.71017	3.70052	3.05233	-
0.5	4.13542	4.12330	3.39165	3.391

* Shah & London (1971)

Table A.3 Overall fluid flow results for the triangular ducts

2τ	$f_D \cdot \text{Re}$ [Present]	$f_D \cdot \text{Re}$ [*]	$f_D \cdot \text{Re}$ [**]
10°	50.1083	49.896	50.188
30°	52.3495	52.260	52.520
60°	53.3889	53.332	53.744
90°	52.6543	52.612	52.936
120°	50.9914	50.976	51.224

* Shah (1975)

** Baliga & Azrak (1986)

Table A.4 Average Nusselt numbers with $\Omega = \infty$ for the triangular ducts

2τ	Nu_{av}^{H} [Present]	Nu_{av}^{H} [*]	Nu_{av}^{H} [**]	Nu_{av}^{T} [Present]	Nu_{av}^{T} [***]	Nu_{av}^{T} [**]
10°	2.43236	2.446	2.467	1.69224	1.61	1.726
30°	2.88957	2.910	2.921	2.24768	2.26	2.284
60°	3.08565	3.111	3.111	2.46106	2.47	2.500
90°	2.95508	2.982	2.979	2.31750	2.34	2.359
120°	2.65588	2.680	2.681	1.98548	2.00	2.031

* Shah (1975)

** Baliga & Azrak (1986)

*** from graphical results of Schmidt & Newell, from Shah & London (1978)

Table A.5 Overall heat transfer results for the triangular plate-fin ducts

2τ	10°				30°			
Ω	Nu_{av}^{H} [Present]	Nu_{av}^{H} [*]	Nu_{av}^{H} [Present]	Nu_{av}^{H} [*]	Nu_{av}^{H} [Present]	Nu_{av}^{H} [*]	Nu_{av}^{H} [Present]	Nu_{av}^{H} [*]
∞	2.4325	2.467	1.6922	1.726	2.8897	2.921	2.2477	2.284
25	2.2265	2.254	1.6444	1.676	2.7326	2.761	2.1763	2.210
10	1.9775	1.997	1.5673	1.594	2.5314	2.555	2.0738	2.105
5	1.6704	1.682	1.4296	1.450	2.2646	2.283	1.9175	1.944
2	1.1516	1.154	1.0574	1.065	1.7593	1.770	1.5573	1.575
1	0.7757	0.774	0.7077	0.710	1.3424	1.348	1.2073	1.218
2τ	60°				90°			
Ω	Nu_{av}^{H} [Present]	Nu_{av}^{H} [*]	Nu_{av}^{H} [Present]	Nu_{av}^{H} [*]	Nu_{av}^{H} [Present]	Nu_{av}^{H} [*]	Nu_{av}^{H} [Present]	Nu_{av}^{H} [*]
∞	3.0857	3.110	2.4611	2.500	2.9551	2.979	2.3175	2.359
25	2.9504	2.972	2.3878	2.424	2.8367	2.859	2.2595	2.299
10	2.7770	2.797	2.2879	2.322	2.6896	2.711	2.1824	2.220
5	2.5474	2.564	2.1444	2.174	2.5017	2.521	2.0758	2.110
2	2.1127	2.124	1.8392	1.862	2.1671	2.184	1.8620	1.890
1	1.7543	1.762	1.5568	1.574	-	1.924	-	1.701

* Baliga & Azrak (1986)

Table A.6 Overall fluid flow results for the circular duct
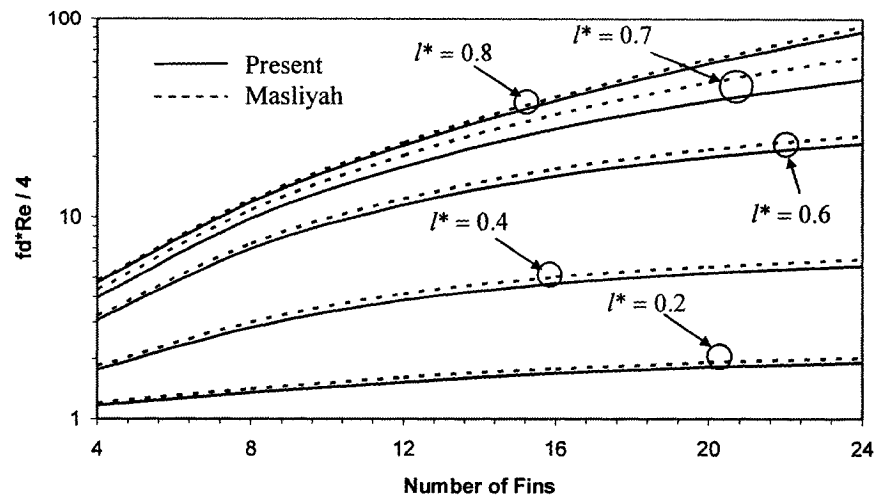with triangular fins ($2\tau = 3°$)

l *	0.2		0.4		0.6		0.7		0.8	
number of fins	$\dfrac{f_D \cdot Re}{4}$ [Present]	$\dfrac{f_D \cdot Re}{4}$ [*]	$\dfrac{f_D \cdot Re}{4}$ [Present]	$\dfrac{f_D \cdot Re}{4}$ [*]	$\dfrac{f_D \cdot Re}{4}$ [Present]	$\dfrac{f_D \cdot Re}{4}$ [*]	$\dfrac{f_D \cdot Re}{4}$ [Present]	$\dfrac{f_D \cdot Re}{4}$ [*]	$\dfrac{f_D \cdot Re}{4}$ [Present]	$\dfrac{f_D \cdot Re}{4}$ [*]
4	1.1694	1.2000	1.7588	1.8344	3.0813	3.2331	3.9756	4.3475	4.7169	4.8275
8	1.3544	1.4100	2.8225	3.0100	6.9413	7.4000	9.8131	10.8875	11.8288	12.1375
12	1.5331	1.6113	3.8448	4.1331	11.5019	12.3938	17.8500	20.3938	22.7869	23.5438
16	1.6869	1.7813	4.6544	5.0225	15.9538	17.3375	27.5256	32.7188	38.2731	39.8813
20	1.8113	1.9131	5.2563	5.6663	19.9169	21.7500	38.1519	47.4625	58.8300	61.8875
24	1.9088	2.0163	5.6988	6.1344	23.2625	25.4563	48.9450	63.8625	84.7875	90.0313

* Masliyah from Shah & London (1978)

Table A.7 Overall fluid flow results for the circular duct
with triangular fins ($2\tau = 6°$)

l *	0.2		0.4		0.6		0.7		0.8	
number of fins	$\dfrac{f_D \cdot Re}{4}$ [Present]	$\dfrac{f_D \cdot Re}{4}$ [*]	$\dfrac{f_D \cdot Re}{4}$ [Present]	$\dfrac{f_D \cdot Re}{4}$ [*]	$\dfrac{f_D \cdot Re}{4}$ [Present]	$\dfrac{f_D \cdot Re}{4}$ [*]	$\dfrac{f_D \cdot Re}{4}$ [Present]	$\dfrac{f_D \cdot Re}{4}$ [*]	$\dfrac{f_D \cdot Re}{4}$ [Present]	$\dfrac{f_D \cdot Re}{4}$ [*]
4	1.1756	1.2056	1.7825	1.8588	3.1738	3.3281	4.1419	4.4944	4.9731	5.0881
8	1.3706	1.4231	2.9025	3.0863	7.4375	7.9313	10.8956	12.0625	13.5900	13.9625
12	1.5581	1.6306	3.9769	4.2656	12.6894	13.7000	21.0994	24.2813	28.8844	29.9625
16	1.7169	1.8038	4.8125	5.1744	17.8625	19.4875	34.2069	41.5938	53.7731	56.4875
20	1.8431	1.9388	5.4188	5.8281	22.3594	24.5438	48.9300	63.3313	91.3925	97.5563
24	1.9394	2.0406	5.8544	6.2875	25.9725	28.5500	63.5888	87.6375	144.088	156.388

* Masliyah from Shah & London (1978)

FigureA.1 Overall fluid flow results for the circular duct with triangular fins ($2\tau = 3°$)
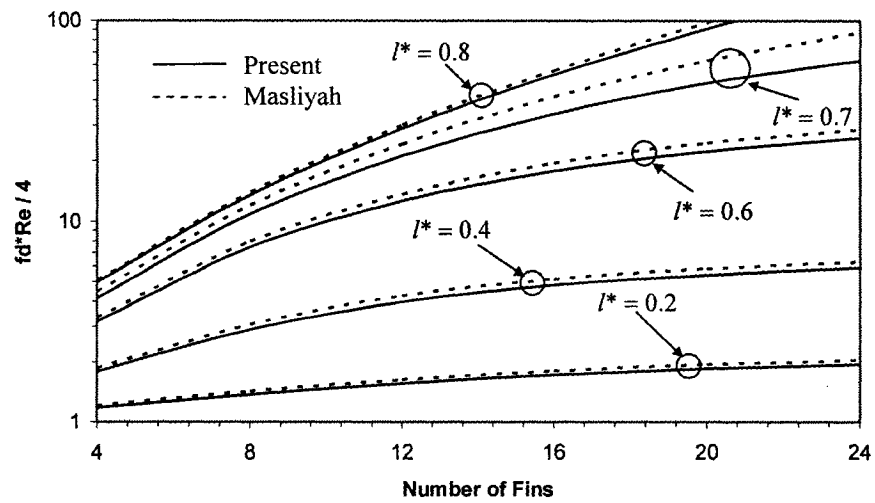
FigureA.2 Overall fluid flow results for the circular duct with triangular fins ($2\tau = 6°$)

Table A.8 Average Nusselt numbers with $\Omega = \infty$ for the circular duct with triangular fins ($2\tau = 3°$)

| l^*	0.2		0.4		0.6		0.7		0.8	
number of fins	$\frac{Nu_{av}^H}{4.37}$ [Present]	$\frac{Nu_{av}^H}{4.37}$ [*]	$\frac{Nu_{av}^H}{4.37}$ [Present]	$\frac{Nu_{av}^H}{4.37}$ [*]	$\frac{Nu_{av}^H}{4.37}$ [Present]	$\frac{Nu_{av}^H}{4.37}$ [*]	$\frac{Nu_{av}^H}{4.37}$ [Present]	$\frac{Nu_{av}^H}{4.37}$ [*]	$\frac{Nu_{av}^H}{4.37}$ [Present]	$\frac{Nu_{av}^H}{4.37}$ [*]
4	1.0499	1.0481	1.3533	1.3799	2.5529	2.6819	3.7217	4.1236	4.3487	4.4142
8	1.0854	1.0824	1.5410	1.5675	4.2545	4.5789	8.7208	9.8993	9.9911	9.9771
12	1.0945	1.0870	1.4645	1.4691	3.8325	4.0778	10.7217	14.7780	17.4224	17.4302
16	1.0881	1.0778	1.3426	1.3318	2.9055	3.0092	8.6117	14.4645	25.2265	25.6545
20	1.0762	1.0618	1.2487	1.2288	2.2588	2.2769	5.9908	10.5652	28.9499	30.1831
24	1.0641	1.0481	1.1844	1.1602	1.8584	1.8352	4.2124	7.0618	25.5277	26.8879

* Masliyah from Shah & London (1978)

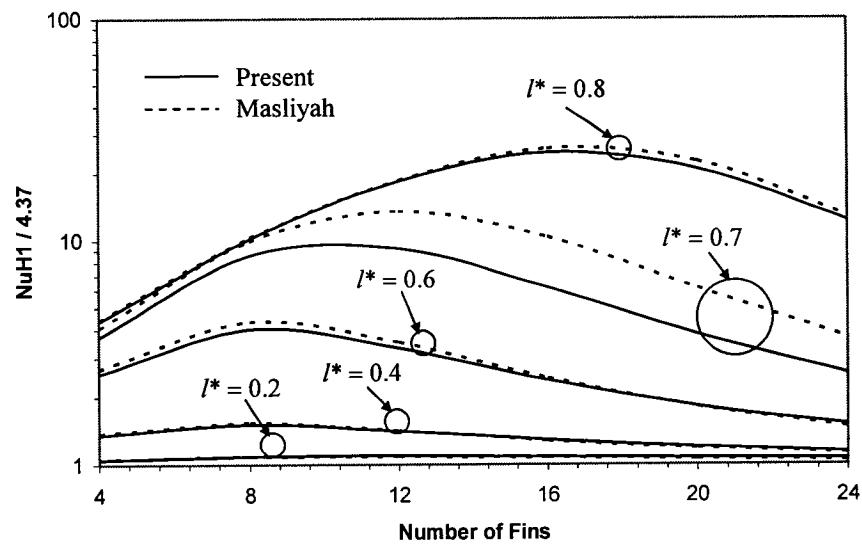**Table A.9** Average Nusselt numbers with $\Omega = \infty$ for the circular duct with triangular fins ($2\tau = 6°$)

l^*	0.2		0.4		0.6		0.7		0.8	
number of fins	$\frac{Nu_{av}^H}{4.37}$ [Present]	$\frac{Nu_{av}^H}{4.37}$ [*]	$\frac{Nu_{av}^H}{4.37}$ [Present]	$\frac{Nu_{av}^H}{4.37}$ [*]	$\frac{Nu_{av}^H}{4.37}$ [Present]	$\frac{Nu_{av}^H}{4.37}$ [*]	$\frac{Nu_{av}^H}{4.37}$ [Present]	$\frac{Nu_{av}^H}{4.37}$ [*]	$\frac{Nu_{av}^H}{4.37}$ [Present]	$\frac{Nu_{av}^H}{4.37}$ [*]
4	1.0492	1.0481	1.3483	1.3730	2.5341	2.6613	3.7092	4.0778	4.3471	4.4142
8	1.0833	1.0778	1.5140	1.5355	4.0227	4.3181	8.5586	9.9108	10.1906	10.2700
12	1.0892	1.0824	1.4142	1.4165	3.3174	3.5011	9.2265	13.4737	18.3867	18.4920
16	1.0801	1.0686	1.2860	1.2746	2.3817	2.4348	6.1746	10.3616	24.6725	25.7323
20	1.0664	1.0526	1.1954	1.1762	1.8199	1.8101	3.8190	6.1213	20.8840	22.4714
24	1.0538	1.0389	1.1373	1.1144	1.5053	1.4691	2.5581	3.6636	12.2373	12.8238

* Masliyah from Shah & London (1978)
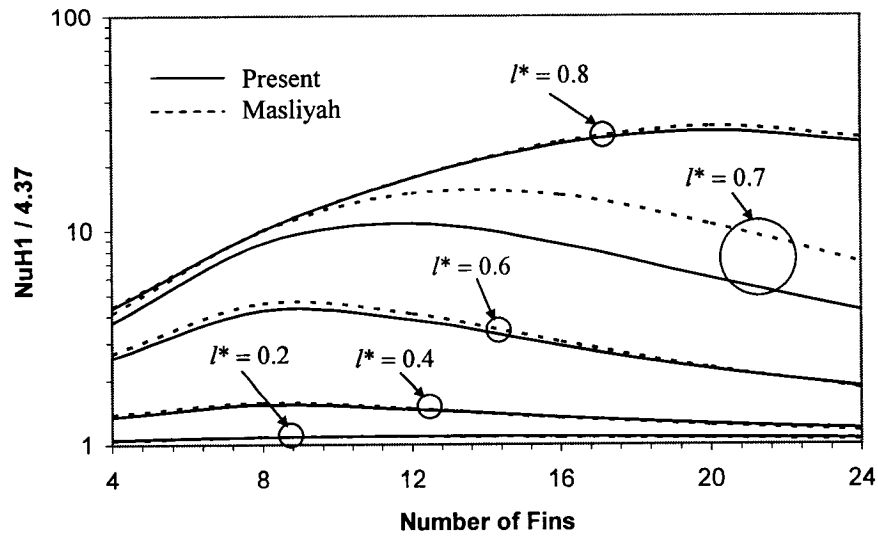
FigureA.3 Average Nusselt numbers with $\Omega = \infty$ for the circular duct with triangular fins ($2\tau = 3°$)

**FigureA.4** Average Nusselt numbers with $\Omega = \infty$ for the circular duct with triangular fins ($2\tau = 6°$)

Appendix B. Optimization Results with Different Initial Design Points for Case 3

Table B.1 Optimization results for different initial design points for Case 3

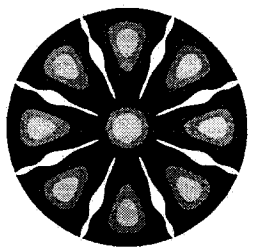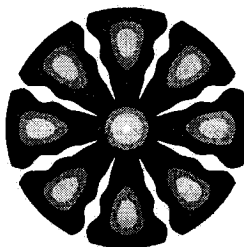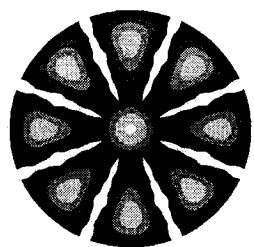| Run No. | Dimensionless design variables | | | | | | | | | | | | $(f_D \cdot Re)_d$ | $f_{circ}^H(X)$ |
	x_1	x_2	x_3	x_4	x_5	x_6	x_7	x_8	x_9	x_{10}	x_{11}	x_{12}		
1	0.3	0.3	0.3	0.3	0.3	0.3	0.3	0.3	0.3	0.3	0.3	0.8	226.9	86.83
2	0.4	0.4	0.4	0.4	0.4	0.4	0.4	0.4	0.4	0.4	0.4	0.6	244.3	83.18
3	0.4	0.4	0.4	0.4	0.4	0.4	0.6	0.6	0.6	0.6	0.6	0.6	262.8	80.54
4	0.1	0.1	0.1	0.1	0.1	0.1	0.1	0.1	0.1	0.1	0.1	0.2	214.0	88.30
5	0.1	0.1	0.1	0.1	0.1	0.4	0.4	0.4	0.4	0.4	0.4	0.4	259.8	81.65
6	0.5	0.5	0.5	0.5	0.1	0.1	0.1	0.3	0.3	0.3	0.3	0.8	215.9	82.63
7	0.1	0.1	0.1	0.1	0.1	0.1	0.1	0.1	0.1	0.1	0.1	0.1	212.8	88.45
8	0.1	0.1	0.3	0.3	0.1	0.1	0.3	0.3	0.1	0.1	0.3	0.5	228.8	84.93
9	0.2	0.4	0.2	0.4	0.2	0.4	0.2	0.4	0.2	0.4	0.2	0.5	227.6	84.75
10	0.6	0.6	0.6	0.6	0.6	0.6	0.4	0.4	0.4	0.4	0.4	0.6	241.8	81.50
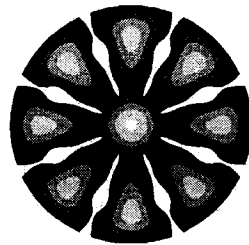
Run 1
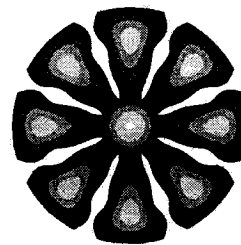
Run 2
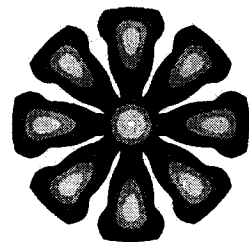
Run 3
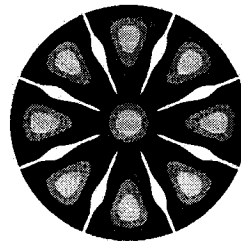
Run 4
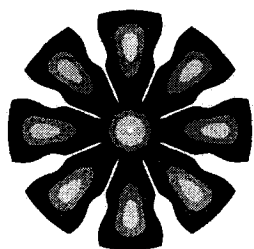
Run 5
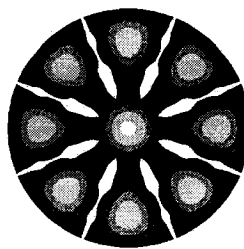
Run 6

Run 7

Run 8

Run 9

Run 10